AN ABSTRACT OF THE DISSERTATION OF

Eric P. Young for the degree of Doctor of Philosophy in Nuclear Engineering presented on August 18, 2006.
Title: On the Effects of Centrifugal Forces in Air-Water Two-Phase Flow Regime Transitions of an Adiabatic Helical Geometry.

Abstract approved: _____

José Reyes Qiao Wu

Two-phase flow in helical conduits is important in many industries where reaction between components, heat transfer, and mass transport are utilized as processes. The helical design is chosen for the effects of secondary flow patterns that reduce axial dispersion, increased heat transfer, and also their compact design. The first is a result of the secondary flow, which continually transports fluid from the near wall region to the bulk of the flow. In single-phase chemical reactor design this secondary flow increases radial mixing and reduces axial dispersion. In heat exchanger design it increases laminar heat transfer while extending the Reynolds number range of laminar flow.

A literature review of the work on helical pipe flow shows that the vast majority of the work is on toroidal single-phase flow, and analyses of two-phase flow are sparse. This dissertation addresses this void by presenting an analytical model of the stratified and annular flow regime transitions in helical conduits, by consideration of the governing equations and mechanisms for transition in the toroidal geometry including the major impact of pitch. Studies have taken a similar approach for straight inclined horizontal and vertical geometries, but none have been found which resolve two-phase flow in the curved geometry of a helix. The main issue in resolving the flow in this geometry is that of determining appropriate inter-phase momentum transfer, and the appropriate friction correlations for wall interaction. These issues are resolved to yield a novel attempt at modeling helical two-phase flow. Pitch is considered negligible in introduction of torsion, while the dominating influence of the centrifugal force is retained. The formulation of the governing equations are taken from a general vector form that is readily extended to a true helix that includes torsion. The predictive capability of the current model is compared to the data and observations of the two-

phase helical flow studies available in the open literature. The new model is found to be accurate in the linear asymptote, and to correctly predict the trends of increased liquid hold-up, a shift in the transition boundary between non-stratified and stratified flows such that the non-stratified regimes are favored, and the new liquid equilibrium height calculations shift the transition between annular and intermittent flows such that the intermittent regime is favored. The current model is an improvement over the previous methods in that it has the same accuracy of prediction of linear flowing inclined flows as methods developed for the linear flow condition, and improves the prediction of curved flow regimes by correctly shifting the boundaries as described above.

On the Effects of Centrifugal Forces in Air-Water Two-Phase Flow Regime Transitions in an Adiabatic Helical Geometry

by

Eric P. Young

A DISSERTATION

submitted to

Oregon State University

in partial fulfillment of
the requirements for the
degree of

Doctor of Philosophy

Presented August 18, 2006
Commencement June 2007

Doctor of Philosophy dissertation of Eric P. Young presented on August 18, 2006.

APPROVED:

Co-Major Professor, representing Nuclear Engineering

Co-Major Professor, representing Nuclear Engineering

Head of the Department of Nuclear Engineering and Radiation Health Physics

---

Dean of the Graduate School

I understand that my dissertation will become part of the permanent collection of Oregon State University libraries. My signature below authorizes release of my dissertation to any reader upon request.

Eric P. Young, Author

ACKNOWLEDGEMENTS

The author would like to thank his family and friends for all the support and encouragement they have provided over the years; especially the loving support of his wife Silia, who has made all things possible, his father Monte and mother Karin, whose never ending love carried me through the many trials of my life. Appreciation is due José Reyes and Qiao Wu for their help in writing, reviewing, and providing the impetus for this work. Specifically, it was Qiao Wu's observation that the helical flow regime formulation had yet to be undertaken, that started this research, and José Reyes for the continual support and guidance that has been a major part of attaining this degree. Not in the least is the fact that José Reyes introduced myself to this field of study, on the recommendation of my close friend Kent Welter. These acknowledgments would be remiss if they did not mention the financial support provided by Qiao Wu & José Reyes that allowed this dissertation to ever even exist. It has also been my pleasure to have had many enjoyable conversations, which have stimulated and encouraged a large part of this research, with both the major professors of this dissertation. Finally I would like to thank Scott Franz for providing the guidance and support required for completion of this work.

TABLE OF CONTENTS

TABLE OF CONTENTS (Continued)

TABLE OF CONTENTS (Continued)

LIST OF FIGURES

LIST OF FIGURES (Continued)

LIST OF TABLES

ON THE EFFECTS OF CENTRIFUGAL FORCES IN AIR-WATER TWO-PHASE FLOW REGIME TRANSITIONS OF AN ADIABATIC HELICAL GEOMETRY

1 INTRODUCTION

Two-phase flow in helical conduits is important in many industries where reaction between components, heat transfer, and mass transport are utilized as processes. The helical design is chosen for the effects of secondary flow patterns that are induced by curvature and their resulting compact design. Secondary flow has the benefit of continually transporting fluid from the near wall region to the bulk of the flow. In single-phase chemical reactor design this secondary flow increases radial mixing and reduces axial dispersion. In heat exchanger design the secondary flow increases laminar heat transfer, while the centrifugal force broadens the Reynolds number range of laminar flow (to the advantage of the increased laminar heat transfer). As a result of these characteristics, helical pipe flow has been studied since the later part of the 19th century. The earliest found published mention of secondary flow effects of curvature on open water flows of rivers was that of Thomson in 1876, and for closed pipes by Grindley & Gibson in 1908. These preliminary investigations were followed by Eustice's investigation in 1911, who made some amazing insights about the flow in curved pipes of varying curvatures. However, analytic study of this flow did not occur until 1927 when Dean published his pioneering work. It wasnt until thirty-seven years after Dean (1927) that the first two-phase research started to enter the literature (Carter 1965, Morton et al. 1964, Gilli 1964, and Rippel et al. 1966). Given that the whole of research into helical flow has evolved in the last century alone, it is nice to see a single piece of work like Dean's endure. This is particularly true between 1927 and 1962, during which time researchers either made refinements to Deans analysis, or applied the boundary layer concept to the secondary flow, for finding flow solutions in this geometry. Around 1962 the first numerical solutions were applied as a method of extending the series analysis of Dean to greater flow rates and/or tighter bends (Barua 1963). Almost all these studies follow the basics of Dean's approach, by considering both the simplifying assumption of zero pitch and negligible curvature, i.e. they do not consider helicity. Hence, the vast majority of studies of helical flow are essentially large radius of curvature studies of a torus.

Given that significant differences in secondary flow structure are introduced with helicity (Wang 1981), it is unfortunate that torque effects of helicity were not considered fundamentally until 1981 (Murata et al. 1981, Wang 1981). Disconcerting is that the few studies considering finite pitch are not in agreement. The main discrepancy seems to stem from the choice of an appropriate coordinate system. Germano (1982) provides an analysis with an orthogonal coordinate system that shows that pitch effects on secondary flow are second order. In contrast, Wang (1981) provides an analysis with a non-orthogonal coordinate system and shows the effects are of first order. Germano (1988) later rectifies this difference by adjusting Wangs equations to match the equations in his work. The qualitative effect of torque in single-phase flow is, however, agreed upon and is described along with the effect of curvature in Figure 1.1. Regardless of whether helicity's influence on secondary flow is first or second order, its influence on multi-phase flow transition is not fully understood and needs to be investigated.

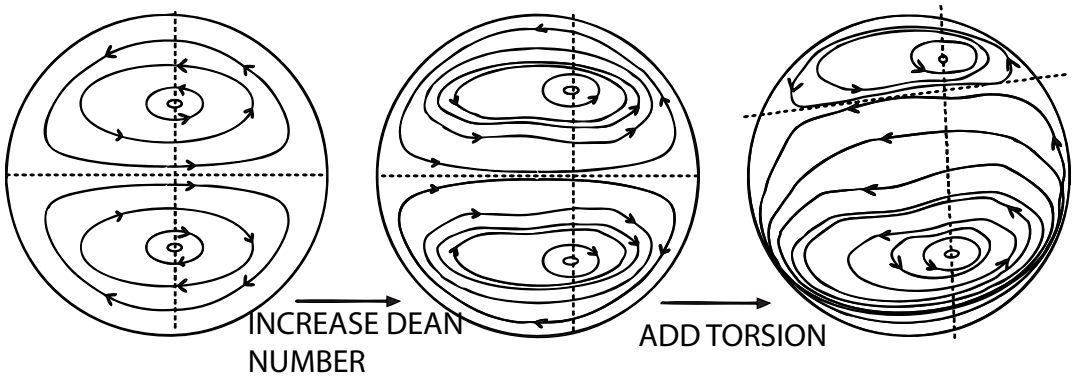

Figure 1.1: Torsion and curvature effects on single-phase helical flow.

The review of literature showed the vast majority of the work as being not only toroidal, but also for single-phase flow. The study of two-phase helical flow regimes has been undertaken in relatively few cases, and a fundamental formulation of the flow regimes for helical geometry is not found in the literature. This is not to say that two-phase flow regime studies are non-existent, only that they exclusively address the horizontal and vertical systems. Probably the most quoted horizontal flow studies were those of Baker (1954), Mandhane (1974), and Taitel & Dukler (1976).

Benefiting the two-phase analysis, the multitude of single-phase helical analyses make clear the effects of centrifugal and torsion forces on the fluid domain. This

provides that these forces indeed do have a non-negligible effect on the flow structure; and with proper consideration, the mechanisms of transitions found accurate for the two-phase flow regime prediction in the linear inclined geometry can be applied to a helical flow. The published results show agreement on the effects of torsion and centrifugal forces on a flowing fluid domain, which can be surmised as follows:

- Curvature increases resistance
- Pitch decreases resistance
- Secondary flow in the plane normal to the pipe axis is induced
- Laminar flow is present over an extended range of Reynolds numbers
- Intermittent flow regimes are present over an extended range in two-phase flow

Even though the first four of the above observations are for single-phase helical flow, it is reasonable to assume a similar degree of secondary flow effects would manifest within the mixture and/or individual phases. Spedding et al. (1981) showed that this is at least found to be true in the slug flow regime of linear horizontal two-phase flows. This implies that the resolution of the secondary flow patterns in each phase for a given regime may eventually be required for an absolute helical flow map. However, this dissertation will make simplifying assumptions to reasonably allow the systems treatment.

With the system defined and the history chosen, one must choose a method of analysis. There are three different one-dimensional approaches in resolving two-phase flow in pipes: the Homogeneous Equilibrium Model (HEM), the Drift Flux Model, and the Two-Fluid Model. Each of the methods are described in more detail later. It is understood that the easiest and least accurate of these is the HEM, because of the simplified manner in which it treats the system as an approximate single-phase flow. The most fundamental is the Two Fluid Model, as it retains the conservation equations for each phase individually. However, the Two-Fluid Model requires that the equations for the individual phases be related in a manner depicting their interaction and influence of each other. These closure relations are directly dependent on the two-phase flow structure (regime) due to the influence of the mechanics of the flow, requiring a starting regime to be chosen. This work will formulate the system using the two-fluid model approach.

This work will follow the analysis of Taitel & Dukler (1976) by assuming a stratified regime as a starting point for the formulation. This is based on the viewpoint that the development of a given regime is not path dependent, and any regime can be considered to have developed from a stratified regime.

The choice of an appropriate coordinate system for the formulation will determine what effects of the flow structure are considered. As was pointed out, the vast majority of researchers choose to operate in the orthogonal toroidal system. This is in spite of the fact that the natural coordinate system for a helix is non-orthogonal. This issue is disused in the literature review, and justification for use of the toroidal coordinate system is provided.

1.1 Dissertation Outline

> *"Things should be made as simple as possible, but not any simpler."* – Albert Einstein

The current study follows an intuitive evolution of the ideas, tools, previous work, and novel calculations applied to the resolution of the helical geometry two-phase flow problem. First, the helical system and two-phase flow regimes are described, along with the currently accepted methodology for rendering calculable two-phase fluid systems. This provides a sufficient foundation to assemble all the previous works on the subject, such that it is followed by a thorough review of the literature to identify all the methods applied in the study of helical fluid flow (single and two-phase systems). The literature review is concluded by a description of effective two-phase flow regime prediction methods used in linear geometries. The lack of an analytical two-phase flow regime map for the helical system is identified, and resolved by the novel use of the successful methods found in the study of the linear system with the inclusion of the centrifugal forces. The outline of the dissertation is summarized in Figure 1.2.

1.2 Description of Helical Geometry and Flow Regimes

The helical geometry flow problem has its history in the investigations of Sir William Thomson (1876) on the cause of windings of rivers of alluvial planes. Thom-

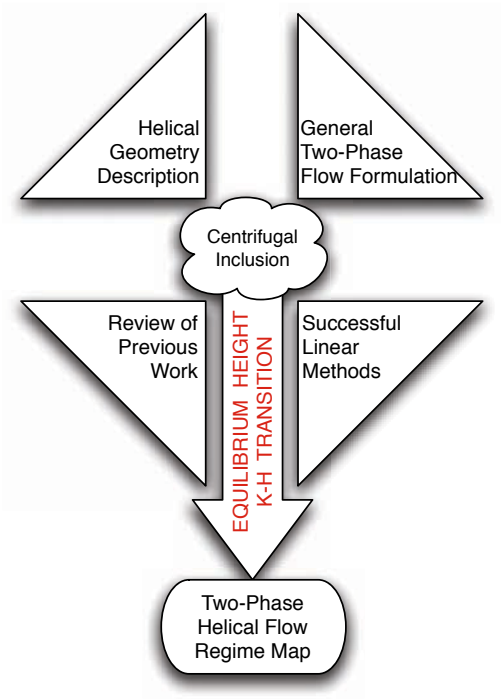

Figure 1.2: Schematic of the dissertation

son correctly determined that the wearing down of the outside edge of curves, and build up along the inside of the curve, was an effect of a secondary cross-stream flow. He used a description similar to Figure 1.3 to describe the river flow. As the flow enters a curve in the direction of s, the centrifugal force on the surface is greater than on the river bed due to the fluid near the bottom, since the flow along the bottom is being retarded from viscous forces. This sets up a circulation outwards on the surface (from A to B) and inwards along the bottom (from B to A), which removes material from the outer edge and deposits it on the inner edge of the river bank. This is the same mechanism that must be considered in the current study, and this study will use the same approach of a stream wise direction, denoted as s.

However, unlike the river, the helical geometry is enclosed by a solid interface on all sides and has an inclination that introduces a second consideration, that of torsion. The geometry description of a helix includes a measurement of the inclination: the of pitch, p. Along with the pitch and the stream wise direction coordinate, measurements are also needed to describe the radius of curvature a, and the radius of the conduit r_0. These parameters are depicted in Figure 1.4.

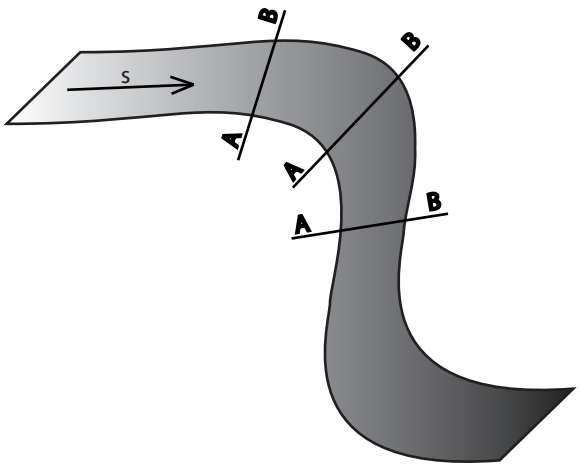

Figure 1.3: A reproduction of Thomson's original work that identified secondary flow effects in curved geometries.

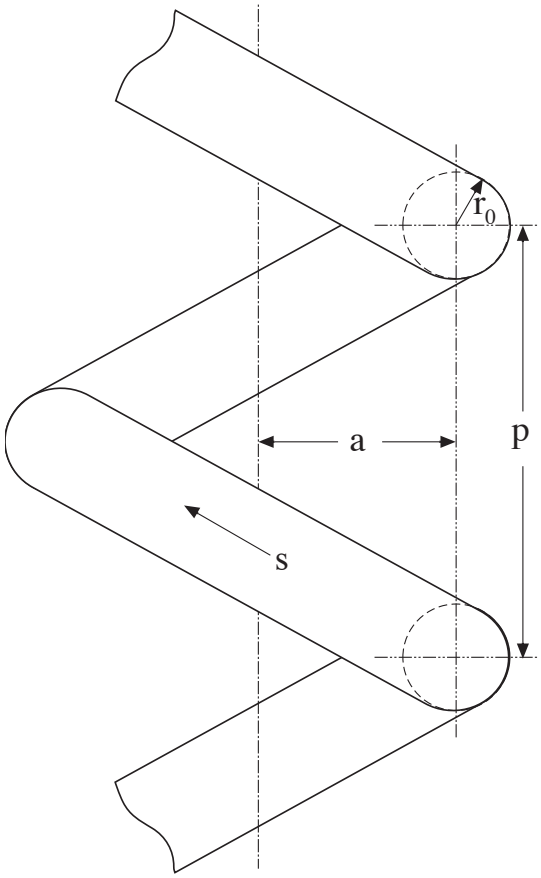

Figure 1.4: Dimensions of helical coil used in analysis.

In addition to the geometric influence, the concurrently flowing phases in a conduit must align themselves relative to one another, given that they do not occupy the same space during the same time. This relative positioning is naturally due to the relative forces felt by the phases, and is described macroscopically as morphologic arrangements. These patterns have been extensively studied in linear inclined and linear horizontal geometries. In the linear inclined geometry there are six basic patterns, shown in Figure 1.5. A vertical arrangement is similar, with the exclusion of the stratified and wavy regimes, and is shown in Figure 1.6. The patterns for the inclined geometry are the same as those for helical flow, and the designations of Figure 1.5 will be used in this study.

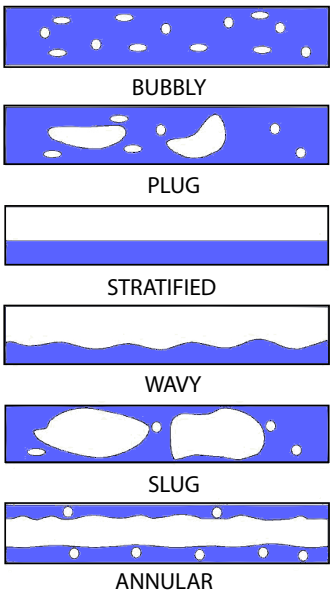

Figure 1.5: Two-phase flow regimes found in horizontal and inclined linear flows.

The relative forces between the phases influence the pattern development. These consist of momentum, turbulence, dynamic pressure, body force, surface tension, and interfacial drag. Examining the above list exposes the importance of the fluid flow rates, and as a result, the methods used to identify the particular flow regime are based on mapping the mass flow rates or velocities of the phases against each other. Example representations are the superficial velocity mapping of Taitel & Dukler (1976), and the mass flux mapping of Baker (1954). These are shown in Figure 1.7 and Figure 1.8 respectively. As discussed in the literature review, mapping with these types of coordinates produces maps that are accurate only for a single inclination angle,

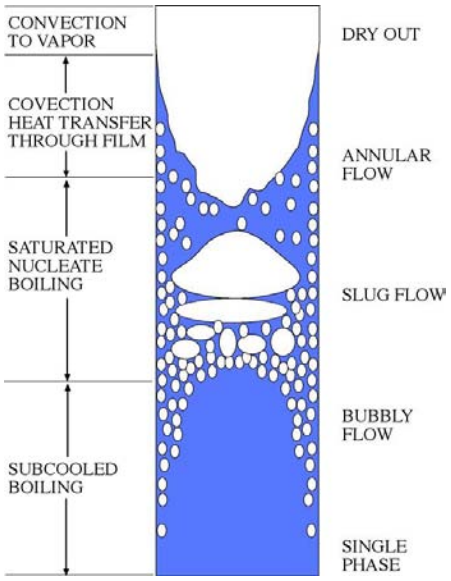

Figure 1.6: The flow regimes of the linear vertical geometry. The case shown is a vertical heated channel with upward flow.

which implies dependence on gravity. This is noted at this point to bring attention to the similarities of gravity and centrifugal forces, and their importance. More importantly, the Taitel & Dukler map of Figure 1.7 is an example of the goal of this thesis; an analytical flow regime map. This topic is described in the linear two-phase flow section of the literature review.

1.3 Two-Phase Flow Modeling Methodologies

Multi-phase fluid flows are some of the most common phenomena in our world. This is apparent when one considers that any continuum material movement which is not in rigid translation is a fluid movement, and when more than one of these materials is present, the system is a multi-phase flow. This describes actions such as blood flow, combustion, rain, boiling eggs, dust storms, and drinking soda. In the way of understanding and control of these systems, the dynamicist provides predictive capabilities for such systems through the formulation of the fundamental concept of conservation. The resulting field equations require additional information describing the interaction of components at the interface of the continua, being that they are only valid within each continuum. The two-phase methodologies that have developed are attempts to solve this issue. The major one-dimensional methodologies are the Two-

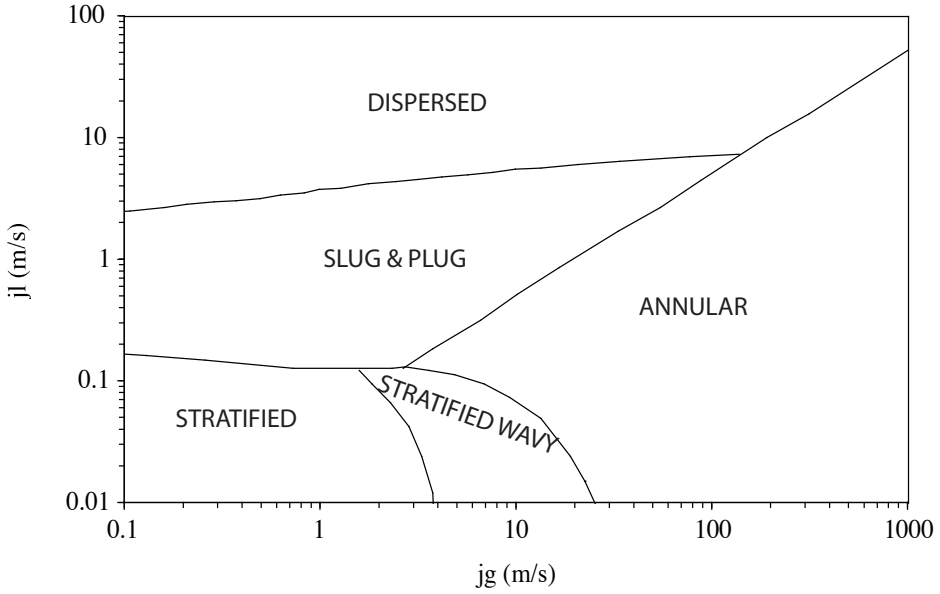

Figure 1.7: Flow regime map of Taitel & Dukler (1976), for air/water horizontal cocurrent flow.

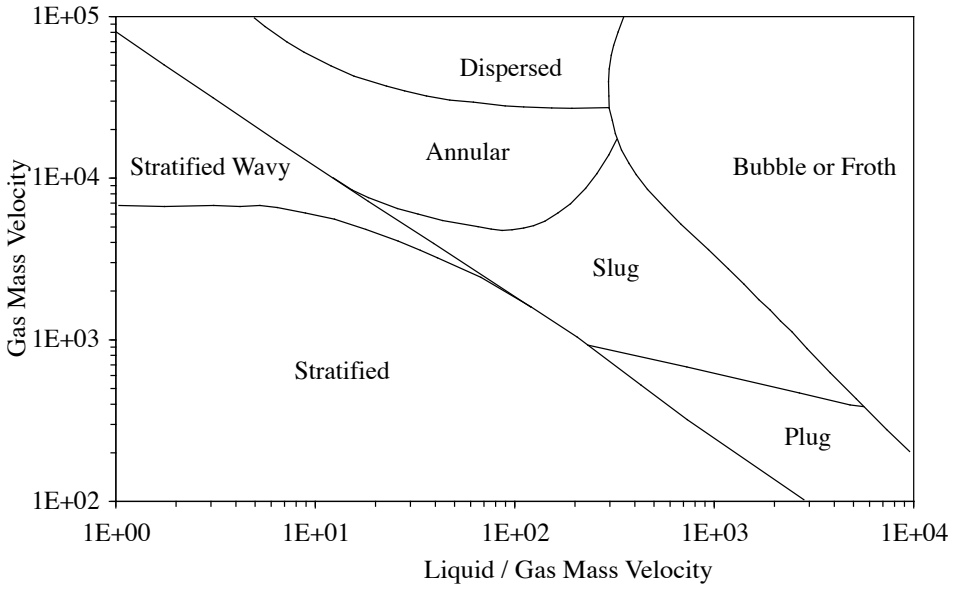

Figure 1.8: Flow regime map of Baker (1954), for oil/water horizontal concurrent flow.

Fluid model, Homogeneous Equilibrium Model (HEM), and the Drift Flux model.

1.3.1 Homogeneous Equilibrium Model

The simplest of the modeled strategies is the Homogeneous Equilibrium Model, which considers the phases as a mixture in thermal equilibrium and without relative motion between phases. This model requires that the properties of the mixture be appropriately defined such that the combination of the components are accurately described as an artificial fluid. Additionally, the flow components of the artificial fluid should be near to thermodynamic and mechanical equilibrium, in order to minimize the transfer of energy between components. This is not the case when the velocity and temperature are different, i.e. separated flows and/or during pressure dynamics sufficient to flash one of the components, and must be understood as a limitation. However, if these conditions are sufficiently met, the artificial fluid can be easily modeled as a single phase flow with standard methods. As a result, examples of the use of HEM in flow analysis are abundant and found in all two-phase flow textbooks. The field equations for the one-dimensional case of HEM flow are given by Wallis (1969):

$$\frac{\partial \rho_m}{\partial t} + \frac{\partial}{\partial z}\left(\rho_m v\right) = 0 \tag{1.1}$$

$$\rho_m \left(\frac{\partial v}{\partial t} + v\frac{\partial v}{\partial z}\right) = -\frac{\partial P}{\partial z} + \rho_m g\cos\theta - \frac{P}{A}\tau_w \tag{1.2}$$

$$\frac{\partial}{\partial t}\left[\rho_m\left(e + \frac{v^2}{2}\right)\right] + \frac{\partial}{\partial z}\left[\rho_m v\left(h + \frac{v^2}{2}\right)\right] = \frac{1}{A}\left(\frac{\partial q_e}{\partial z} - \frac{\partial v}{\partial z}\right) + \rho_m v g\cos\theta \tag{1.3}$$

where the mixture density, void fraction, and quality are defined as:

$$\rho_m = \alpha\rho_g + (1-\alpha)\,\rho_l \tag{1.4}$$

$$\frac{1}{\rho_m} = \frac{x}{\rho_g} + \frac{1-x}{\rho_l} \tag{1.5}$$

$$\alpha = \frac{\dot{V}_g}{\dot{V}_g + \dot{V}_l} = \frac{j_g}{j} \tag{1.6}$$

$$x = \frac{\dot{m}_g}{\dot{m}_g + \dot{m}_l} = \frac{m''_g}{m''} \tag{1.7}$$

1.3.2 Drift Flux Model

The Drift Flux Model is a mixture flow model that considers the relative velocity of the gas to the mixture rather than the individual phase velocities as in the Two-Fluid Model, or the equilibrium velocity of HEM. The model has a wide range of applicability and is considerably less complicated than the Two-Fluid Model. Its simplification is accomplished by eliminating one of the momentum equations and one energy equation, and making up for the insufficient number of equations by including constitutive relationships that describe the relative motion and energy exchange. The set of Drift Flux Model equations are given by Ishii (1976).

Mixture Continuity Equation

$$\frac{\partial < \rho_m >}{\partial t} + \frac{\partial}{\partial z} < \rho_m > \bar{v}_m = 0 \tag{1.8}$$

Dispersed Phase Continuity Equation

$$\frac{\partial < \alpha_d > \rho_d}{\partial t} + \frac{\partial}{\partial z} \left(< \alpha_d > \rho_d \bar{v}_m \right) =< \Gamma_d > - \frac{\partial}{\partial z} \left(\frac{< \alpha_d > \rho_d \rho_c}{< \rho_m >} \bar{V}_d j \right) \tag{1.9}$$

Mixture Momentum Equation

$$\begin{aligned} &\frac{\partial < \rho_m > \bar{v}_m}{\partial t} + \frac{\partial}{\partial z} \left(< \rho_m > \bar{v}_m^2 \right) = - \frac{\partial}{\partial z} < \rho_m > + \\ &\frac{\partial}{\partial z} < \tau_{zz} + \tau_{zz}^T > - < \rho_m > g_z - \frac{f_m}{2D} < \rho_m > \bar{v}_m |\bar{v}_m| - \\ &\frac{\partial}{\partial z} \left(\frac{< \alpha_d > \rho_d \rho_c}{(1 - < \alpha_d >) < \rho_m >} \bar{V}_{dj}^2 \right) - \frac{\partial}{\partial z} \sum_k COV \left(\alpha_k \rho_k v_k v_k \right) \end{aligned} \tag{1.10}$$

Mixture Energy Equation

$$\begin{aligned} &\frac{\partial < \rho_m > \bar{h}_m}{\partial t} + \frac{\partial}{\partial z} \left(< \rho_m > \bar{h}_m \bar{v}_m \right) = - \frac{\partial}{\partial z} < q + q^T > + \frac{q_w'' \xi_h}{A} \\ &- \frac{\partial}{\partial z} \left(\frac{< \alpha_d > \rho_d \rho_c}{< \rho_m >} \Delta h_{dc} \bar{V}_d j \right) - \frac{\partial}{\partial z} \sum_k COV \left(\alpha_k \rho_k \bar{h}_k v_k \right) \\ &+ \frac{\partial < \rho_m >}{\partial t} + \left(\bar{v}_m + \frac{< \alpha_d > (\rho_c - \rho_d)}{< \rho_m >} \bar{V}_{dj} \right) \frac{\partial < \rho_m >}{\partial z} + < \Phi_m^\mu > \end{aligned} \tag{1.11}$$

Drift Velocity Constitutive Equation

$$\alpha_k \rho_k \left(\frac{\partial v_k}{\partial t} + v_k \frac{\partial v_k}{\partial z} \right) = -\alpha_k \nabla p_k + \nabla \circ \left(\alpha_k \left(\overline{\overline{\tau}}_k + \overline{\overline{\tau}}_k^T \right) \right) + \alpha_k \rho_k g_z +$$

$$(p_{ki} - p_k) \frac{\partial \alpha_k}{\partial z} + (v_{ki} - v_k) \Gamma_k + M_{ki} \tag{1.12}$$

Where $< \phi >$, $<< \phi >>$, and $COV\,(\phi)$ are defined in Eq. 3.15, Eq. 3.16, and Eq. 3.26 respectively.

1.3.3 Two Fluid Model

Of the three models considered here, the Two Fluid Model is the most general, and is the basis for the analysis presented in this dissertation. The model is constructed using a set of field equations written for each phase and closed with interfacial terms that account for the interaction of phases. The development of the equations is accomplished by application of the concept of conservation. This axiom provides that all quantities are conserved, and must be accounted for in the mathamatics by use of a general balance equation. A novel production of this equation would be unnecessary given that its derivation is quite mature. Instead the development of the general balance equation given by Ishii (1975), Delhaye (1969), or Hsu (1986) is presented.

Figure 1.9 depicts the application of the the mathematical theorem of Green (also known as Gauss, Lagrange, or the divergence theorem) and Leibnitz (also known as Reynold's transport theorem) to the concept of a general integral balance to produce the general balance equation. This process is formalized in Eq. 1.13 to Eq. 1.16. The description of Leibnitz is constructed from information found in the text by Aris (1962). First the axiom of conservation is put in mathematical form, i.e.: the time rate of change of the integral of any specific quantity per unit mass (ψ) being equal to the flux ($\mathbf{J}$) into the region of interest, and any source (ϕ) of the quantity.

$$\frac{d}{dt} \int_V \rho_k \psi_k dV = - \int_S \mathbf{n}_k \cdot \mathbf{J}_k dS + \int_V \rho_k \phi_k dV \tag{1.13}$$

Green's theorem,

$$\int_V \nabla \cdot \mathbf{F} dV = \int_S \mathbf{n} \cdot \mathbf{F} dS,$$

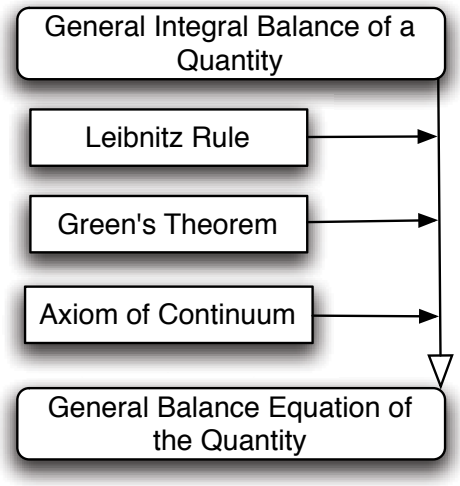

Figure 1.9: Diagram of concepts included in the general balance equation (Ishii 1975).

is applied to the second term of Eq. 1.13, transforming the surface integral to a volume integral, i.e.:

$$\frac{d}{dt}\int_V \rho_k \psi_k dV = -\int_V \nabla \circ \mathbf{J}_k dV + \int_V \rho_k \phi_k dV \tag{1.14}$$

Parallel to the formulation of the conservation axiom, the theorem of Leibnitz is written. This theorem considers the contribution to an integral quantity, by distinguishing between the effects within the control volume occupied by the material region to those at the surface of the control volume (i.e. surface flux). Its derivation is informative, an important tool of the averaging used in two-phase flow, short, and

interesting, so it is quickly covered here.

$$\frac{d}{dt}\int_V F dV = \frac{d}{dt}\int_V F dV \tag{1.15a}$$

$$= \int_{V_0}\left(\frac{dF}{dt}\mathsf{J} + F\frac{d\mathsf{J}}{dt}\right)dV_0 \tag{1.15b}$$

$$= \int_{V_0}\left(\frac{dF}{dt} + F\left(\nabla\circ\mathbf{v}_k\right)\right)\mathsf{J}dV_0 \tag{1.15c}$$

$$= \int_{V}\left(\frac{\partial F}{\partial t} + F\nabla\circ\mathbf{v}_k\right)dV \tag{1.15d}$$

$$= \int_V \frac{\partial F}{\partial t}dV + \int_S F\mathbf{v}_k\circ\mathbf{n}dS \tag{1.15e}$$

Where F is any function and J is the Jacobian of the transformation between the material and spatial coordinates. The step between Eq 1.15a and Eq. 1.15b is simply the change of spatial volume integral to a material volume, the step between Eq 1.15b and Eq. 1.15c is the application of the relationship between the Jacobian and the divergence, the step between Eq. 1.15c and Eq. 1.15d is the application of the definition of the material derivative, and the step between Eq 1.15d and Eq. 1.15e comes from applying Green's theorem. Equation 1.15e is the Leibnitz rule that is referenced in all the fluid texts. Specifics about the steps, and the definition of the Jacobian, can be found in Chapter 4 of Aris (1962).

The next step is accomplished by letting $F = \rho_k\psi_k$, setting Eq. 1.15d equal to Eq. 1.14, and requiring the integrand vanish everywhere. The result is the differential form of the balance equation that is valid instantaneously for a differential volume of a single continuum, Eq. 1.16. For comparison to the HEM and Drift-Flux models, Eq. 1.16 is written in its one-dimensional form. Noting that the divergence of a vector quantity is the trace of the vector ($\nabla\cdot\mathbf{\Phi} = \delta_{ij}\partial_i\Phi_j = \partial_x\Phi_x + \partial_y\Phi_y + \partial_z\Phi_z$) and that the functional dependence is only on the one-dimension ($\mathbf{\Phi} = \mathbf{\Phi}(z)$), the divergence is simply the gradient in the one dimension ($\nabla\cdot\mathbf{\Phi} = \partial_z\Phi_z$). Thus, Eq. 1.16 becomes Eq. 1.17.

$$\frac{\partial\rho_k\psi_k}{\partial t} + \rho_k\psi_k\nabla\circ\mathbf{v}_k = -\nabla\circ\mathbf{J}_k + \rho_k\phi_k \tag{1.16}$$

$$\frac{\partial \rho_k \psi_k}{\partial t} + \rho_k \psi_k \frac{\partial v_k}{\partial z} = -\frac{\partial J_k}{\partial z} + \rho_k \phi_k \tag{1.17}$$

Note: J is a surface flux, and $\mathbf{J}$ is the Jacobian of the material & spatial coordinates.

It is the identity of the quantities ψ, J, and ϕ that distinguishes between different equations for fluid kinematics, or for the equations governing neutronics, electricity and magnetism, etc.. The set of field equations for fluid dynamics are given by substitution of the values given in Table 1.1.

Table 1.1: Values used to produce the fluid kinematic field equation (Ishii 1975).

Eq.	Equation Type	ψ	ϕ	J
i.	Continuity	1	0	0
ii.	Momentum	$\mathbf{v}_k$	$\mathbf{g}$	$\mathbf{P}_k - \tau_k$
iii.	Energy	$e_k + \frac{{\mathbf{v}_k}^2}{2}$	$\mathbf{g} \circ \mathbf{v}_k + \frac{{q_k}'''}{\rho_k}$	$\mathbf{q}_k - (\mathbf{P}_k - \tau_k) \circ \mathbf{v}_k$

2 LITERATURE REVIEW

The literature review completed for this dissertation considers both analytical and experimental studies of helical and linear flows. The purpose of this dissertation is the formulation models of two-phase helical systems. However, single-phase helical and linear two-phase flow literature are covered to provide insight into successful modeling techniques of simplified systems, and to provide guidance on model development. The literature review is broken into individual sections for analytical and experimental studies, where similar works are grouped accordingly. The first author of the works covered in this literature review, are listed in the appropriate section of Table 2.1. It should be noted that the works of these authors are not necessarily restricted to their location in the table, e.g. analytical works often include experimental contributions. Also, many more studies than those listed in Table 2.1 were reviewed, though the table and literature review only cover the most applicable. A complete listing of the work reviewed by the author, to determine the novelty of this research, is found in the Bibliography.

Table 2.1 implies, that for the existing techniques, there is an analytical helical two-phase flow regime model shortage. Of the two lone works in this category, the first is a flow map created by data correlation, and the second, an ad hoc modification to the linear theory of Taitel & Dukler (1976), that provides no additional framework. No first basis mechanistic formulation of the helical two-phase flow regimes was found to exist in the literature. It was also found that the majority of studies are within the realm of single-phase analytical work, whose methods can be broken up into four groups:

- The original work of Dean (1927), and similar series analyses.
- Boundary layer analyses.
- Numerical solutions of the field equations.
- Helical coordinate system formulation (for torsion inclusion).

The model of this dissertation relies on the natural coordinates for a helix. Hence the coordinate system formulation is provided last, and in its own subsection. The development of this literature review follows the classification of the layout in Table 2.1.

Table 2.1: First author listing of the major work covered in the literature review.

Section	**Authors**	—	—
1Φ Helical *Experimental*	Eustice 1911 Koutsky 1964	Taylor 1929 Webster 1997	Ito 1959
1Φ Helical *Analytical*	Dean 1927 McConalogue 1968 Joseph 1975 Nandakumar 1982	Barua 1963 Ito 1969 Van Dyke 1978 Goering 1989	Mori 1965 Truesdell 1970 Dennis 1982
2Φ Helical *Experimental*	Rippel 1966 Akagawa 1971 Boyce 1969 Hart 1987 Ishikawa 2003	Banerjee 1967 Kasturi 1972 Mujawar 1981 Saxena 1990	Banerjee 1969 Whalley 1980 Rangacharyulu 1984 Yan 1993
2Φ Helical *Analytical*	Uddin 1988	Keshock 1998	
2Φ Linear Flow Regime Transitions *Exp. & Ana.*	Mandhane 1974 Petalas 2000	Taitel 1976	Barnea 1987
1Φ Helical *Coordinate Formulation*	Wang 1981 Germano 1988	Germano 1982 Tuttle 1990	Kao 1987 Zabielski 1998

2.1 Experimental Studies of Helical One-Phase Flow

As with other fluid system studies, the one-phase helical studies focused on determining pressure drop, friction coefficient, and the critical parameter values for transition to turbulent flow. The secondary flow structure analysis found its impetus in offering explanation to the difference between pressure loss of a straight pipe and a curved one. The early work of Eustice (1911), was a classical experiment of our field, and is summed up in his own words:

> ... even a small curvature in the length of a cylindrical pipe affected the quantity of flow ... the experiments showed that in coiled pipes there was apparently no critical velocity region... (*then in response to these earlier findings)*
>
> In an attempt to discover the cause of this departure from the law of flow in straight pipe, the author had tried Osborne Reynolds' colour-band test in a coiled glass tube, but the arrangements were of a primitive character

> and the results obtained were not decisive. At the suggestion of Sir Joseph Larmor the colour tests have been repeated with specially made glass tubes, in which the stream motion could be traced by the introduction of coloured water through capillary nozzles.

In his experiment, Eustice studied the streamline motion of fluid flowing in 90°, 180°, and 360° bends of 1 and 1.7 [cm] diameter glass tubing. His simulation of Reynolds' setup for curved ducts showed that the $< 360°$ bends produced movement in the plane normal to the pipe axis that was restricted to either side of the bend plane. These movements, when viewed normal to the pipe axis, would complete a single revolution back to the origin of injection. When the bend was extended to $> 180°$, the movements would begin another rotation, implying a repeating cycle. Eustice's study also shows the relationship between the flow rate and the secondary velocity as being proportional for a similar geometry, i.e. the secondary velocity increased proportionally to axial velocity increases. The color injections would consistently flow from the internal region of the pipe to the outer wall. Once the injection reached the outer wall, it would spread into a flattened band that would flow along the wall back to the inner wall then partially re-combine into a single strand. An interesting result was the backward (upstream) velocity for outer bend dye streams, found in sharp right angle bends. The outer dye would actually flow back upstream along the wall until it reached the inside bend, then reverse direction and exit the bend. The most interesting result of Eustice's study is that the secondary flow effects are present in turbulent flow. Eustice makes the point that the curvature effects are present at the wall streamlines first, and if a sufficiently long curve is present, then all parts of the flow are affected. This is to say that a given length of curved pipe must be provided for the complete secondary effects to manifest. He noted that when dye was smeared on the surface of the pipe, it was most quickly removed from the outside of the bend and relatively slower from the inside of the bend. This is in direct agreement with the heat transfer and friction loss observations of authors to follow. All of Eustice's qualitative observations were repeatedly verified by all subsequent studies.

Taylor (1929) verified the findings of White (1929) and the statement by Eustice (1911), that the critical Reynolds number for transition between laminar and turbulent flow is larger for a helical pipe than a straight one. In his experiment he injected a dye into a stream of water in a glass helix with a ratio of coil to tube diameter of 18. Taylor found that the critical Reynolds number is indeed increased, and in this

case, by a factor of 2.8 ($Re = 5830$). An interesting part of his study is that the fluid flow was definitely turbulent at the entrance of the helix. So the flow had actually been laminarized by the presence of helicity and curvature.

Ito (1959) pressed this idea further, and also proposed empirical formulas for calculation of the turbulent pressure loss in curved pipes, and a formula to calculate the critical Reynolds number. These are empirical formulas based on his data for 5 different radii of curvature flows. The setup had only a single loop (360° bend), so it is not rigorously applicable to a helical geometry with non-zero helicity. However, his formula for the laminar/turbulent transition Reynolds number, see Eq. 2.1, compared well to his data and the data from previous work (including White (1929), and Taylor (1929)). None of Ito's undisturbed data showed a Reynolds number less than 5000. This is an important point of the study: that unless the flow is intentionally disturbed by an orifice plate upstream of the curved section, the critical Reynolds number is underestimated by his formula. The use of the orifice plate was included to model the upstream turbulence, and laminarization mentioned in previous work.

$$Re_{crit} = 2\left(\frac{r_0}{a}\right)^{0.32} \times 10^4 \quad for \quad 15 < a/r_0 < 860 \tag{2.1}$$

Koutsky (1964) experimentally studied the mechanisms affecting axial dispersion that are important to continuous chemical reactor design. This is the phenomena characterizing the dispersing of product along the axis of flow. He states the three main mechanisms effecting dispersion are a non-uniform velocity profile (laminar), turbulent mixing (eddies), and secondary flow. Secondary flow and turbulent mixing are both beneficial if the goal is to minimize the axial dispersion, and a non-uniform velocity is detrimental. Secondary flow is more efficient at the reduction due to it being an ordered flow, which does not dissipate large amounts of energy (i.e. pressure losses) and is not isotropic (i.e. acts only in the plane perpendicular to the helix axis). The isotropic nature of turbulent flow means that both radial and axial mixing are increased, and it is desirable in chemical reactors to only increase the radial mixing. Koutsky found that the reduction in axial dispersion is proportional to the Reynolds number, and has a minimum at a Reynolds number of approximately 3000. Koutsky also compares the pressure loss as a function of Reynolds number, for helical tubes, straight tubes, and packed beds, and finds that for similar axial dispersion, a minimum in pressure loss is achieved by the helical flow case. This finding is the design basis for helical chemical reactors, and might be applicable to home biodiesel design in the near

future (due to the reduced size and increased efficiency). His experimental pressure drops correlated well with the equation of Ito (1959), with an added observation that the transition to turbulence is sufficiently smooth in helical flow to allow a continuous function to represent the friction losses.

Webster and Humphrey (1997) completed an experimental and numerical study, similar to Taylor (1929) and Ito (1959), to determine the transition Reynolds number in helical flow, based on the idea that traveling wave instabilities are present during the "transition" to turbulence. Here, the transition is not as is observed in the traditional linear flows, where the linear regime feels the onset of small turbulent fluctuations that eventually increase to fully developed turbulent flow, as the flow rate is increased. Instead, the helical system, and the linear portion of piping preceding the helical region, is characterized by three distinct conditions:

1. Laminar upstream linear section; Laminar helical section. ($Re < 2300$)
2. Turbulent upstream linear section; Laminar helical section. ($2300 < Re < 8000$)
3. Turbulent upstream linear section; Turbulent helical section. ($8000 < Re$)

This mismatch with the linear section is from the additional forces of helical flow stabilizing the turbulent structure of the upstream flow through damping of the turbulent fluctuations. The transition region of $2300 < Re < 8000$ shows a stable (i.e. laminar) fluctuation that is characterized as a traveling wave instability, and explains the observations of previous authors (Taylor 1929). Notice that Webster & Humphrey list the transition to turbulence for a helical flow as occurring at a Reynolds number of 8000, instead of 5830 as found by Taylor (1929) (both are for coil to tube diameter ratios of $\sim$18). This is from differences in the definition of laminar flow, where Taylor's finding of $Re = 5830$ is related to "steady" laminar flow, and Webster & Humphrey's findings are related to actual turbulent mixing. The "unsteady" flows of Taylor (1929) are observed as fluctuations in the streams of dye, without dissipation of the dye streams, as would be seen in a turbulent flow. These are the in situ traveling wave referred to by Webster & Humphrey (1997), and actually shows agreement between the two studies.

2.2 Analytical Studies of Helical One-Phase Flow

2.2.1 Dean Style Series Analysis

Dean (1927) is attributed with first developing the analytical treatment of the helical one-phase system. In his paper presented to the Royal Society of London in 1927, Dean twice refered to Eustice's work of 1911, implying the origin of the motivation for his own work. In the first reference, Dean takes note of the stream line nature of the flow, and uses a stream line description that leads to a sketch of a symmetric secondary flow pattern that is now known as "Dean Flow". In the next reference, Dean points out that the influence of curvature is present at even minute values, and the dependence of flow rate on curvature should be of first order (Dean is commenting on the same text as quoted in section 2.1 of this dissertation), which in turn leads to his second seminal work in 1928. Dean's approach was to work with a simplified system that allowed an analytical solution. His assumptions were:

- Steady flow (fully developed)
- Incompressible single-phase flow
- Toroidal coordinate system (negligible torsion)
- Small curvature (loosely coiled pipe)

Considering the above assumptions, Dean formulated equations for a first order curvature. This set of equations is then solved in his 1927 work by separation of variables, and in his 1928 work by a series expansion in powers of the Dean number. The Dean number being a similarity parameter for curved flows that includes the Reynolds number and the curvature (De). Though unlike Reynolds' number, the Dean number does not enjoy a consistent definition, and shows up in the literature in at least 4 different forms (Van Dyke 1968). Because of the variation in definitions, direct comparison between authors is confusing, and someone studying the flow in helices should be aware of the forms being used. The original form is given in Eq. 2.2, and the form used by Barua (1963), Mori & Nakayama (1965), Ito (1969), is given in Eq. 2.3. The latter is applicable to both developing and fully developed flows, where the former is strictly applicable only to fully developed cases (Berger et. al. 1983). As such, Berger et. al. (1983) recommended that the form of Eq. 2.3 be used. The

present work heeds this recommendation.

$$De = 2\left(\frac{r_0}{a}\right)\left(\frac{r_0 C}{\nu}\right)^2 \tag{2.2}$$

$$k = \left(\frac{r_0}{a}\right)^{1/2}\left(\frac{2r_0 < w >}{\nu}\right) = R_0^{1/2} Re \tag{2.3}$$

Where C is a constant representing the flow that has the dimensions of velocity, and $< w >$ is the average axial velocity.

The solutions found by Dean (1927/1928) exhibit the secondary flow observed in Eustice's (1911) work, but not the expected pressure gradient dependence on first order terms of the radius of curvature. Because of this disagreement with Eustice's (1911) experimental results, Dean completed another analysis up to the fourth order terms (Dean 1928). His extended work concluded that curvature has a "slightly reduce(ing)" effect on the flow, and identified its dependence on the second order and higher terms. A schematic of the system and coordinates used by Dean (1927/1928) are given in Figure 2.1, the conservation equations solved are given in Eqs. 2.4, and the series expansion used by Dean (1928) is given in Eqs. 2.5.

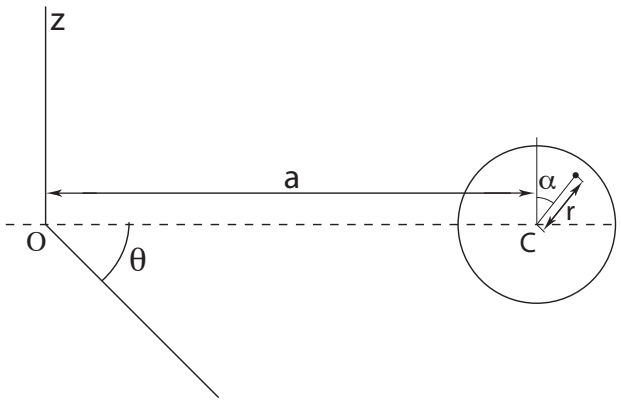

Figure 2.1: Toroidal coordinates used by Dean (1927/1928).

$$\frac{\partial u}{\partial r} + \frac{u}{r} + \frac{1}{r}\frac{\partial v}{\partial \alpha} = 0 \tag{2.4a}$$

$$u\frac{\partial u}{\partial r} + \frac{v}{r}\frac{\partial u}{\partial \alpha} - \frac{v^2}{r} - \frac{w^2 \sin\alpha}{a} = -\frac{\partial}{\partial r}\left(\frac{P}{\rho}\right) - \frac{\nu}{r}\frac{\partial}{\partial \alpha}\left(\frac{\partial v}{\partial r} + \frac{v}{r} - \frac{1}{r}\frac{\partial u}{\partial \alpha}\right) \tag{2.4b}$$

$$u\frac{\partial v}{\partial r} + \frac{v}{r}\frac{\partial v}{\partial \alpha} + \frac{uv}{r} - \frac{w^2 \cos\alpha}{a} = -\frac{1}{r}\frac{\partial}{\partial \alpha}\left(\frac{P}{\rho}\right) + \nu\frac{\partial}{\partial r}\left(\frac{\partial v}{\partial r} + \frac{v}{r} - \frac{1}{r}\frac{\partial u}{\partial \alpha}\right) \tag{2.4c}$$

$$u\frac{\partial w}{\partial r}+\frac{v}{r}\frac{\partial w}{\partial \alpha}=-\frac{1}{a}\frac{\partial}{\partial \theta}\left(\frac{P}{\rho}\right)+\nu\left(\frac{\partial^2 w}{\partial r^2}+\frac{1}{r}\frac{\partial w}{\partial r}+\frac{1}{r}\frac{\partial^2 w}{\partial \alpha^2}\right) \tag{2.4d}$$

$$w=\sum_{n=0}^{\infty}k^{2n}w_n \tag{2.5a}$$

$$\Psi=k\sum_{n=0}^{\infty}k^{2n}w_n\Psi_n \tag{2.5b}$$

McConalogue & Srivastava (1968) did a numerical extension of Dean's analysis of toroidal flow, using a Fourier series expansion. The importance of this extension was obvious even to Dean (1928), where he states that the helical flow should be considered for values of Dean number up 100,000, but only offers them up to 576. McConalogue & Srivastava take off from where Dean left off, and cover the range of Dean numbers between $576 \leq De \leq 22,931$. Their paper is a very nice presentation of the general formulation, variation of parameters, and numerical scheme required for the analysis.

McConalogue & Srivastava's numerical analysis was stable at low Dean numbers, but became unstable at higher Dean numbers. An actual critical Dean number is not defined, as the calculation diverged at different Dean numbers, depending on the initial approximations for the numerical scheme. They did note that the stability was dominated by the behavior of the axial velocity and detailed the modifications to the numerics to allow calculation up to $De = 22,931$. Some of the most interesting conclusions are for the higher Dean number flows. First the pressure gradient inferred from the streamlines shows that this is the force resisting the centrifugal force, and it induces a central region of uniform secondary flow velocities. Second, the effect of increasing Dean number on the maximum axial velocity and secondary flow, identifies this effect as the reason for the relative increase over straight pipes. Specifically, the increase of Dean number shifts the location of the maximum axial velocity towards the outside wall of the helix, which presents a stronger velocity gradient at the wall, and results in greater shear losses.

Van Dyke (1978) took a different approach to extending Dean's original analysis. His approach was to simply increase the number of calculated terms of the expansion, which was not possible by hand calculation at the time of Dean's work. Van Dyke pushed the original 4^{th} order series to 24 terms via computer calculations. Van Dyke

also mentions the diversity of Dean number definition, and concludes that the form introduced by White (1929) is the most appropriate (see Eq. 2.6). He also proposed that the laminar friction factor should vary as the White form of the Dean number to the 1/4 power for loosely coiled helices, and to the 1/2 power for tightly coiled helices. 5 previous accepted works with an exponent value of 1/2 are given as examples of correlations that agree well with available data sets. The exact forms of the friction ratios are given in Eq. 2.7.

$$k \equiv \frac{2r_0 < w >}{\nu} \left(\frac{r_0}{a}\right)^{1/2} \tag{2.6}$$

$$\frac{f_{helix}}{f_{straight}} \propto \begin{cases} 0.1064k^{1/2} & \text{Adler} \quad 1987 \\ 0.0919k^{1/2} & \text{Barua} \quad 1963 \\ 0.1080k^{1/2} & \text{Mori} \quad 1965 \\ 0.1033k^{1/2} & \text{Ito} \quad 1969 \\ 0.1028k^{1/2} & \text{Collins} \quad 1975 \end{cases} \tag{2.7}$$

Dennis & Ng (1982) numerically solve the series expansions of the conservation equations, in a circular cross-section toroidal coordinate frame. This is similar to McConalogue & Srivastava (1968), with the addition that they are the first to note a four-vortex solution in circular cross-sections (along with Nandakumar & Masliyah (1982), who did work in this same year). They are also the first to characterize the vortex type that develops in this flow as Taylor-Goertler vortices. This is an interesting step, as the Taylor-Goertler vortices are formed on stream-wise surfaces with curvature, and have distinct effects on the boundary layer (see a paper by Dris and Johnson, 2004). This topic is studied extensively in the gas turbine field for the effects on heat transfer coefficients on blade surfaces. Investigation into this relationship could lead to information as to why boundary layer analyses' of helical flow show discrepancies.

The four-vortex flow structure is not reported in any other work for the circular case, and its existence is disputed. Though Dennis & Ng (1982) provide support for the existence of the four-vortex solution by reference to two experimental visualization studies in which observation of this flow structure was reported for non-circular cross-sections. Dennis & Ng's results seem dubious in the same manner as the solutions of Nandakumar & Masliyah (1982), since neither directly calculates the four-vortex solution. Rather they had to impose the structure as an initial condition and see if the structure could be maintained. This would suggest that the solution is valid but not

probable, i.e. purely academic. The results also show that the four-vortex solution is accompanied by dual maximum axial velocity locations. This effect is another reason why the structure is not probable, since the flow would have to develop from a single maximum and split into two. Dennis & Ng's presentation of their results and grid check are concise, with good agreement for the friction ratio across the range of Dean numbers calculated.

2.2.2 Boundary Layer Analysis Solutions

Three main studies were carried out during the 1960's that formulate the laminar friction factor based on a Boundary Layer (BL) analysis, in an attempt to extend the applicable range to more prototypic flows. The three works described are Barua (1963), Mori & Nakayama (1965), and ito (1969). The boundary layer analysis used in this section plays an important part in the general scheme of fluid mechanics. Its history comes from the initial attempts to model fluid motion where the viscid region was initially neglected (potential flow). The issue arises that without viscosity there isn't any friction loss, and objects like spheres and rocks fly around uninhibited by all but gravity and the confines of earth, i.e. the no-slip condition at the wall is lost. Addressing this issue showed that increasing the Reynolds number didn't make the viscous effects disappear, rather it makes the viscous effect's influence tend toward smaller and smaller regions of the fluid domain. This observation answered the work of D'Alembert, and implied to Prandlt the compromise of separating the flow into the viscid region (boundary layer) and the inviscid region (potential flow), and to solve them separately. This history exposes the boundary layer theory as applicable to high Reynolds number flows, and somewhat forgives the errors seen in Figure 2.3 at lower flow rates. It also quickly explains the methods of our three authors. The full story is found in many fluid mechanics texts, and is not rigorously referenced and detailed here.

Barua (1963), Mori & Nakayama (1965), and Ito (1969) all take the approach of splitting the flow into the viscid and inviscid regions, with the simplifying assumptions of:

- Small curvature (loosely coiled)
- Negligible pitch (toroidal geometry)

- Fully developed flow
- Incompressible single-phase flow

The system analyzed is shown in Figure 2.2. Note the change in the location from which the polar angle is measured, in comparison with the analysis of Dean (1928) (Fig. 2.1). This is quite similar to the torus and large radius of curvature analyses of previous works. Since this method is not utilized in this dissertation, it suffices to list the steps for obtaining the boundary layer solution. These are:

1. Develop the conservation equations for the core region.
2. Assume a velocity distribution in the BL that matches the boundary conditions.
3. Integrate the BL velocities over δ, to obtain the momentum integrals.
4. At any given polar angle, equate the fluid flowing into the BL to the flow inside the BL.
5. Calculate the transverse velocity and boundary layer thickness (Mori & Nakayama assume they are both a series expansion in Dean number)

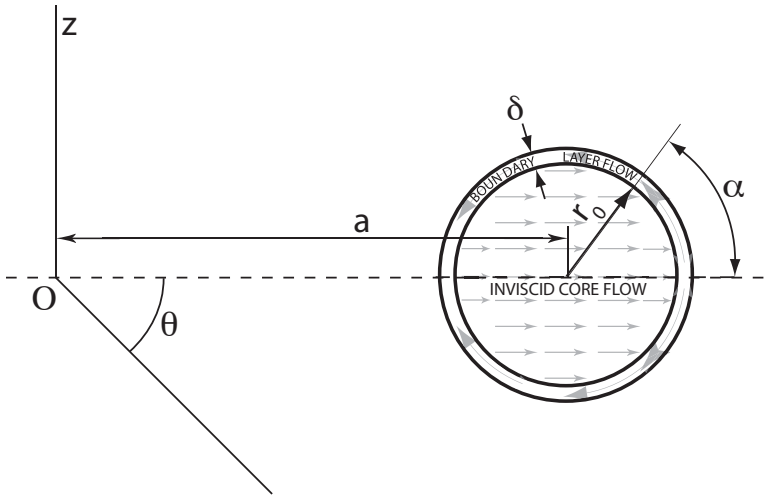

Figure 2.2: Flow regions used in the boundary layer analyses.

Ito's (1969) study, being the most recent, compares the different author's ratio of friction factors, against an empirical fit of the data sets of Ito (1959) and White (1929). The comparison is reproduced in Figure 2.3, using the equations given in the

respective publications. The analytic model of Ito shows the closest agreement to the empirical fit, especially at lower Dean number flows. Important is the agreement of the proportionality of the friction ratio by all the analyses, i.e. the relative friction is asymptotically proportional to the Dean number to the 1/2 power (Eq. 2.7). This does not support the conclusion of a 1/4 power relation by Van Dyke (1978).

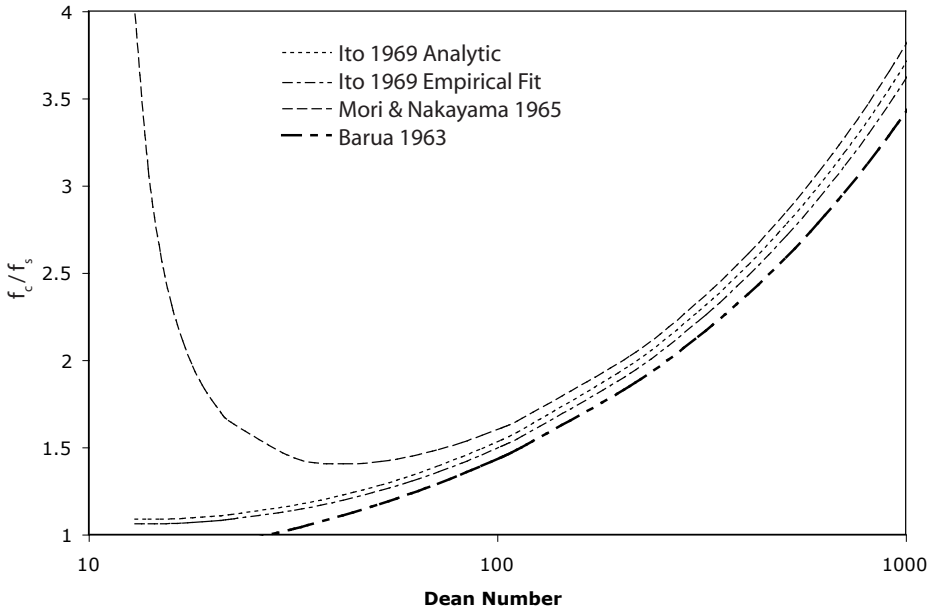

Figure 2.3: Comparison of the forms for relative friction factor of curved to straight flows.

2.2.3 Numerical Methods Solutions

The use of numerical methods in determining the flow structure and friction factor in the helical geometry is well represented by the works of Truesdell & Adler (1970), Joseph et. al. (1975), Nandakumar & Masliyah (1982), and Goering (1989). This method utilizes the brute force of the computer to iteratively solve the governing equations for the given geometry. The prevailing simplification of a toroidal geometry is continued in the numerical studies, with all covered studies making this assumption. Goering (1989) provides a great review of previous works in the field, and attacks the problem on including heat transfer and buoyancy into the calculations. Goering also details the issues with solving the coupled non-linear equations. He explains why the coupling of the equations requires the equations to be solved in a given order,

and use under-relaxation techniques. His details the issue well, with clear examples and references to previous works. In short, the coupling issue that Goering explains can be summed up with Figure 2.4. The accuracy of the results of these numerical studies, with respect to friction factor and secondary streamline patterns, are inline with the boundary layer and series solutions. The numerical analyses cover helical flows up to a Dean number of approximately 1000. The numerical works considered the following assumptions:

- Small curvature (loosely coiled)
- Negligible pitch (toroidal geometry).
- Fully developed flow
- Incompressible single-phase flow

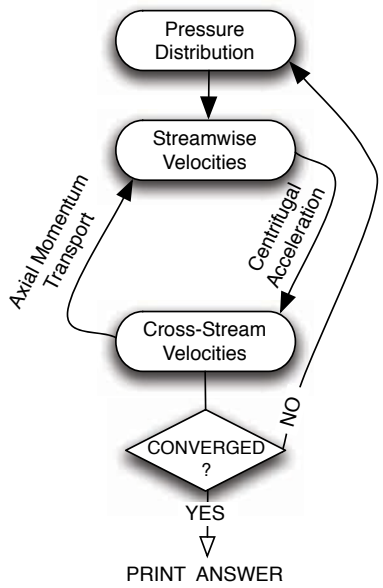

Figure 2.4: Iteration direction, and coupling of the streamwise and cross-stream velocities.

The specifics of each numerical method for the individual works can be found in the respective publications. All have are similar in that they solve the appropriate forms of the governing equations by iterating on the pressure and velocity. These equations can be developed from Eq. 1.16 and Table 1.1 of Sec. 1.3.3. In short, a very simplified version of the steps is as follows:

1. Develop the conservation equations for the system.
2. Reduce the differential equations to algebraic form, by introducing finite differences.
3. Calculate the pressure distribution using velocity (velocities are estimated the first time though).
4. Use the calculated pressure to calculate new velocities, go to the next step if the velocities are unchanged, and back up a step if they have changed (within the tolerance).
5. Print the final values for velocities (or stream function) and pressure.

These numerical studies have provided some important results and recommendations that are utilized or referenced by subsequent works. The first mentionable result has to do with the impact of finite pitch. The finite pitch of a helix has the effect of increasing the radius of curvature, and changing how the centrifugal force applies to the flow. Centrifugal forces in a toroidal system are strictly perpendicular to the axial flow; in contrast, the helix translates the centrifugal force so that it acts both in the plain perpendicular and along the helix axis. This translation removes symmetry and shows up as a difference in mass flux between the upper and lower halves of the duct. Truesdell & Adler (1970) reference unpublished tracer experiments that show the difference in velocity of the upper half from the lower half of a helical cross-section as being approximately 1% (for $r_0/a \approx 0.09$, $p/s\pi a \approx 0.03$). Both Truesdell & Adler (1970) and Goering (1989) use these unpublished results as the basis for neglecting helicity in their own work.

Truesdell & Adler (1970) also proposed compensating for the increase in radius of curvature, due to pitch, by introducing a modified curvature. A helix of constant diameter has a curvature defined by Eq. 2.8, and a radius of curvature defined by Eq. 2.9 (Lipschultz 1969, Truesdell 1970). Truesdell considers these expressions and recommends making the substitution described in Eq. 2.10, to compensate for the change in radius of curvature when the pitch is "small". He does not state what is meant by "small".

$$\kappa = \frac{a}{a^2 + \left(\frac{p}{2\pi}\right)^2} \tag{2.8}$$

$$\frac{1}{\kappa} = a + \frac{1}{a}\left(\frac{p}{2\pi}\right)^2 \tag{2.9}$$

$$\text{substitute} \quad \frac{a}{a + \frac{1}{a}\left(\frac{p}{2\pi}\right)^2} \quad \text{for} \quad R_0 \tag{2.10}$$

Joseph et al. (1975) changed things up a bit, and studied the toroidal flow in a square cross-section. The square cross-section inherently matches the grid setup, eliminates the placement of grid points outside the fluid domain, and explores the influence of cross-section shape. His calculations showed a four vortex secondary flow structure for Dean numbers greater than 100. Joseph explains the four-vortex structure by noting that the flat outer wall flattens the axial streamline, and on increasing Dean number, dimples the streamline such that the axial velocity maximum is moved off of the centerline. Since this study ignores torsion, this creates a *symmetric* pattern with a maximum axial velocity location on either side of the $\alpha = 0$ centerline. The maximum axial velocity forms the location of the interface between the secondary flow counter rotating vortices, and with dual maximums present, the pattern bifurcates into that of a four vortex. This shift is described in the Figure 2.5, where the boxed crosses are the location of the maximum axial velocity in the plane perpendicular to the pipe axis, the lower two figures are the streamlines for the axial velocities, the upper two figures are the streamlines of the secondary flow in the plane perpendicular to the pipe axis, the arrows on the streamlines indicate the direction of the cross-stream flow, the left two figures are a pair at a single Dean number, and the right two figures are a pair at a greater Dean number. The greatest centrifugal force is located at the maximum axial velocity, i.e. when the axial flow splits with two maximums there are two locations of maximum centrifugal force. These locations are bound by re-circulating flow that provides the material moving due to the centrifugal force, hence two maximum locations means two re-circulating flow interfaces and four vortices. Joseph also completed visualization studies to verify his calculations. Both the calculations and visualizations showed a transition to a four vortex structure around a Dean number of 100, and a greater pressure loss / lesser axial dispersion when the Dean number was greater than 100. Nandakumar & Masliyah (1982) reported similar results for a circular cross-section, where the flow could be *made* to bifurcate into a four vortex solution, by starting with a flat outside edge similar to Joseph. Next the flow is allowed to develop a four vortex solution, and the grid is gradually shifted to the circular cross-section. They found that with a sufficiently gradual transition, the four vortex solution could be maintained for flows of Dean number greater than 113.

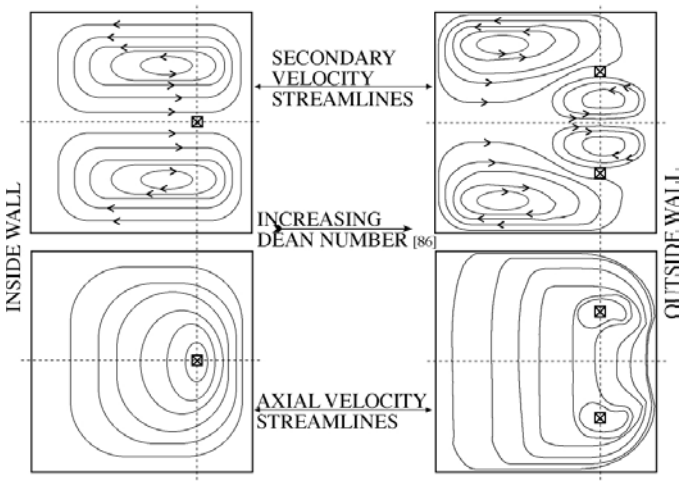

Figure 2.5: Secondary flow streamlines by the numerical calculations of Joseph (1975).

2.3 Experimental Studies of Helical Two-Phase Flow

Experimental investigations of helical two-phase flow can be grouped into work on pressure drop formulation with liquid hold-up/void fraction modeling, and flow regime mapping studies. With this in mind, the studies covered here are presented in a manner consistent with the previous sections, and grouped accordingly. The range of parameter values of the helical systems covered by the author of this review are listed in Table 2.2. Considering the principal importance of pressure drop on fluid system design, it is not surprising to find that all of the works investigate pressure drop, while only six report flow regime observations. The studies that report flow regimes are marked with double asterisks (**). This flow regime data is valuable, and is used for assessing the helical flow model of this dissertation.

2.3.1 Pressure Drop and Liquid Hold-Up Studies

The methods of Lockhart & Martinelli (1949) are heavily used in the helical pressure drop formulations, and requires a bit of explanation. Their work was focussed on developing the predictive capability for two-phase pressure loss in horizontal linear flows. Their formulation can be described with the following steps:

1. The Fanning form of pressure loss is written for each phase.
2. The Blasius form of the friction factor is written for each phase.

Table 2.2: First author listing of the two-phase works covered in the helical two-phase experimental section. *(** - includes flow regime observations.)*

Author	j_g $[m/s]$	j_l $[m/s]$	d_0 $[mm]$	A_0 [non-dim]	p $[m]$	$2a$ $[m]$
Rippel 1966	0.470 - 1.194	0.0004 - 1.194	10.20	19.9	0.0020	0.203
Boyce 1969**	0.409 - 1.769	0.001 - 0.027	31.75	9.6 2.4 48.0 96.0	0.062 0.154 0.308 0.616	0.305 0.762 1.524 3.048
Banerjee 1969**	0.527 - 38.33	0.0064 - 0.5153	15.53	9.8 14.7 19.6	0.017 - 0.135	0.152 0.229 0.305
Akagawa 1971	0.00 - 5.00	0.35 - 1.16	9.90	11 22.7	Not Listed	0.665
Kasturi 1972	0.005 - 4.329	0.005 - 0.112	12.5	53.2	0.0299 - 0.0616	0.109 0.225
Whalley 1980 **	10.74 - 29.17	0.023 - 0.063	20.20	49.5	0.330	1.0
Mujawar 1981**	0.20 - 1.20	0.05 - 0.124	24.20	14.4 21.0 50.4 100.0	0.019 0.26 0.57 0.136	0.017 0.025 0.061 0.121
Rangacharyulu 1984	1.131 - 1.826	0.005 - 0.1347	11 13	18.5 23.4	0.030 0.025	0.203 0.304
Hart 1987	10 - 40	0.0008 - 0.030	14.66	287.2	0.085	4.210
Saxena 1990**	0.070 - 0.516	0.041 - 0.078	9.70	11 51.6 156.5	0.015 0.008 0.017	0.106 0.500 1.516
Yan 1992**	0.50 - 400	0.04 - 0.20	8.26	9.085	0.025	0.150
Ju 2001	varies w/ length	varies w/ length	14 12	8.0 9.3	0.023	0.112
Ishikawa 2003**	0.088 - 3.560	0.088 - 3.110	20	13.5	0.100	0.270

3. Modify the hydraulic diameter definition so that it includes a parameter that is a measure of phasic fraction.
4. Substitute (3) into (2), then the result into (1).
5. Equate the pressure drop of each phase, and determine the non-dimensional parameters that govern the system.

Their analysis results in three new non-dimensional parameters. Two ratios of two-phase pressure loss to each superficial phasic pressure loss, and one for the ratio of the superficial liquid pressure loss to the superficial gas pressure loss. The superficial pressure loss is analogous to superficial velocity, and is the pressure loss if only one phase is flowing in the duct. With these new parameters, the liquid hold-up and two-phase pressure loss are ascertainable. Pressure loss is calculated by taking a simply product. The new parameters are given in Eqs. 2.11 and the two possible products for determining the pressure loss are given in Eqs. 2.12.

$$\phi_g^2 = \frac{\left(\frac{dP}{ds}\right)_{TP}}{\left(\frac{dP}{ds}\right)_g} \tag{2.11a}$$

$$\phi_l^2 = \frac{\left(\frac{dP}{ds}\right)_{TP}}{\left(\frac{dP}{ds}\right)_l} \tag{2.11b}$$

$$X^2 = \frac{\left(\frac{dP}{ds}\right)_l}{\left(\frac{dP}{ds}\right)_g} \tag{2.11c}$$

$$\left(\frac{dP}{ds}\right)_{TP} = \phi_g^2 \left(\frac{dP}{ds}\right)_g \tag{2.12a}$$

$$\left(\frac{dP}{ds}\right)_{TP} = \phi_l^2 \left(\frac{dP}{ds}\right)_l \tag{2.12b}$$

Rippel (1966) was one of the first to look at downward gas-liquid cocurrent flow in a helical geometry. He applied the method of Lockhart & Martinelli (1949) described above, to correlate his data. Rippel carried out a series of tests, and made comparisons to the L-M model. His results showed that for the downward helical flow case, the horizontal L-M correlation predicted reasonably well the helical pressure drops (+40% -30%). Rippel postulates that the ratio form of the L-M correlation (shown in Eqs. 2.11 & Eqs. 2.12) allows some of the curvature effects to cancel out, i.e.even

though the geometry can change the absolute pressure loss markedly, it should not have as strong an effect on the ratio of the liquid to gas pressure loss.

Akagawa et al. (1971), Kasturi & Stepanek (1972), and Rangacharyulu et al. (1984) investigate the upward cocurrent gas-liquid helical flow case. They all present comparisons with the Lockhart Martinelli prediction of pressure loss. Akagawa et al. (1971) showed that the influence of curvature on pressure drop becomes more apparent as the liquid flow rate is increased. In Fig. 9 of his paper, the lower liquid flow rate ($j_l = 0.35$ $[m/s]$) shows similar pressure gradients for the curvature ratios of 11 and 22.77. When the liquid superficial velocity is increased to 0.85 $[m/s]$, the curvature dependence becomes apparent, and the tighter coil ratio of 11 is no longer coincident with the looser coil of ratio 22.77. For the flow rates utilized, it was shown that the ratio of the frictional pressure drop in a helix versus that in a straight pipe is always greater than unity, and in the limiting case of a coil to tube ratio of 7 (stated as the practical limit expected) was highest with a ratio of 2. This is in line with the observations of all the single-phase helical works. Even though the magnitude of pressure loss is strongly dependent on the flow rate, Akagawa's results showed that the entrance length was similar for all flow rates in both coil ratios.

It is interesting that the data collected by Akagawa et al. (1971) better matched the modified L-M method of Ripple (1966), than Ripples own data (+- 15% for Akagawa, compared to +40% -30% for Rippel). In addition, Akagawa's data spans a larger range of L-M values. Akagawa takes this as indication that his data collection is more accurate than Ripple's. Akagawa does make some indirect measurement of flow patterns in the opaque copper tubing, inferring the pattern from the frequency of the gas phase presence. He noted that the patterns (void frequencies) were similar to those found in horizontal pipe, though variations introduced by the centrifugal force were present. Early in his paper he talked of the effects of the centrifugal force being unresolved by the comparison of the frequency of the void regions before, in, and after the helical test section. This would imply that the void frequency measurement is inappropriate for identifying flow regimes in helical geometries.

Kasturi & Stepanek (1972) only used a single coil, and focused on the effects of fluid properties and flow rate on the pressure drop and void fraction. The results of this study showed the data to be well represented by the turbulent liquid-turbulent gas L-M correlation, with an average deviation of +30% when the X parameter had

a value greater than unity. Kasturi & Stepanek (1972) additionally propose a new pressure loss model. Their analysis is similar to that of Taitel & Dukler (1976). In fact, there are actually few discrepancies between the two. His model does not compare well to the available helical data sets, and could be a result of his formulation effectively being for a linear pipe. Their assumptions are:

- No cross-stream pressure gradient
- Interfacial and wall shear stresses are functions of slip friction factors,
- Negligible inertia forces
- Steady flow that yields consistent time averaged properties.

More recently, Rangacharyulu et al. (1984) recommended another model for pressure drop based on another modification of the L-M approach. Rangacharyulu compared his results with his, Boyce's (1969), and Rippels (1969) work (about 400 data points). These comparisons showed that his modified model produced good results. In the last couple of pages of his paper he sums up his recommended important helical flow parameters for future analyses. On page 42 of his paper:

> ... two-phase flow through pipes has been shown to be a function of the flow pattern and the superficial liquid Reynolds number Re_l ... for flow through coils, the additional pressure drop should also include other effects, namely, the effect of secondary flow phenomena, the effect of the compressibility of the gas phase, the effect of interfacial instability between the gas and the liquid, and the geometry effect of the helical coils.

Hart et al. (1987) contributed friction factors for single-phase flow through curved tubes, and pressure gradient data for two-phase flow through a helical tube. Hart also proposed models for prediction of film inversion and liquid hold-up. He looked at the pressure imbalance induced by the centrifugel force, and a formulation of these forces as a function of the velocity. This is the same approach Banerjee (1967) used to explain the phenomenon. He extended the analysis and steps through a method for determining the coil friction factor. The coil friction factor is the key for the analysis, because the formulation for a straight pipe is used with the friction factor replaced by the coil friction factor. The coil friction factor is dependent on the Dean number, which in turn is a function of the Reynolds number. The coil friction factor is formulated so that it asymptotically approaches the linear flow factor as the

curvature decreases. This is better than previous models of White (1929) or Mishra (1979), who were not asymptotically correct. Given the accuracy of the White and Mishra models, it is important to note that the model by Hart (1987) matches these. Hart notes a 30% maximum increase in friction factor from single to two-phase flow for the helical system. This is in contrast with contemporary work, such as Hamersma (1987). Hamersma (1987) observed increases in friction factors of up to 70 percent over straight pipes.

Ju et. al. (2001, 2004) of the Institute of Nuclear Energy Technology at Tsinghua University, has published the most current work on helical two-phase flow. The Beijing group looked into the hydraulic performance of helical flows specific to the heat exchanger design of the High Temperature Reactor (HTR-10), located at the university. This heat exchanger design consists of 30 identical helical coils that experience single-phase liquid through single-phase gas flows. The studies completed included theoretical prediction of the pressure gradients and heat transfer coefficients, and values for the critical Reynolds number, along with experimental verification of the predictions. Analytical portions use the form of Dean number originally formed by White (1929) and recommended by Berger et. al. (1983), shown in Eq. 2.3. Ju et. al. compared their data to calculated single-phase friction factors for the formulas of Ito (1959) and Mori & Nakayama (1967). The results showed that Mori & Nakayama's formula compares better (within 20 %). For their coil to tube ratio of 6.22, the data was well represented by Eqs. 2.13 for laminar flows, and by Eqs. 2.14 for turbulent flows. Notice that this ratio is less than the assumed minimum value of 7 by Akagawa et. al. (1971).

$$\frac{f_{helix}}{f_{straight}} = 1 \quad for \quad k < 11.6 \tag{2.13a}$$

$$\frac{f_{helix}}{f_{straight}} = 1 + 0.015 Re^{0.75} \left(\frac{r_0}{a}\right)^{0.4} \quad for \quad k \geq 11.6 \quad Re < Re_{crit} \tag{2.13b}$$

$$f_{straight} = \frac{64}{Re} \tag{2.13c}$$

$$\frac{f_{helix}}{f_{straight}} = 1 + 0.11 Re^{0.23} \left(\frac{r_0}{a}\right)^{0.14} \tag{2.14a}$$

$$f_{straight} = \frac{0.316}{Re^{0.25}} \quad for \quad \text{smooth pipe} \tag{2.14b}$$

$$f_{straight} = 0.1\left(\frac{1.46\delta}{d_0} + \frac{100}{Re}\right)^{0.25} \quad when \quad \delta = \text{pipe roughness} \tag{2.14c}$$

The data of Ju et. al. displayed the expected trends of increases in pressure loss, heat transfer, and critical Reynolds number, over the linear geometry. An interesting observation was made when comparing the heat flux at the inside, outside, and top of the coil in the two-phase flow regions. It was noted that the energy transfered at the top and inside of the coil was greater than at the outside, and that the differences are up to a factor of five ($\sim$ 2000 $[W/m^2K]$ along the outside of the bend vs. $\sim$ 10000 $[W/m^2K]$ along the top surface). This exposes the strong dependence of transport processes on the flow regime, and the importance of accurate prediction of the regimes in helical flow designs.

2.3.2 Flow Regime Studies

Of the 7 authors listed in Table 2.2 as publishing helical flow regime data, only five sets of data are found usable. These five publications provide approximately 200 data points that span all flow regimes expected, and one transition line for the stratified to annular transition. The five authors that published consistent data are: Boyce (1969), Whalley (1980), Saxena (1990), Yan (1992), and Ishikawa (2003). Each of these author's published works is discussed in more detail, and the data extracted from the works are shown in Figure 2.6.

The studies turned up in the literature search, but whose data are not consistent or used in this dissertation, are explained. These are the works of Banerjee (1967/1969) and that of Mujawar & Rao (1981). Banerjee et al. (1967/1969) was one of the first studies of the effects of coil diameter and pitch on helical two-phase flow patterns. His 1967 study specifically investigated the phenomena of film inversion. This phenomena is the situation where the liquid and gas phases flow opposite to intuition, with the denser phase traveling along the inside of the helix bend. This situation is simply explained as follows: under the condition where the slip velocity is great enough that the centrifugal force on the gas exceeds that of the liquid, in spite of the much greater liquid density, the force imbalance inverts their relative position. It is simple to show this occurs for low pressure air-water systems when the air velocity is 31 times that of the liquid. In 1969, Banerjee extended his contributions to helical flow studies by making pressure drop, liquid hold-up, and flow pattern observations for

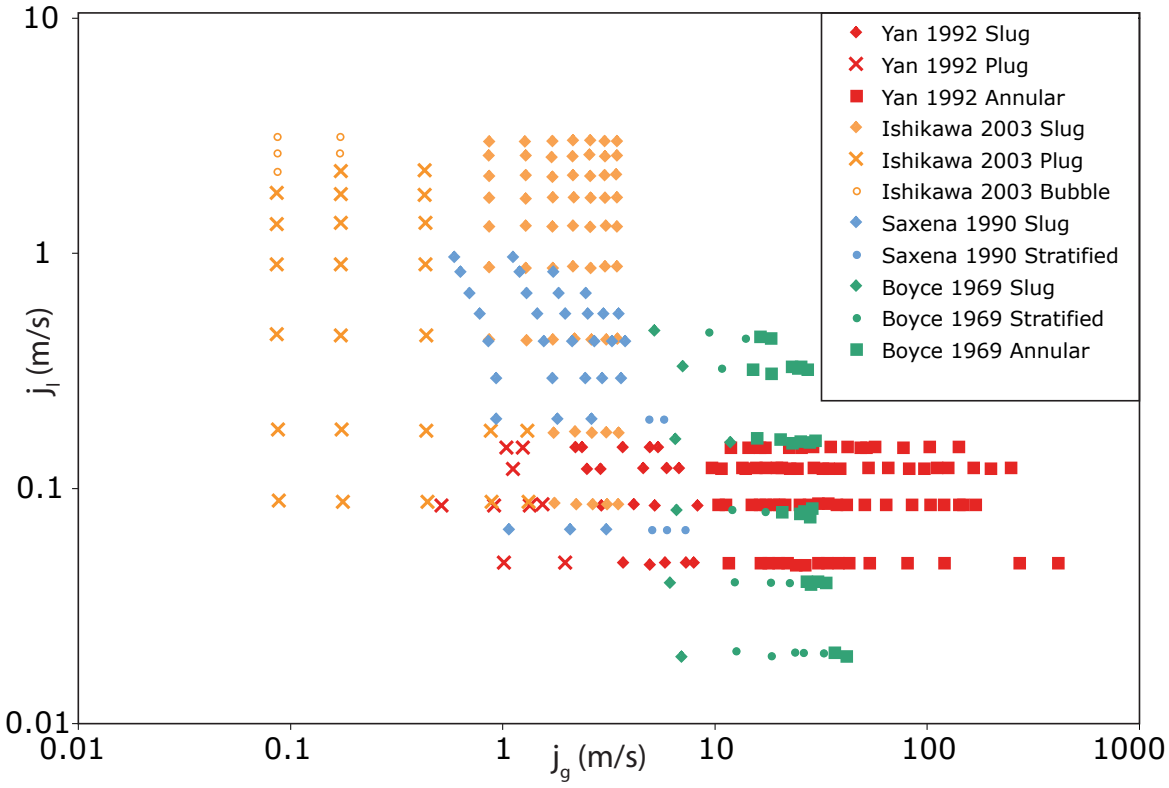

Figure 2.6: Helical two-phase flow regime observations from Boyce (1969), Whalley (1980), Saxena (1990), Yan (1992), and Ishikawa (2003).

air-water cocurrent flow in several different helices. Banerjee observed all the regimes normally found in an inclined linear flow, and compared his observations to the regime map developed by Baker (1954) for linear systems. The agreement between Banerjee (1969), for the data range, and Baker (1954) is remarkably good. However, significant discrepancies exist between Banerjee's data and other helical flow regime observations. As a result, Baker's flow regime map is for linear systems, and Banerjee's data are not utilized here for model development purposes.

Mujawar & Rao (1981) extended the Lockhart & Martinelli (1949) method to Non-Newtonian helical flows. This publication also includes flow regime observations for air-water flow, however the observations are only for the helix with the curvature ratio of 0.0695. The results showed that the slug regime was more pronounced in the helical geometry, reducing the presence of the stratified regime to a narrower window of gas flow rates. The annular flow regime was also shown to include a dispersed mist that is not seen in horizontal systems. Mujawar & Rao (1981) showed that the Lockhart & Martinelli (1949) model agrees well with hold-up data for the Newtonian liquid, but was 20–40 % high for the Non-Newtonian liquids. Mujawar & Rao made the same conclusion as Banerjee (1969), that the flow regimes for helices are essentially similar to horizontal two-phase flow. This observation showed up in his pressure loss calculations, hold up, and friction factor correlation. Mujawar & Rao's (1981) study is mainly for non-Newtonian fluids, and their annular data set falls completely inside the intermittent data sets of all the other authors. This inconsistency with the other helical data sets, and that the study is basically for non-Newtonian flows, is why their data were not used in this dissertation.

Boyce et al. (1969) noted early on, the effects of secondary flow on two-phase pressure loss in helical coils. He provided a clear graphical representation of the flow regimes observed in the helical system, and proposed a flow regime map for the design of helical coil steam generators in nuclear power systems, operating at 2700 [$psia$]. The extension method is the same as that originally introduced by Baker (1954), where Baker attempted to extend linear horizontal air-water data of atmospheric pressure to oil-gas systems, by using correction factors which are functions of fluid properties. Since Baker's analysis is for a linear horizontal system and Boyce is upward helical, Boyce considered an additional correction factor for curvature that multiplies the friction factor of the linear system. This approach of Baker has been shown to be only approximately correct for the linear system (Boyce 1969), so the accuracy of the

extension by Boyce is somewhat in question. Boyce actually refered to the extension as "highly speculative". Comparison of Boyce (1969) with Baker (1954) shows strong disagreement in flow regime transitions, in contrast to the observations of Banerjee (1969). Boyce (1969) only presented data points of flow regime observations for a 5 $[ft]$ diameter coil.

Whalley (1980) experimentally investigated helical cocurrent air-water flow in the stratified and annular regimes. His study focussed on the stratified and annular regime film thickness distribution, and identification of the stratified to annular transition. The results showed that for most cases studied the liquid film flow rate was greatest on the inside of the bend, and that liquid drop entrainment was minimized because of centrifugal force de-entrainment of liquid drops on the outside of the bend. Whalley observed the same phenomenon of film inversion that Banerjee et al. noted in 1967, and used the same explanation of the phenomenon. For the stratified and annular regimes, Whalley (1981) made the following observations:

- A comparatively small fraction of the liquid flows is entrained as drops. Whalley's data shows a maximum of 30 percent of the flow as entrained, with increasing entrainment related to increasing liquid and gas flow rates (more so with liquid flow rate increases.)
- The location of the liquid film, and the maximum film flow rate, is positioned on the inside of the curve for a matched high gas / low liquid flow, and on the outside for a matched low gas / high liquid flow. The former occurs most often for the flow rates considered in this study.
- Deposition can introduce a secondary peak flow rate at the outside edge when a matched high gas / high liquid flow is present. In this case, there is a pronounced amount of liquid being entrained and deposited on the outside surface.

When Whalley compares his pressure gradients with previous works, he found contradiction and poor comparison. Whalley pointed out that the models he considered did not take into account flow in directions other than axial, and concluded that the lack of consideration of the secondary flow influence was the reason for the poor comparisons. Whalley's (1981) data used in this dissertation is the observed stratified to annular transition.

Saxena et. al. (1990) completed an experimental investigation of the pressure

drop, hold-up, and flow regime observations in 3 helices of constant tube diameter, and varying coil diameter. The results showed that the most common regime in upward flow was slug, and stratified for downward flow. The slug pattern increasingly dominated a greater portion of the upflow mapped region with decreasing coil to tube diameter ratio. Saxena noted NO slug flow in the cocurrent downward flow case, even though the liquid hold-up for the downward case was greater than the upward case. He compared this to observations made by Spedding et al. (1981), and finds good agreement. This characteristic of downward helical flow is the reason for its use in the design of slug dissipaters of oil wells, see Mateo (2003). From these results, he concluded that tube inclination, and not the curvature, is the dominant parameter value that affects flow pattern presence in helical geometries. Another interesting observation made in this study, is that the curvature also showed very little influence on frictional pressure loss for coil to tube ratios greater than 51.6. Again he compares with a previous study (Rippel et al. 1966), and finds agreement. Saxena (1990) only provides flow regime observation data for the coil to tube diameter ratio of 11.

Yan (1992) investigated the two-phase flow of both air-water and R113 vapor-liquid flows, in helical coils and spiral coils. The difference between spirals and helices being that the helix has a constant coil diameter, and a spiral coil has a variable radius of curvature. The vapor phase in the R113 tests was generated by heating all but the sight glass section of the facility. In keeping with the other experiments of this section and the goal of this dissertation of modeling an adiabatic situation, only Yan's air-water test data is used. The flow regime observations were decided on by reviewing high-speed camera film of the flow. Yan's data showed similar results for the circular and rectangular cross-sections, when the hydraulic diameters were the same. Yan's data is in agreement with the other helical studies, in that he notes the absence (or strong reduction) of the stratified flow regime in the helical up-flow case, being replaced by the slug flow pattern. This study is the first found to apply the helical map of Uddin (1988), which was one of only two known to exist for the helical flow case. Comparison to Uddin's map showed poor agreement.

Ishikawa et al. (2003) published the most current two-phase helical flow regime data found. This study reported visualizations of helical two-phase flow of large Dean number. The results showed an increase in the range of the intermittent and bubbly regimes and an expiration of the stratified regime, in comparison to the horizontal case. They explain the increase seen in the bubbly regime as being due to the sec-

ondary flow prevention of coalescence. Ishikawa et al. noted that the secondary flow may also exist in the intermittent regimes, but there are no data to support the claim. The two-phase linear study of Spedding et. al. (1981) supports this statement, and reportes recirculation flow patterns within slugs of liquid of the intermittent regime. The existence and character of the secondary flow in the bubbly regime have been numerically studied by Oiwa et al. (2001), which also supported the statements of Ishikawa et. al. about bubbly flow secondary patterns. In this numerical study, Oiwa et. al. artificially turned off the gravity force and found that the introduction of air, to generate a two-phase bubbly regime, had negligible effect on the symmetric secondary flow. He concluded that the two-phase bubbly regime was affected similarly to a single-phase flow by the centrifugally induced secondary flow. These studies suggest that the secondaryflow is present in the helical geometry, and that it affects the force balances that determine the transition between different patterns. Ishikawa et. al. (2003) published the data on helical flow regimes for a helix with a radius of curvature of 0.540 $[m]$.

2.4 Analytical Studies of Helical Two-Phase Flow

Only two studies were found to report analytical work on two-phase helical flow. These are the contributions of Uddin (1988) and Keshock (1998). Uddin approached the generation of a helical flow regime map by first determining the correct correlating parameters to represent the system. These parameters are gotten from Uddin's formulation of the helical system, which he based on the boundary layer analysis of Mori & Nakayama (1965). It is noted that the solution of the secondary flow intensity (i.e. non-dimensional core velocity) provides measurement of the additional shear introduced from this flow, and allows the desired parameters to be identified. This solution is said to be obtained by "special numerical techniques", though it exactly matches the first order approximation to the series solution given in Mori & Nakayama's paper. No additional information of the analysis is presented in this paper, rather it is implied that the specifics are to be found in an earlier internal university progress report. Uddin considers this analysis, and chooses the gas phase dimensionless acceleration and modified Lockhart & Martinelli factor as appropriate correlating parameters, and applied them to the flow pattern observations from the above-mentioned internal report. The resulting map expectantly compares very well

to the internal report's data, and also to some data Uddin extracted from the Boyce et. al. (1969) paper. An important feature of the Uddin (1988) map is its inconsistency with the expanded slug presence characteristic of upward helical flow. The map does not predict any slug flow regime for upward helical flow, even though it has been shown in *all* studies that the slug regime is actually quite prevalent! Notwithstanding of this, and that the transition boundaries are set by correlation of a relatively small quantity of data (28 data points), it represents the first attempt at improving flow maps for helical flow by consideration of the underlying physics. The proposed map of Uddin (1988) is shown in Fig. 2.7.

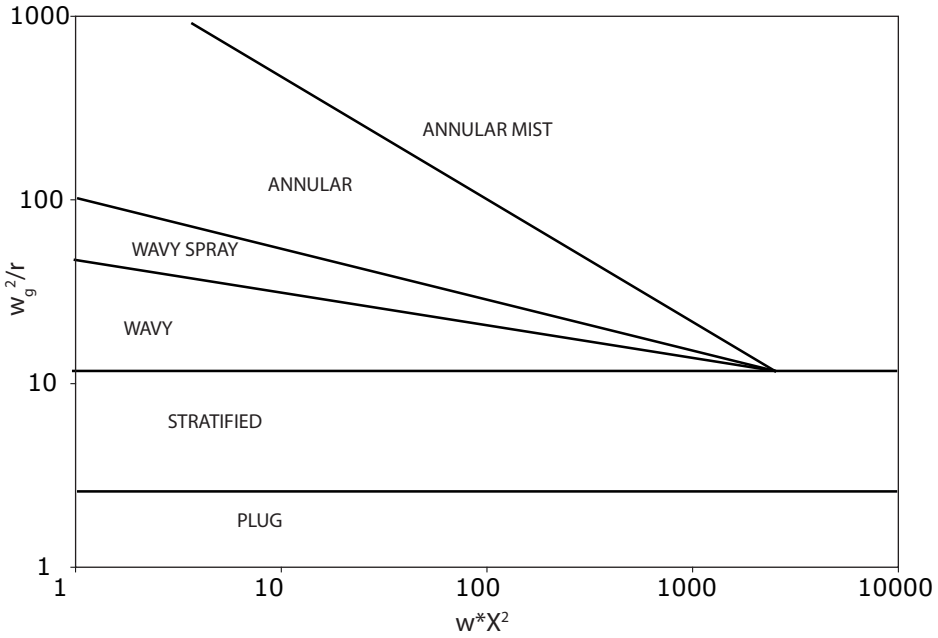

Figure 2.7: Helical two-phase flow regime map by Uddin 1988.

The second attempt at developing an analytically based helical flow regime map was not intentionally undertaken. This is to say, the work of Keshock (1998) was directed at the measurement of two-phase flow under microgravity, and the experiment length was constrained to fit into a KC-135 airplane. Keshock noted that a length greater than that allowed by this constraint was required for accurate pressure drop measurements, so he simply by wrapping the duct into a coil. The helices of this study would be considered loosely coiled, with coil to tube diameter ratios between 27–40, and in fact "were designed to minimize complexities induced by curvature . . . ,

so that the flows would not differ substantially from straight-channel flows." Keshock accounts for the necessary curvature by introducing the idea of an effective gravity, which accounts for the centrifugal acceleration, and is also effectively used in a later study by Matteo (2003). The form of effective gravity used by Keshock (1998) is given in Eq. 2.15, where w_k represents is the axial velocity for phase k. This effective gravity is substituted into the Froude number, and a modified microgravity Taitel & Dukler style transition map is proposed for the annular to slug transition. This method showed good results for the small data set of his study (16 data points), and produces good agreement when Matteo (2003) applied the same idea for determining slug dissipation rates. It should be noted that both Matteo (2003) and Keshock (1998) examining the downward flow situation, so the mapping technique is very preliminary and represents, as with Uddin (1988), a step towards identifying the underlying mechanics that differentiate curved flow regimes from linear.

$$g_{eff} = \sqrt{(g \cdot cos)^2 + w_k^2 r_c} \tag{2.15}$$

2.5 Successful Studies of Linear Two-Phase Flow Regime Prediction

This section provides a look at the most successful models for predicting two-phase flow regime transitions in the horizontal/inclined linear geometry. The importance of linear work to the present study stems from the similarities between the helical and linear two-phase flow, where the difference is simply two body forces. In line with all engineering models, linear two-phase flow transition modeling consists of experimental and analytical formulations. The study of linear two-phase flow is covered by considering the often referenced and utilized studies of Mandhane et. al. (1974), Taitel & Dukler (1976), Barnea (1987), and the quite recent study on diabatic horizontal flow regime transitions by Petalas & Aziz (2000). These studies provide a clear evolution of the methods that allow the prediction of flow structure in near horizontal linear geometries, and much insight into an appropriate method for the helical geometry.

2.5.1 Experimental Linear Two-Phase Flow Regime Transition Mapping

The earliest experimental works of linear two-phase flow transition mapping were completed in the early 1940's. These early models were later optimized as more data

became available to the reasearchers. Possibly the most referenced works are those of Baker (1954) and Mandhane et. al. (1974). Baker was possibly the first accepted flow regime map, and was based on air-water flow data of previous authors. Baker's map is shown in Figure 2.8. Mandhane et. al. (1974) utilized the University of California Multiphase Pipe Flow Data Bank of 5,935 flow regime observations to assess the accuracy of some regime maps available in 1974. The study identified shortcomings in the empirical models' ability to predict the flow patterns of the database, where the models have average accuracies of 69% and 55%, for air-water data and all data respectively. The deficiency was that the individual models were accurate in different specific areas, but lacked an overall application. Mandhane addressed this deficiency by effectively averaging the three maps, and adding correction factors for fluid properties. With this, the accuracy of the predictions for the University of California database were increased to 81% and 68%, respectively. Mandhane noted two things: that the use of superficial velocities included the pipe diameter effects well, and that the effects of the property correction was not very strong, and could usually be neglected. The map of Mandhane et. al. (1974) represented an accurate empirical map, and is shown in Figure 2.9.

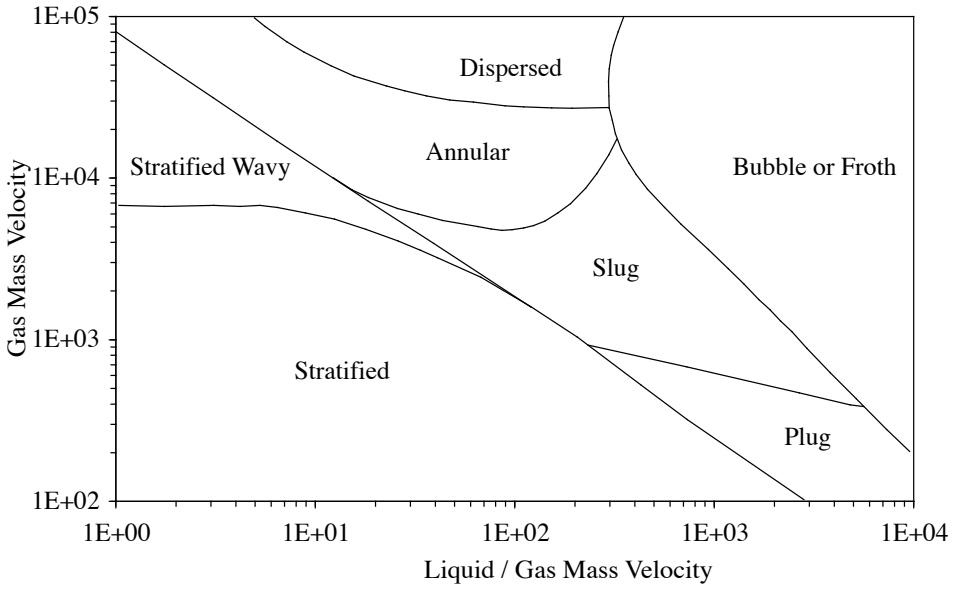

Figure 2.8: Flow regime map of Baker (1954), for air-water & oil-water horizontal cocurrent flow.

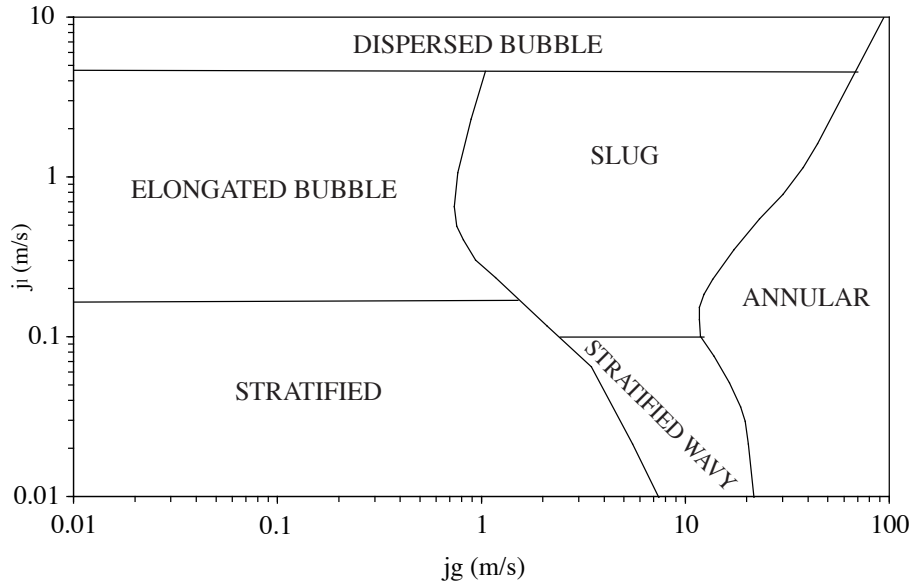

Figure 2.9: Flow regime map of Mandhane (1974), for horizontal gas/liquid cocurrent flow.

2.5.2 Analytical Linear Two-Phase Flow Regime Transition Mapping

Mechanistic modeling of horizontal linear flow regime transitions was first undertaken successfully by Taitel & Dukler (1976). The basis of their analysis is the assumption that all flow regimes can develop from the stratified regime, *regardless* of whether or not the stratified regime actually exists in the flow. Following this assumption, an one-dimensional momentum balance is written for each component, the axial pressure gradients equated, and the equation non-dimensionalized. This produces a single equation for the equilibrium stratified interface height, based on calculable values of the flow. The equilibrium height is defined as the depth of liquid if the flow is constrained to a stratified condition, and represents a calculation of the system void fraction. Next, the mechanisms of transition from the equilibrium stratified regime are formulated, and mapped as transition lines with respect to the non-dimensional parameters of the momentum equation. To determine the flow regime present, the parameters are calculated for the system and checked against the transition locations of the general map.

The schematic of the system analyzed by Taitel & Dukler is shown in Figure 2.10, the general map is depicted in Figure 2.11, and a comparison of the analytic map

of Taitel & Dukler (1976), to the empirical map of Mandhane (1974) is shown in Figure 2.12. The momentum equation and the non-dimensional parameters for the general map (Figure 2.11) are given in Eqs. 2.16 to 2.21. The transition mechanisms are given in Eqs. 2.22 to 2.26.

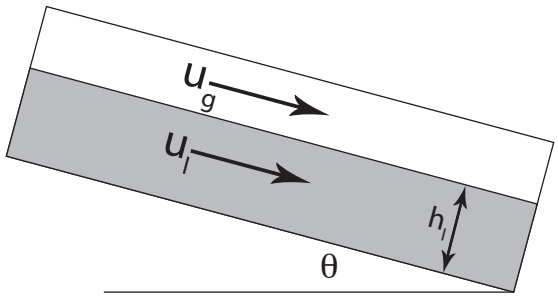

Figure 2.10: Schematic of the system analyzed by Taitel & Dukler (1976).

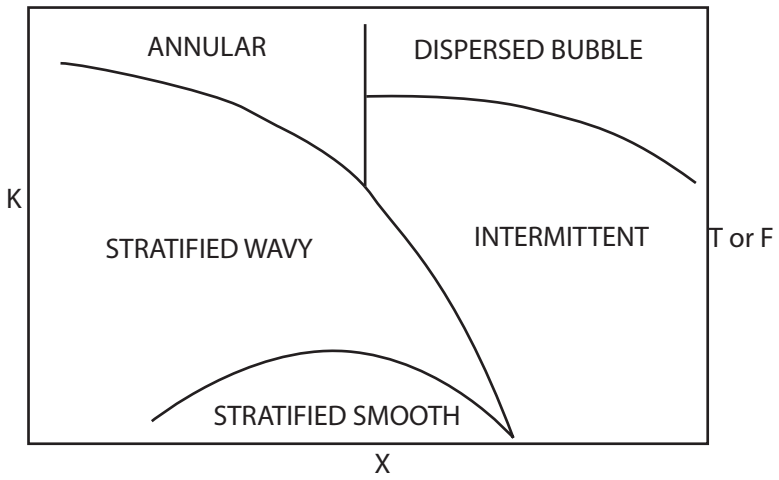

Figure 2.11: General flow regime map of Taitel & Dukler (1976), for horizontal gas/liquid cocurrent flow.

$$X^2 \left[\left(u_l^* D_l^*\right)^{-n} u_l^{*2} \frac{S_l^*}{A_l^*} \right] -$$

$$\left[\left(u_g^* D_g^*\right)^{-m} u_g^{*2} \left(\frac{S_g^*}{A_g^*} + \frac{S_i^*}{A_l^*} + \frac{S_i^*}{A_g^*} \right) \right] - 4Y = 0 \tag{2.16}$$

$$X^2 = \frac{\frac{4C_l}{D} \left(\frac{j_l D}{\nu_l} \right)^{-n} \frac{\rho_l j_l^2}{2}}{4C_g} D \left(\frac{j_g D}{\nu_g} \right)^{-m} \frac{\rho_g j_g^2}{2} = \frac{\left| \left(dP/dx\right)_{j_l} \right|}{\left| \left(dP/dx\right)_{j_g} \right|} \tag{2.17}$$

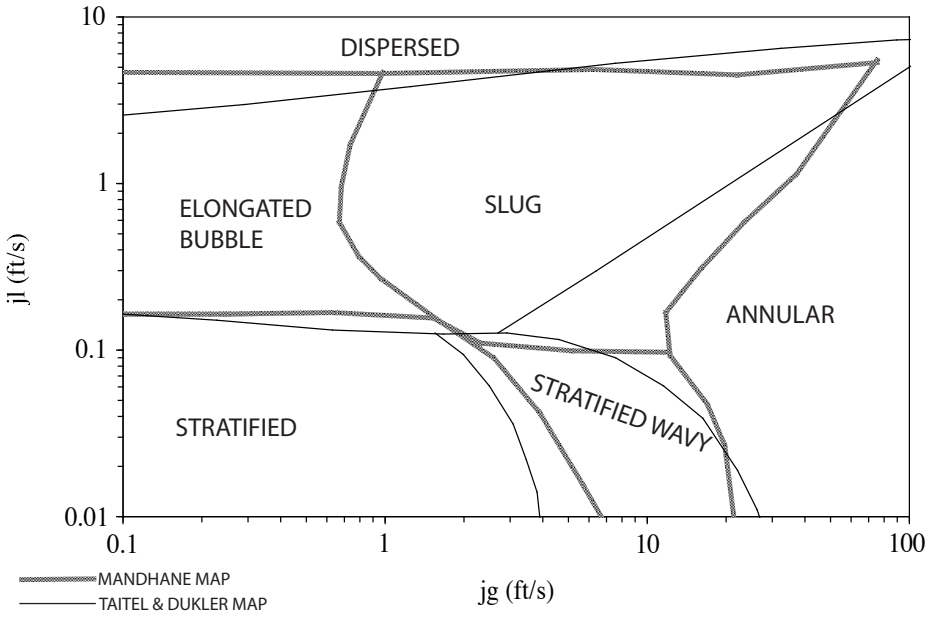

Figure 2.12: Comparison of the analytic map of Taitel & Dukler (1976), with the empirical map of Mandhane (1974). 1" dia. pipe for air-water flow.

$$Y = \frac{(\rho_l - \rho_g)\, g \sin\alpha}{\frac{4C_g}{D}\left(\frac{j_g D}{\nu_g}\right)^{-m} \frac{\rho_g j_g^2}{2}} = \frac{(\rho_l - \rho_g)\, g \sin\alpha}{|\,(dP/dx)_{j_g}\,|} \tag{2.18}$$

$$F = \left(\frac{\rho_g}{(\rho_l - \rho_g)}\right)^{1/2} \frac{j_g}{(Dg\cos\alpha)^{1/2}} \tag{2.19}$$

$$T = \left(\frac{|\,(dP/dx)_{j_l}\,|}{(\rho_l - \rho_g)\, g\cos\alpha}\right)^{1/2} \tag{2.20}$$

$$K = \left(\frac{\rho_g j_g^2 j_l}{(\rho_l - \rho_g)\, g\nu_l \cos\alpha}\right)^{1/2} \tag{2.21}$$

Transition from stratified to either intermittent or annular regimes is defined by the ability of a finite amplitude wave on the surface of the liquid to grow. In the case where sufficient liquid is present to form a competent bridge over the pipe cross-section, an intermittent flow will be established, i.e. $h_l/D \geq 0.5$. If sufficient liquid is *not* present, than the liquid cannot span the core of the flow and will be swept along the sides of the duct to form annular flow, i.e. $h_l/D < 0.5$. Surface wave growth is governed by the mechanism of the Kelvin-Helmholtz instability, i.e. the balance of gravity and inertia forces (Eq. 2.22). Application of this mechanism to the circular

pipe with inclination results in the criterion for this transition (Eq. 2.23).

$$u_g > (1 - h_l^*) \left(\frac{g\,(\rho_l - \rho_g)\,A_g \cos\alpha}{\rho_g \frac{dA_l}{dh_l}} \right)^{1/2} \tag{2.22}$$

$$1 \geq Fr^2 \left(\frac{1}{(1 - h_l^*)^2} \frac{j_g^* \frac{dA_l^*}{dh_l^*}}{A_g^*} \right) \tag{2.23}$$

where

$$Fr = \left(\frac{\rho_g}{(\rho_l - \rho_g)} \right)^{1/2} \frac{j_g}{(Dg\cos\alpha)^{1/2}} \tag{2.24}$$

The transition between stratified and stratified wavy is governed by the balance of pressure and shear forces with those of viscous dissipation, Eq. 2.25.

$$K = Fr^2 Re_{j_l} = \left(\frac{\rho_g j_g^2 j_l}{(\rho_l - \rho_g)\,g\cos\alpha\nu_l} \right)^{1/2} \geq \frac{2}{(0.01 u_l^*)^{1/2} u_g^*} \tag{2.25}$$

Transition between intermittent and dispersed bubble regimes is governed by the balance of forces due to turbulent fluctuations in the liquid and the buoyancy force of the gas phase bubbles, Eq. 2.26. When the former overcomes the latter, the bubbles are pulled into the liquid phase stream.

$$T^2 = \frac{|\,(dP/dx)_{j_l}\,|}{(\rho_l - \rho_g)\,g\cos\alpha} \geq \frac{8A_g^*}{S_i^*\,(u_l^*)^2\,(u_l^* D_l^*)^{-n}} \tag{2.26}$$

2.5.3 Extension of the Analytical Linear Two-Phase Flow Regime Transition Map

The empirical model covered in section 2.5.1 shows the Mandhane map as having $> 80\%$ accuracy in predicting the regimes in an air-water system. The comparison in Figure 2.12 validates the analytical model of Taitel & Dukler (1976) for the data used for Mandhane's (1974) map, and shows the mechanisms considered in the study as appropriate for a large set of experimental observations. Based on the long history of success that this analytical model has enjoyed, many optimizations and modifications have been completed (Barnea 1987, Petalas & Aziz 1998/2000, Wu 1996, Thome 2003, Chen 2001, Zürcher 2002). Precedence for flow regime modeling is taken from the the most popular linear work, and included in the helical model development of section 3.

However, a complete review of the linear mapping methods is not the purpose of this dissertation and only a couple of more recent studies are covered. To this end, the linear mapping techniques of Barnea (1987) and Petelas & Aziz (2000) are taken as appropriate examples of advancement to the original work of Taitel & Dukler (1976).

Barnea and Petalas & Aziz focus on transition criteria that is valid for all inclination angles. For the stratified transition to intermittent flow, both use the Kelvin-Helmholtz stability criteria of the original work (Eq. 2.22). For the sub-regime of stratified-wavy, the authors apply an additional requirement to the shear vs. viscous dissipation of Eq. 2.25. This requirement considers the case of downward flow and the Froude number that represents sufficient dominance of inertia to induce waves. The range of Froude numbers that depict this scenario is 0.5 – 2.2 (Petalas & Aziz 2000), with Barnea and Petalas & Aziz recommending 1.5 and 1.4, respectively. Barnea checks this transition criteria by comparison with data, for downward angles of $\geq$ -1°, and finds good agreement.

$$Fr = \frac{j_l}{\sqrt{h_l g}} = \begin{cases} 1.5 & : \text{ Barnea (1987)} \\ 1.4 & : \text{ Petalas \& Aziz (2000)} \end{cases} \tag{2.27}$$

Both Barnea and Petalas & Aziz push this scenario further by considering an even greater downward inclination, at which point the stratified wavy regime transitions into annular at reduced gas flow rates, as compared to the horizontal and small inclinations. When the inclination has a strong downward angle, the liquid film *falls* down the duct with a high liquid velocity and small liquid height. The gravity effects begin to shear droplets from the wavy interface, entrain them into the gas core, and deposit them onto the wall. This produces an annular regime similar to the case where the droplet removal was from gas shear alone. Barnea checks this transition criteria by comparison with data, for downward angles of $\geq$ -80°, and finds good agreement. The condition is:

$$j_l \geq \sqrt{\frac{2gr_0\left(1 - h_l^*\right)\cos\alpha}{f_l}} \tag{2.28}$$

The mechanism which separates the annular and intermittent flow regime is similar to the original of Taitel & Dukler (1976), and is considered to exist when sufficient liquid is present to form a competent liquid bridge across the pipe. Taitel & Dukler effectively assumed a sinusoidal development of a wave on the interface, as shown

in Fig. 2.13. If the wave formation is sinusoidal, than an equilibrium liquid height corresponding to $(1 - h_l^*) \leq 0.5$ would have the crest of the wave reaching the top of the pipe before or at the same time as the trough reaching the bottom of the pipe, hence forming a competent bridge. This proved a lucky guess for the intermittent–annular transition, since the wavy interface is rarely a symmetric sine wave.

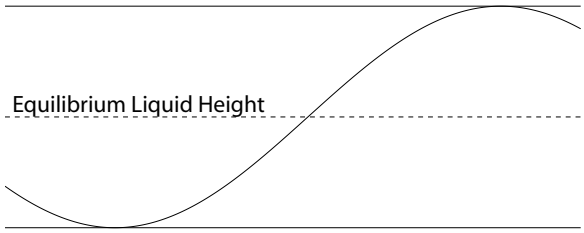

Figure 2.13: Taitel & Dukler assumed wave shape for horizontal gas/liquid cocurrent flow.

The modification by Barnea and Petalas & Aziz is more realistic, and shows where Taitel & Dukler's guess found its lucky value of 0.5. These newer models assume that the transition from intermittent to annular regime occurs when the void fraction *within* a slug body is sufficient that the slug cannot maintain its structure, and breaks up. This condition is met when the maximum volumetric bubble packing fraction inside the slug is reached, with an internal slug void fraction of 0.52. This corresponds to a time averaged equilibrium liquid height around 0.5, and shows the coincidence that assisted Taitel & Dukler. The distinction between models lies in the correlation or model used in calculating the liquid hold up or void fraction. This condition is similar to when bubble migration fails to cause agglomeration, but is specific to vertical and off-vertical geometries with relatively large cross-sections. Basically bubbles in a tank, raising independent of the wall effects.

2.6 Helical Coordinate System Formulation

The previous sections have shown most studies prefer to make the simplifying assumption of toroidal geometry. This completely neglects the effects of torsion and is obviously not an accurate description of a helix, but authors take this approach because the coordinates are orthogonal, and normal education preconditions us for these systems. Moving to a natural coordinate system of a helix will automatically include the relations between the curved geometry and the changes to the formal

equations. However, they are non-orthogonal, a bit tough to handle, and require additional consideration as to the physical components and how they are used. Germano (1988) tried to reconcile the situation by developing a set of governing equations that have the convenience of orthogonality, which was the original reason for using the torus, that is also valid for a non-zero pitch. However, at this point its applicability is contended and it carries the requirement that the curvature and torsion be small ($\kappa < 1$ & $\tau < 1$). The approaches used for the analysis of the helical system with non-negligible torsion are grouped into the orthogonal approaches similar to Germano's, and the non-orthogonal approaches similar to Wang (1981). However, Zabielski & Mestel (1997) note that helical flow cannot be decomposed into components which are orthogonal, so any (including Germanos) orthogonal system is not appropriate. This is in agreement with the findings of the other somewhat contemporary work of Tuttle (1990). The recommendations of Zabielski & Mestel and Tuttle are accepted for this dissertation's development, and the equations will be developed in the more general non-orthogonal forms. However, for completeness, the two methods are contrasted. All other works discovered in the literature review do not vary far from the works of these authors, and are simply listed in the bibliography and not covered in this section.

So what is the actual difference between an orthogonal and non-orthogonal coordinate system, and why is the former preferred? Simply put, the orthogonal basis consists of three mutually orthogonal base coordinate vectors, with intuitively defined physical meanings of the components. A non-orthogonal system does not have these qualities, and its use requires a distinction be made between the covariant and contravariant forms of the basis vectors, introduction of complicated forms for derivatives and metric tensors, and their component's physical meaning is not as simple as the orthogonal definitions. The coordinate system of Tung & Laurence (1975) is a good example of a non-orthogonal system formed by transformation from the orthogonal polar cylindrical system (shown in Fig. 2.14). If any of the terminology of this section is not fully understood, the reader is directed to Appendix A for a short coverage of some background material important to this section.

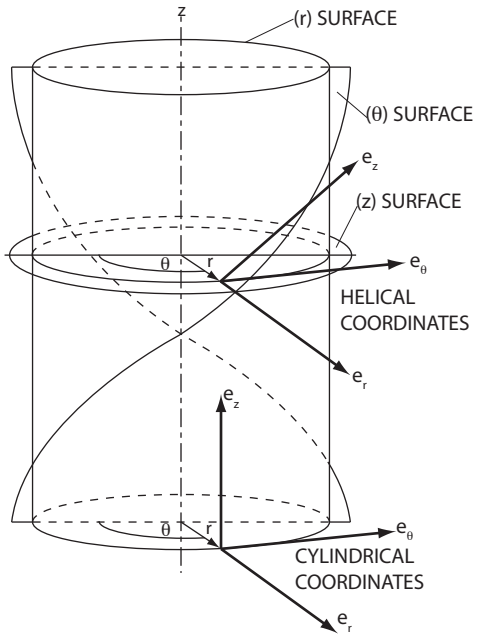

Figure 2.14: Helical Coordinate formulation of Tung (1975). Includes the polar cylindrical frame used for the transformations.

2.6.1 Orthogonal Helical Coordinate Systems

The works of Germano (1982, 1988) and Kao (1987) represent the main orthogonal methods used in helical flow modeling. In Germano's first paper (1982), he developed a locally accurate orthogonal coordinate system that follows a spatial curve (i.e. helix centerline), based on the Frenet triad. He concluded that the torsion is of second order and the curvature is of first order (in their effects on the secondary flow velocities.) His formulation is restricted to small values of curvature and torsion, and did not consider the helix angle effect on gravity's influence with respect to the obliqueness between the plane perpendicular to the axial flow (the plane in which the secondary flow exists.) Germano discusses the coordinate system used by Wang (1981) and how Wang's axial velocity component is not always normal to the perpendicular plane of the secondary flow, and how in his system it is defined as perpendicular. It is uncertain which system this statement is implying as the more physical; especially when considering that the streamwise velocity is indeed *not* perpendicular to the cross-stream plane. This idea brings to the surface the importance of considering the velocity as not being aligned with the base, and how this allows contribution

to made to the secondary flow by axial flow and potentially introduce error in the determination of these quantities.

Germano (1982, 1988) considers a fully developed incompressible single-phase flow through a helix. Since the system is assumed to be fully developed, the velocities are not a function of position along the centerline of the duct, and the problem is essentially a 2-dimensional one. This is the concept of symmetry that will be developed fuller in the helical coordinate formulation in Sec. 3. The coordinate system for this development is defined in Fig. 2.15. In the figure, $\mathbf{x}$ is a position vector describing locations in the cross-stream plane, $\mathbf{R}(s)$ a vector describing the location of the cross-stream plane origin along the duct centerline, $\mathbf{b}$ is the binormal base vector, $\mathbf{n}$ is the normal base vector, $\mathbf{t}$ is the tangent base vector, s is the parameter along the centerline, and P is the point located by $\mathbf{x}$.

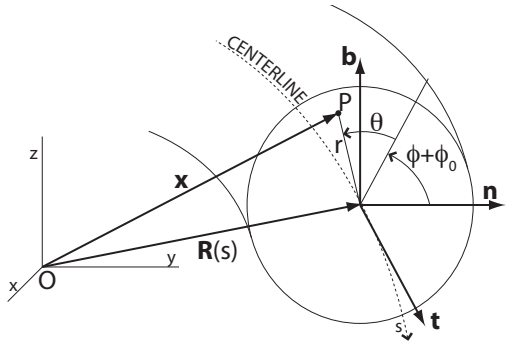

Figure 2.15: Helical Coordinates used by Germano (1982, 1988). Note that the azimuthal angle is measured from a position that is rotated away from the normal $\mathbf{n}$ base, and a function of the.

In order to define the new helical coordinate system, its components must be referenced to a known system. Germano chooses to make the transformation from the Cartesian system, whose origin is the point O, and whose axes are the lines x, y, and z, of Fig. 2.15. Using the Cartesian system as the originator, the position vector $\mathbf{x}$ can be constructed with the Cartesian position vector $\mathbf{R}(s)$ and the components of the normal and binormal bases that place the point P in the cross-plane. Since the position vector $\mathbf{R}(s)$, the normal base $\mathbf{n}$, and the binormal base $\mathbf{bB}$ all lie in the same plane, and the plane is a function only of the symmetry parameter s, the construction is simply a linear combination of these components (Eq. 2.29). It is the offset from the normal base by an arc length dependent value that provides for an orthogonal system in Germano's approach. Germano determines this value of offset

rotation $\phi(s)$, by integrating the torsion from an initial rotation from the normal base of $\phi_0 = \pi/2$ (Eq. 2.30), and effectively integrates the torsion contribution into this $\phi(s)$ term. This integration results in the orthogonal metric given in Eq. 2.31, and a set of conservation equations found in the publication.

$$\mathbf{x} = \mathbf{R}(s) + r\cos\left(\theta + \phi(s) + \phi_0\right)\mathbf{n}(s) + r\sin\left(\theta + \phi(s) + \phi_0\right)\mathbf{b}(s) \tag{2.29}$$

$$\phi(s) = -\int_{s_0}^{s} \tau(\bar{s})d\bar{s} \tag{2.30}$$

$$d\bar{x}\cdot d\bar{x} = \left(1 + \kappa r\sin\left(\theta + \phi\right)\right)^2 (ds)^2 + (dr)^2 + r^2\left(d\theta\right)^2 \tag{2.31}$$

Kao (1987) looked at the effect of torsion for steady helical pipe flow. His analysis took two routes: a series solution representing the analytical analysis and a numerical solution; both of which are based on Germano's approach. The series expansion solution is not applicable for larger curvature and/or larger Dean numbers ($De >$ 96), so the numerical analysis was completed to extend the work to more flows. Kao concludes that the effect of helicity (torsion) is not negligible for ratios of curvature to torsion around unity or greater. This does not seem to have an appreciable effect on the pressure gradient, but it can greatly distort the secondary flow pattern and presumably the regime transitions: The results obtained in these cases for both small and moderately high Dean numbers seem to show that a small torsion may cause a significant change in the secondary flow pattern. The series solution results show that the effect of helicity is to render the flow asymmetric, as compared to the symmetric solutions for zero pitch.

Kao finds, for similar Dean numbers, that the numerical and analytical solutions show good qualitative agreement. Kao is also in agreement with previous authors results that the flow resistance in a helical pipe is less than in a curved pipe with zero pitch. This shows the effect of pitch is to reduce the resistance to flow. Since curvature increases resistance and helicity reduces it, the effects can cancel each other out and give false understanding of the flow in helical pipes, especially when just considering the pressure gradients as many studies have done. Kao shows for Dean numbers between 2000 and 5000 that the flow structure is definitely changed with helicity. The upper vortex being diminished while lower vortex structure becomes dominant. These effects are found to be a function of the ratio of torsion to curvature, which is simply the ratio of the pitch to the coil radius, more than simply on either parameter alone. This set of observations are generally in agreement with previous

works. However, the results of Kao (1987) and Germano (1982) are not in total agreement, even though they use the same coordinate system. The difference is in Kao's finding an effect on the secondary flow of the power of 1.5, instead of the second order effect of Germano. Kao offers the explanation that the helical systems requirement of a non-orthogonal coordinate system for fundamental formulation of the governing equations is the major impediment to advances in the study of this system, and implies that the orthogonality of these equations is not completely realistic.

2.6.2 Non-Orthogonal Helical Coordinate Systems

Non-orthogonal helical flow modeling can be summed up by the works of Wang (1981) and Tuttle (1990). The first author, Wang (1981), introduced a non-orthogonal coordinate system in a fashion very similar to that of Germano (1982); and in fact is the starting point for Germano's formulation. Wang uses a similar transformation from the Cartesian system, and also similarly defines the position within the helical pipe cross-stream plane as the linear combination of helix centerline position vector and local two-dimensional cross-stream vectors. This approach is detailed in Sec. 2.6.1, so it is not repeated here. Wang also uses the Frenet triad and accompanying definitions of torsion and curvature. The system differs from Germano's approach in that the θ value is measured from the normal vector $\mathbf{n}$, and not advanced as a function of the torsion. Wang's system is shown in Fig. 2.16. Not using an advancing θ coordinate results in the cross-stream position defined by Eq. 2.32, and the metric of Eq. 2.33.

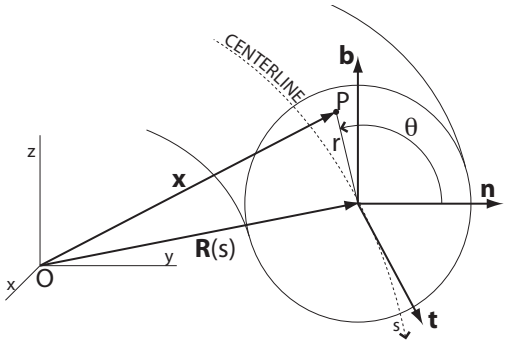

Figure 2.16: Helical Coordinates used by Wang (1981). Note that the azimuthal angle is measured from the normal $\mathbf{n}$ base.

$$\mathbf{x} = \mathbf{R}(s) + r\cos\theta\mathbf{n}(s) + r\sin\theta\mathbf{b}(s) \tag{2.32}$$

$$d\bar{x}\cdot d\bar{x} = \left((1-\kappa r\cos\theta)^2 + \tau^2 r^2\right)(ds)^2 + (dr)^2 + r^2(d\theta)^2 + 2\tau r^2 ds d\theta \tag{2.33}$$

The last term on the right hand side of Eq. 2.33 is where the non-orthogonality of Wang's approach first shows up. If one notes that the metric is given by $ds^2 = g_{ij}dx^i dx^j$, using the covariant metric tensor of g_{ij}, then the components of the covariant metric tensor are simply the coefficients in Eq. 2.33. Using the definitions given in Appendix-A, the contravariant metric tensors and non-zero Christoffel symbols are determined to be those of Eq. 2.34 and Eq. 2.35, respectively. With these objects defined, Wang presents the tensorial form of the Navier-Stokes & conservation of mass equations as Eq. 2.36 and Eq. 2.37, respectively. The variables G and M are given by Eqs. 2.38, and the covariant derivative ($v^i_{,jk}$) is given in Eq. 2.39.

$$\begin{aligned} g^{11} &= 1 & g^{22} &= \frac{\left((1-\kappa r\cos\theta)^2 + \tau^2 r^2\right)}{r^2(1-\kappa r\cos\theta)^2} \\ g^{13} &= 0 & g^{23} &= \frac{-\tau}{(1-\kappa r\cos\theta)^2} \\ g^{12} &= 0 & g^{33} &= \frac{1}{(1-\kappa r\cos\theta)^2} \end{aligned} \tag{2.34}$$

$$\begin{aligned} \Gamma^1_{22} &= -r & \Gamma^2_{13} &= \frac{\tau}{M}\left(\frac{G}{r} - \frac{1}{2}\frac{\partial G}{\partial r}\right) \\ \Gamma^1_{23} &= -\tau r & \Gamma^3_{13} &= -\frac{r\tau^2}{M} + \frac{1}{2M}\frac{\partial G}{\partial r} \\ \Gamma^1_{33} &= -\frac{1}{2}\frac{\partial G}{\partial r} & \Gamma^3_{23} &= \frac{1}{2M}\frac{\partial G}{\partial \theta} \\ \Gamma^2_{21} &= \frac{1}{r} & \Gamma^2_{33} &= \frac{G}{r^2 M}\left(r^2\frac{d\tau}{ds} - \frac{1}{2}\frac{\partial G}{\partial \theta}\right) - \frac{\tau}{2M}\frac{\partial G}{\partial s} \\ \Gamma^2_{23} &= -\frac{\tau}{2M}\frac{\partial G}{\partial \theta} & \Gamma^3_{33} &= \frac{\tau}{M}\left(r^2\frac{d\tau}{ds} - \frac{1}{2}\frac{\partial G}{\partial \theta}\right) + \frac{1}{2M}\frac{\partial G}{\partial s} \end{aligned} \tag{2.35}$$

$$\frac{\partial v^i}{\partial t} + v^j \left(\frac{\partial v^i}{\partial x^j} + \Gamma^i_{\alpha j} v^\alpha \right) = -\frac{g^{ij}}{\rho} \frac{\partial p}{\partial x^j} + \nu g^{kj} v^i_{,jk} \tag{2.36}$$

$$\frac{\partial v^i}{\partial x^i} + \Gamma^i_{\alpha i} v^\alpha = 0 \tag{2.37}$$

$$where \quad M \equiv (1 - \kappa r \cos\theta)^2 \quad and \quad G \equiv (1 - \kappa r \cos\theta)^2 + \tau^2 r^2 \tag{2.38}$$

$$v^i_{,jk} = \frac{\partial^2 v^i}{\partial x^k \partial x^j} + \Gamma^i_{j\alpha} \frac{\partial v^\alpha}{\partial x^k} + \Gamma^i_{\alpha k} \frac{\partial v^\alpha}{\partial x^j} - \Gamma^\alpha_{jk} \frac{\partial v^i}{\partial x^\alpha} + \left(\frac{\partial \Gamma^i_{j\alpha}}{\partial x^k} + \Gamma^i_{\beta k} \Gamma^\beta_{j\alpha} - \Gamma^\beta_{jk} \Gamma^i_{\beta\alpha} \right) v^\alpha \tag{2.39}$$

Here one starts to feel the complexity of the non-orthogonal methods, and understands why they are usually avoided! Wang takes the physical velocities in the (r, θ, s) directions and relates them to the tensorial velocity components; then he develops and solves the equations for small curvature and torsion. He concludes that the effects of curvature and torsion are most pronounced in low Reynolds number flows ($Re \approx 1$), and that they may dominate the secondary flow pattern while destroying the Dean flow. Wang (1981) concludes that torsion is not negligible when the Reynolds number is less than 20, and can disrupt the dual rotating pattern to the point of setting up a single vortex. Wang observed that though the torsion can dominate the secondary flow, it has negligible effect on axial flow rates. Wang's findings add to the disagreement seen in the previous section between the results of Kao (1987) and Germano (1982), and are actually not in agreement with either! Kao calculates a torsion effect on secondary flow to the power of 1.5, Germano calculates a second order effect, and Wang calculates a first order effect! It seems that the more work that is done on this topic, the less understanding one gains. This is not actually the case, and it comes to light that the individual works are not incorrect in their formulation, rather the differences stem from their interpretation! Particularly, the different interpretations vary due to the use of tensorial methods and the fact that proper attention is not paid to the differences between the covariant, contravariant, and physical velocities.

These differences were apparent to those working on the helical flow problem, and there have been attempts at reconciling the studies by Germano 1988, Kao 1987, and Tuttle 1990. The analysis and explanation of Tuttle (1990) is presented here; as it is the latest of the studies, considers all the works externally, and is a particularly clear presentation of this issue and its resolution. Tuttle constructs two systems: one orthogonal and similar to the approach of Germano (1982), and one non-orthogonal

and similar to the approach of Wang (1981). In both cases, he uses a rectilinear local cross-plane coordinate system instead of a curvilinear one. Tuttle's orthogonal system rotates the local axes by an angle which matches that of the torsion, where the non-orthogonal local system does not rotate with the torsion. He refers to the two systems as space-centered and body-centered, respectively. The differences of these systems are illuminated by comparing Fig. 2.15, Fig. 2.16, and Fig. 2.17.

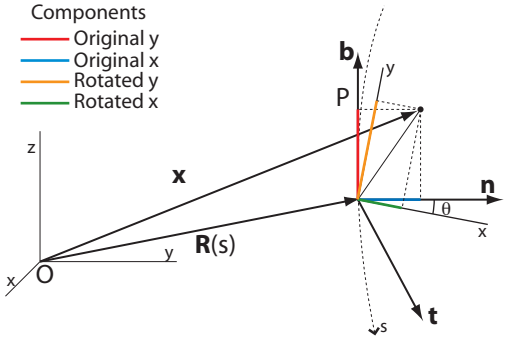

Figure 2.17: Helical Coordinates used by Tuttle (1990). Note that both the x and y local coordinates are transformed by the progression of the angle measured from the normal **n** base.

It is beyond the scope of this dissertation to present all of Tuttle's; rather, it is in the insight provided by this study that its value lies. Tuttle's observations and conclusions are that ***orthogonal local systems***:

- have boundary conditions invariant with respect to s.
- allow vector formulation of the continuity and Navier-Stokes equations.
- do not have a natural relationship between the cross-sectional equations and the local Frenet triad.
- do not allow a stream-function to be defined for the cross-stream velocities.
- do not allow the calculation of a two-dimensional secondary flow, and hence incorrectly predict its dependence on torsion.
- does not correctly describe the flow rate calculation along the helix axis, by integration of the axial velocity.

Tuttle's observations and conclusions are that ***non-orthogonal local systems***:

- do not have invariant boundary conditions with respect to s.

- require tensorial formulation of the continuity and Navier-Stokes equations.
- have a natural relationship between the cross-sectional equations and the local Frenet triad.
- allow a stream-function to be defined for the cross-stream velocities.
- allow the calculation of the two-dimensional secondary flow as first calculated by Dean (1927).
- provide the correct axial velocity (i.e. the covariant form); and as a result, provides the correct calculation of the axial flow rate, by the integration of this velocity over the cross-section.

Tuttle's work comprehensively addresses the issue of the effects of torsion and the natural formulation of the problem for its description. It was shown that the approaches of Germano (1982, 1988) and Wang (1981) are both correct in their construction, and it is only in their interpretation that the differences arise. Tuttle recommends that a non-orthogonal system be used.

2.7 Literature Review Summary

The literature review identified the important aspects of helical flow and the previous works that provide information on how to handle these aspects. The contributions of the different sections found in the literature review, and what information is gotten from each section, is summarized as follows.

In the modeling of the helical flow regime transitions, a two-fluid approach is taken that is similar to that of Taitel & Dukler (1976). This dissertation's approach applies the same "mechanisms of transition" that has been validated many times for the linear system of Taitel & Dukler, and also utilizes similar assumptions about the flow. The linear approach is detailed in section 2.5. The linear and helical systems are apparently different and cannot use the same closure formula. This difference is handled by the works found in the single-phase helical sections (Sections 2.1 and 2.2), which provide validated formula for the friction factors and transition criteria for helical flows. Shear stress takes the usual form for a Newtonian fluid. Data for evaluating the model resulting from this dissertation's work is gotten from the published works presented in Sec. 2.3. Lastly, the desired coordinate system for the helical flow equations is shown in Sec. 2.6 to be a non-orthogonal system in

tensorial form; however, the current effort represents the first attempt of resolving this system with respect to two-phase flow regime transition, and as a first step, the effect of torsion is only identified inasmuch as what part of the mathematics lead to their inclusion. This makes the new model one that includes the stronger of the two forces present in the helical geometry, and is inline with all of the helical single-phase study's conclusion that the curvature effects are of greater import than torsion. The implementation of this idea in the model is affected by considering a general development of the conservation equations from the tensorial form, i.e. the same methods for a model that would eventually include both torsion and curvature, but only proceeding with the case where the pitch is neglected. By taking this approach, instead of simply utilizing a toroidal transformation from Cartesian coordinates, the foundation for a future "all inclusive" model is provided.

3 HELICAL FLOW MODEL DEVELOPMENT

The methods for the helical flow model are based on the insights provided in the literature review. Basically, the helical model is an application of the successful linear methodology to a toroidal coordinate formulation that includes the centrifugal forces. However, as mentioned in the literature review summary, this is a first attempt at the two-phase regime transition modeling, so it is simplified by use of the toroidal assumption. Development evolves by:

- Setting up of an appropriate coordinate system (Sec. 3.1) that provides the foundation for advancement of the new model to the "next stage" of torsion inclusion.
- Writing of the conservation equations in the toroidal coordinate frame (Sec. 3.2).
- Develop the one-dimensional area averaged momentum equations. (Sec. 3.3)
- Develop a predictive method for calculating the equilibrium liquid height, which is accurate in both the linear and curved flows (Sec. 3.4).
- Develop transition mechanisms that describe the physical phenomena which determine flow regime (Sec. 3.5).

3.1 Coordinate System Development

In order that the governing equations be written for the toroidal system, from a general vectoral form, it is required that the metric coefficients be determined. Then the continuity equation and momentum equations can be developed for the toroidal system, by considering the condition of a negligible pitch. This more general approach allows firm understanding of the equations, and the emergence of torsion and curvature terms; and given the universal form of the moving coordinate system, the current development can be logically extended to the finite pitch condition of a helix, or one of its derivatives such as the geometry found in a spiral heat exchanger.

In spite of the disagreement found in the results of the reviewed analyses, the route to the coordinate descriptions are all the same, and can be extended from the works of Wang (1981), Germano (1982), and Tuttle (1990) to be gotten in four steps:

1. Designate a fixed global reference frame.
2. Describe an arbitrary smooth curve through space using a moving trihedron.
3. Define the torus centerline as the smooth curve and symmetry direction.
4. Develop the relation between points in the pipe cross-section back to the fixed frame

The final description of the system is only valuable if the observer can come to grips with the physical quantities of that system. Given the goal of this dissertation to predict flow regimes in a two-phase fluid system, where the prevailing regime is determined by the forces acting on the fluids and their resulting motion, and that the fluid dynamics of this system is embedded in Euclidian 3-space (E^3), the formulation of the system must ultimately be described in terms of this space. This is the reason for the first step in the above list, and the motivation for use of the classical Cartesian system. One achieves this infrastructure by designating a fixed point in space as the origin of the global system (O), and three mutually orthogonal straight lines that pass through the origin (Ox, Oy, Oz) as the coordinate directions. Let unit length vectors originate and coincide with each of these coordinate directions, and define them as the basis for the global system ($\mathbf{e}_x$, $\mathbf{e}_y$, $\mathbf{e}_z$). The global system is shown in Fig. 3.1, and additional information of E^3, the Cartesian system, and the basis is given in Appendix A.

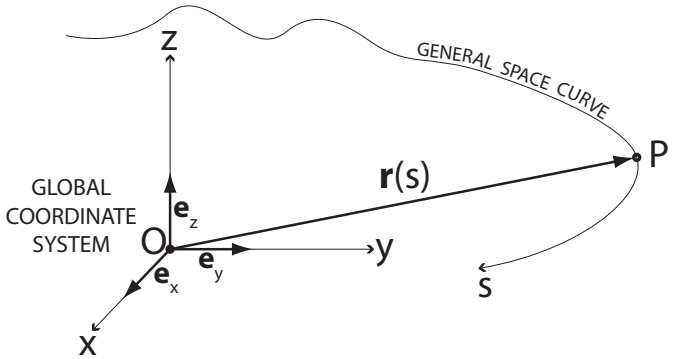

Figure 3.1: Description of an arbitrary smooth space curve with a global coordinate system.

Let the smooth space curve be defined as the parametric function $\mathbf{r} = \mathbf{r}(t)$, where the parameter t is simply an independent value upon which the function $\mathbf{r}$ maps out

a set of points in space as t varies over the real line (i.e. the set of real numbers.) For this parametric representation to be permissible, it is sufficient that the function $\mathbf{r}(t)$ is of class C^2 (i.e. second order differentiable with respect to t) and not everywhere zero valued. It can be helpful in understanding if one visualizes the points in space defined by $\mathbf{r}$ as being constructed sequentially in time, and take the independent parameter t as time-like.

With respect to the global coordinate system defined above, the function $\mathbf{r}(t)$ produces three scalar components ($x(t)$, $y(t)$, $z(t)$) that multiply the base vectors of the system to provide a unique description of the space curve ($\mathbf{r}(t) = x(t)\mathbf{e}_x + y(t)\mathbf{e}_y + z(t)\mathbf{e}_z$). However, since the curve that is to be considered describes a toroidal pipe fixed in space, it is necessary that the curve description be a function of one of the pipe's parameters. A change of parameters from the general one, to the path position along the curve, achieves this. This path position is readily defined by taking an arbitrary curve point as the origin of the parameter related to a value of $t = t_0$, and measuring the distance along the curve from this origin to the path position related to a value of $t = t_1$. It can be shown that this change of parameters is permissible, and the curve distance is defined by the arc length given Eq. 3.1a. The natural representation of the torus is then determined by taking the integral of the parametric representation (substitute Eq. 3.1b into Eq. 3.1a), and substituting $t = t(s)$ back into the parametric representation; this yields Eq. 3.1c.

$$s(t) = \int_{t_0}^{t_1} |d\mathbf{r}/dt| dt \tag{3.1a}$$

$$\mathbf{r}(t) = a\cos t\mathbf{e}_x + a\sin t\mathbf{e}_y \tag{3.1b}$$

$$\mathbf{r}(s) = a\cos\left(\frac{s}{a}\right)\mathbf{e}_x + a\sin\left(\frac{s}{a}\right)\mathbf{e}_y \tag{3.1c}$$

The local moving coordinate system is quickly constructed using this natural representation. The first moving base of the trihedron is defined as the derivative of the natural representation (Eq. 3.1c), and represents a vector of unit length everywhere tangent to the curve. The second moving base is found by normalizing the second derivative of the natural representation, and represents a vector of unit length that is everywhere parallel to the curvature and orthogonal to the tangent base. The third base is simply the cross-product of the tangent and normal bases, and, by the character of the cross-product, is everywhere orthogonal to both the normal and tangent

bases. The moving trihedron is shown in Fig. 3.2, and the mathematical descriptions are given in Eqs. 3.2. It is interesting that Wang (1981) and Germano (1982) appear to have their normal base oriented in the wrong direction; since their definition is exactly the same as the one shown in Eq. 3.2b, the normal should indeed point in the direction of curvature. This can be checked by comparing Fig. 3.2 with Fig. 2.16 or Fig. 2.15. Tuttle (1990) however has the same alignment as that shown in Fig. 3.2, and correctly corresponds to the relationship between the normal vector and curvature.

$$\mathbf{t} = \frac{d\mathbf{r}}{ds} \qquad \text{unit tangent vector} \tag{3.2a}$$

$$\mathbf{n} = \frac{\frac{d^2\mathbf{r}}{ds^2}}{|\frac{d^2\mathbf{r}}{ds^2}|} \qquad \text{unit normal vector} \tag{3.2b}$$

$$\mathbf{b} = \mathbf{t} \times \mathbf{n} \qquad \text{unit binormal vector} \tag{3.2c}$$

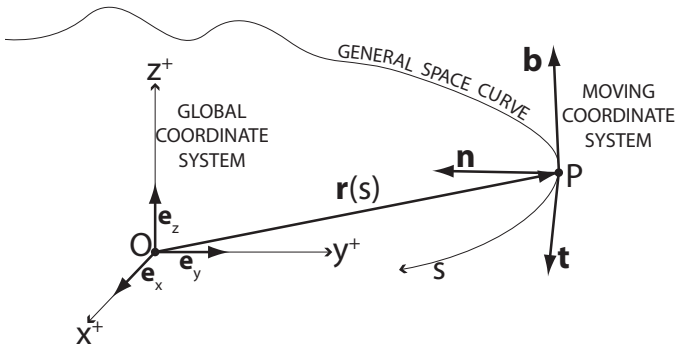

Figure 3.2: Description of an arbitrary smooth space curve with the moving coordinate system.

Eqs. 3.2 have the favorable characteristic of satisfying the set of equations known as the as the Serret-Frenet equations (shown in Eqs. 3.3.) Inspecting these equations illuminates the fact that any smooth curve based on the moving trihedron, and obeying the Serret-Frenet equations, is uniquely defined by the curvature ($\kappa(x^i)$) and torsion ($\tau(x^i)$) scalar fields; and in the toroidal case, have the simpler form of

Eqs. 3.4.

$$\dot{\mathbf{t}} = \frac{d\mathbf{t}}{ds} = \kappa\mathbf{n} \tag{3.3a}$$

$$\dot{\mathbf{n}} = \frac{d\mathbf{n}}{ds} = -\kappa\mathbf{t} + \tau\mathbf{b} \tag{3.3b}$$

$$\dot{\mathbf{b}} = \frac{d\mathbf{b}}{ds} = -\tau\mathbf{n} \tag{3.3c}$$

$$\dot{\mathbf{t}} = \frac{d\mathbf{t}}{ds} = \kappa\mathbf{n} \tag{3.4a}$$

$$\dot{\mathbf{n}} = \frac{d\mathbf{n}}{ds} = -\kappa\mathbf{t} \tag{3.4b}$$

$$\dot{\mathbf{b}} = \frac{d\mathbf{b}}{ds} = 0 \tag{3.4c}$$

The last step in developing the toroidal coordinate system, is to relate the description methods just developed to points inside a toroidal pipe. Since the above method is appropriate for a class C^2 curve, and a circle is of this class, the torus smooth curve is set as a function of the arc length (Eq. 3.1c.) The pipe flow domain is then constructed by projecting the cross-sectional area of the pipe along the length of this curve. In this way, specifying the location of a point in the cross-section and the cross-section's path length, allows all locations inside the domain to be uniquely defined, and extension of the model strategy to a true helix can be started by specifying a helix as the smooth curve instead of a circle. Taking the cross-section point to have a global position vector $\mathbf{x}$, the working toroidal coordinate system is related to the moving triad by choosing the descriptive directions of (r, θ, s). This working system is shown in Fig. 3.3, and is such that the global point position vector $\mathbf{x}$ has the form of Eq. 3.5. It is with these (r, θ, s) coordinates that the continuity and conservation of momentum equations are formulated.

$$\mathbf{x} = \mathbf{r}(s) - r\cos\theta\mathbf{n}(s) + r\sin\theta\mathbf{b}(s) \tag{3.5}$$

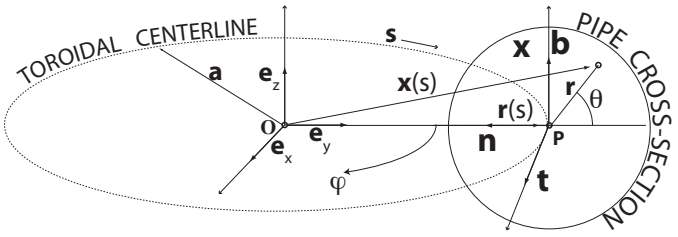

Figure 3.3: Local coordinate system description of the helical pipe.

3.2 Helical Conservation Equations

Given that we are working in Euclidian space, the accuracy of the correct toroidal conservation equations can be checked simply by comparing the vectorally developed equations developed from the derived coordinate description, to the form arived at from transforming the usual Cartesian equations. The first step of this approach is the method of Aris (1962), which in turn relies much on the historic works in *Handbuch der Physik III/1*, by Truesdell, Serrin, and Noll. The metric and metric tensor for the system are found by comparison of Eq. A.14 to the scalar product of total derivative of the position vector, with itself. This derivative is found by considering Eqs. 3.2, when differentiating Eq. 3.5. The steps are shown in Eqs. 3.6, and the resulting metric for the working coordinate system is shown in Eq. 3.7.

$$\frac{d\mathbf{x}}{ds} = \frac{d\mathbf{r}}{ds} - \frac{d}{ds}\left(r\cos\theta\mathbf{n}(s)\right) + \frac{d}{ds}\left(r\sin\theta\mathbf{b}(s)\right) \tag{3.6}$$

$$= \mathbf{t} - r\left(\cos\theta\frac{d\mathbf{n}(s)}{ds} + \mathbf{n}(s)\frac{d\cos\theta}{ds}\right) - \cos\theta\mathbf{n}(s)\frac{dr}{ds} \quad (^{\downarrow})$$

$$+ r\left(\sin\theta\frac{d\mathbf{b}(s)}{ds} + \mathbf{b}(s)\frac{d\sin\theta}{ds}\right) + \sin\theta\mathbf{b}(s)\frac{dr}{ds} \quad (^{\downarrow})$$

$$d\mathbf{x} = \left(1 + \kappa r\cos\theta\right)\mathbf{t}ds + \left(\cos\theta\mathbf{b} + \sin\theta\mathbf{n}\right)rd\theta + \left(\sin\theta\mathbf{b} - \cos\theta\mathbf{n}\right)dr \quad (^{\downarrow})$$

$$d\mathbf{x} = \left(a + r\cos\theta\right)d\phi\mathbf{t} + rd\theta\mathbf{e}_\theta + dr\mathbf{e}_r \quad (.)$$

Where $\mathbf{e}_\theta = \sin\theta\ \mathbf{n} + \cos\theta\ \mathbf{b}$, $\mathbf{e}_r = \sin\theta\ \mathbf{b} - \cos\theta\ \mathbf{n}$, and $ds = a\ d\phi$ $(or\ d\phi^2 = \frac{ds^2}{a^2})$,

the dot product is $\mathbf{f} \cdot \mathbf{g} = f_i g_i$, and the square of the arc length is given by,

$$d\mathbf{x} \cdot d\mathbf{x} = (a + r\cos\theta)^2 \, d\phi^2 + r^2 d\theta^2 + dr^2 \tag{3.7}$$

$$= (a + r\cos\theta)^2 \, \frac{ds^2}{a^2} + r^2 d\theta^2 + dr^2 \tag{.}$$

Note: when equation sets with a single number have many components, the equation number is given on the first component, with continuation arrows (↓) labeling the rest of the components up to the last; the last component is indicated by a period (.).

$$d\mathbf{x} \cdot d\mathbf{x} = g_{ij} dx^i dx^j = \frac{\partial y^k}{\partial x^i} \frac{\partial y^k}{\partial x^j} dx^i dx^j \tag{3.8}$$

$$g_{ij} = \begin{bmatrix} 1 & 0 & 0 \\ 0 & r^2 & 0 \\ 0 & 0 & N^2 \end{bmatrix} \tag{3.9}$$

where $N = \frac{(a + r\cos\theta)}{a} = (1 + r\kappa\cos\theta)$

The metric is found to be orthogonal due to none of the off diagonal terms in the metric tensor matrix having a non-zero value, i.e. $g_{ij} = 0$ for $i \neq j$ of Eq. 3.9. Off diagonal non-zero terms would make the scalar product of the metric tensor with itself not equal to the identity matrix; which is the condition for an orthogonal matrix. Since the system is orthogonal, the metric tensor components of Eq. 3.9 can be related to the scale factors, and used in the vector form of the Navier-Stokes equations, shown in Eq. 3.11 as given on page 350 of Sokolnikoff (1964). The scale factor to metric tensor relationship is described on p. 143 of Aris (1962) as $g_{ii} = h_i^2$, with the resulting scale factors for the current development shown in Eq. 3.10. The toroidal momentum equations are then found by substituting the toroidal form of the vector operations for the toroidal system (Eq. B.13, Eq. B.14, and Eq. B.15) into the vector form of the Navier-Stokes equations (Eq. 3.11). The result is shown in Eq. 3.13, with the individual components shown in Eq. 3.14.

$$h_i = \begin{bmatrix} 1 \\ r \\ N \end{bmatrix} \tag{3.10}$$

$$\rho \left(\mathbf{v} \cdot \nabla \mathbf{v} \right) = -\nabla p + \mu \nabla^2 \mathbf{v} + \rho \mathbf{f} \tag{3.11}$$

$$\rho\left(\left[-\frac{w^2\kappa\cos\theta}{(1+r\kappa\cos\theta)}\right]\mathbf{e}_r+\left[\frac{w^2\kappa\sin\theta}{(1+r\kappa\cos\theta)}\right]\mathbf{e}_\theta\right)= \tag{3.12}$$

$$-\left(\frac{\partial p}{\partial r}\mathbf{e}_r+\frac{1}{r}\frac{\partial p}{\partial\theta}\mathbf{e}_\theta+\frac{1}{(1+r\kappa\cos\theta)}\frac{\partial p}{\partial s}\mathbf{e}_s\right) \quad (^{\downarrow})$$

$$+\mu\left(\left\{\frac{(1+2r\kappa\cos\theta)}{r\,(1+r\kappa\cos\theta)}\frac{\partial w}{\partial r}+\frac{\partial^2 w}{\partial r^2}-\frac{w\kappa^2}{(1+r\kappa\cos\theta)^2}\right\}\mathbf{e}_s\right)+\rho\mathbf{f} \tag{3.13}$$

$$\frac{\partial p}{\partial r}=\frac{\rho\kappa\cos\theta}{N}w^2+\rho f_r \tag{3.14a}$$

$$\frac{1}{r}\frac{\partial p}{\partial\theta}=-\frac{\rho\kappa\sin\theta}{N}w^2+\rho f_\theta \tag{3.14b}$$

$$\frac{\partial p}{\partial s}=\frac{\mu\,(1+2r\kappa\cos\theta)}{r}\frac{\partial w}{\partial r}+\mu N\frac{\partial^2 w}{\partial r^2}-\frac{\mu\kappa^2 w}{N}+\rho f_s \tag{3.14c}$$

A check of the cylindrical asymptotic form of the axial momentum equation is provided in App. C. The above equations show that the centrifugal forces act in the cross-stream direction only, and specifically play their part through the effective gravity in the mechanisms of transition. Eq. 3.14a, Eq. 3.14b and 3.14c are utilized in averaged forms, for description of the system and model development. The averaging of the above equations is given in the next section.

3.3 One-Dimensional Separated Flow Equations

The linear methods on which the current model is founded, are based on the assumption that all flow regimes *can* develop from an equilibrium stratified flow; regardless of whether or not the stratified case was ever present in the system. This assumption leads to the calculation of the liquid interface height of the equilibrium stratified case (e.g. void fraction); followed by the determination of the system's non-dimensional parameters. The use of a separated one-dimensional model is found in many studies of multi-phase fluid flow analysis, not just in flow regime modeling. The general reasoning of these efforts rely on appropriate averaging of the three dimensional equations, and as detailed by Kocamustafaogullari (1971), the accuracy of phase specific average equation development is applicable as long as the interaction

between the phases is modeled, and this interaction is easily included for the adiabatic separated flow condition. As mentioned above, this is exactly what is used in the current modeling strategy.

Production of the area averaged equations requires the definition of individual averaged values that result from the integration of each equation over the control volumes describing the system. Following the forms provided by Kocamustafaogullari, the area and center of mass averaged values of any general quantity $\Psi(r, \theta, s)$, are defined by Eq. 3.15 and Eq. 3.16. Comparison of Eq. 3.15, and Eq. 3.16 indicates that the center of mass and area averages are equivalent when the density is not a function of position, which is the case in the current development.

$$\ll \Psi \gg (s) = \frac{1}{\mathcal{A}} \iint_{\mathcal{A}} \Psi d\mathcal{A} \tag{3.15}$$

$$< \Psi > (s) = \frac{\iint_{\mathcal{A}} \rho \Psi d\mathcal{A}}{\iint_{\mathcal{A}} \rho d\mathcal{A}} \tag{3.16}$$

The results of all the linear analyses conclude that the distortion introduced by applying an area averaged equation, that is not a function of flow area shape, are acceptably small; as long as the forces acting within the body of the flow are limited to a gravity force. The distinguishing quality of the gravity force that allows this simplification is that it acts equally on all positions inside the flow, i.e. gravity is not a function of position in the flow area. Reviewing Eq. 3.14a, Eq. 3.14b and 3.14c, indicates that the centrifugal forces appear in the r and θ momentum equations only, and not in the s-coordinate equation. This characteristic is due to the component form that the equations are written in. Given that the flow field being considered is not a single-phase enclosed flow, the forces in each direction will actually contribute to the axial momentum through variations in the surface shape. However, the pressure is an isotropic force that acts in all three dimensions equally, and the total pressure at any point in the flow will be the sum of the contributions from the momentum forces acting in all the directions. A mathematical description of this fact is generated by summing Eqs. 3.14, and noting that the LHS of the resulting equation is simply the gradient of the pressure field in cylindrical coordinates. Note, in the equations below the Laplacian of the scalar axial velocity is written using the ∇^2 form. This combined equation is given in Eq. 3.17, and is generally applicable to the individual phases that make up the two-phase flow configuration that includes a variable surface

height. The configuration is displayed in Fig. 3.4 and Fig. 3.5.

$$\nabla p = \frac{\partial p}{\partial r}\mathbf{e}_r + \frac{1}{r}\frac{\partial p}{\partial \theta}\mathbf{e}_\theta + \frac{\partial p}{\partial s}\mathbf{e}_s \tag{3.17}$$

$$= \frac{\rho\kappa\cos\theta}{N}w^2\mathbf{e}_r + \rho f_r\mathbf{e}_r - \frac{\rho\kappa\sin\theta}{N}w^2\mathbf{e}_\theta \qquad (^{\downarrow})$$

$$+ \rho f_\theta\mathbf{e}_\theta + N\mu\nabla^2 w\mathbf{e}_s - \frac{\mu\kappa^2 w}{N}\mathbf{e}_s + \rho f_s\mathbf{e}_s \qquad (.)$$

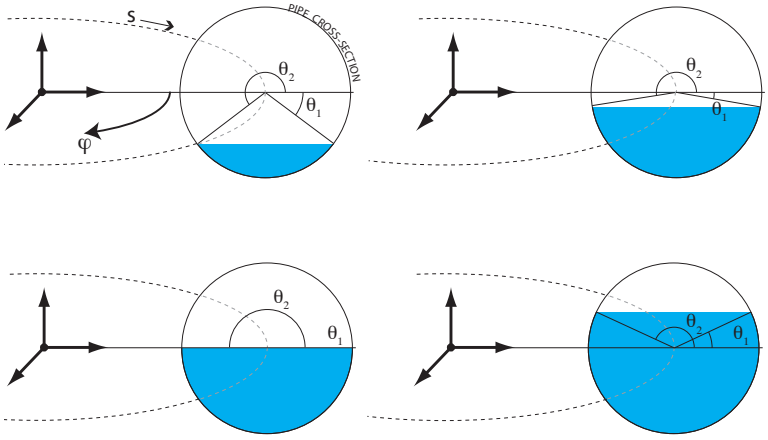

Figure 3.4: Example of the angular limits of integration for area averaging the toroidal axial momentum equation.

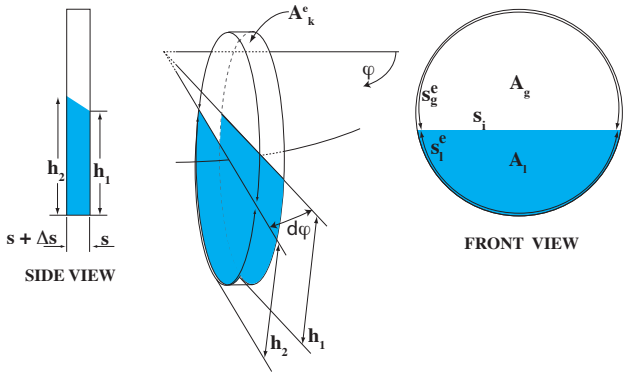

Figure 3.5: Interface locations, and phasic areas, used in development of the axial momentum equation.

Before the momentum equations are integrated over the individual phase regions, it is appropriate to take the projection of the forces acting in the (r, θ) directions onto the vertical direction and the horizontal plane. These projections are physically interpreted as the forces parellel and perpendicular to that of the gravity force. This change in description is a proper one, since the action of the centrifugal forces are always perpendicular to gravity. The transformation is realized by applying the transformations given in Eqs. 3.18 to the RHS of Eq. 3.17, with the resulting axial momentum equation given by Eq. 3.19. As shown in Fig. 3.5, the control volume is the sum of the volume occupied by the gas phase and the volume occupied by the liquid phase; and Eq. 3.19 written for each. For this reason, Eq. 3.19 is not integrated over the entire control volume, rather, it is evaluated for the portion of the control volume occupied by the k^{th} phase.

$$\mathbf{e}_\theta = \sin\theta\ \mathbf{n} + \cos\theta\ \mathbf{b} \tag{3.18a}$$

$$\mathbf{e}_r = \sin\theta\ \mathbf{b} - \cos\theta\ \mathbf{n} \tag{3.18b}$$

$$\nabla p = -\frac{\rho\kappa}{N}w^2\ \mathbf{n} - g\rho\cos\phi\ \mathbf{b} + N\mu\nabla^2 w\mathbf{e}_s - \frac{\mu\kappa^2 w}{N}\mathbf{e}_s - \rho g\sin\phi\mathbf{e}_s \tag{3.19}$$

$$\begin{aligned}
\iiint_{\mathcal{V}_k} \nabla p_k\ d\mathcal{V}_k =& -\iiint_{\mathcal{V}_k} \frac{\rho_k\kappa}{N}w_k^2\ d\mathcal{V}_k\ \mathbf{n} - \iiint_{\mathcal{V}_k} g\rho_k\cos\phi\ d\mathcal{V}_k\ \mathbf{b} && (3.20)\\
&+ \iiint_{\mathcal{V}_k} N\mu_k\nabla^2 w_k\ d\mathcal{V}_k\ \mathbf{e}_s - \iiint_{\mathcal{V}_k} \frac{\mu_k\kappa^2 w_k}{N}\ d\mathcal{V}_k\ \mathbf{e}_s && (\downarrow)\\
&- \iiint_{\mathcal{V}_k} \rho_k g\sin\phi\ d\mathcal{V}_k\ \mathbf{e}_s && (\downarrow)\\
=& -\rho_k\kappa \iiint_{\mathcal{V}_k} \frac{w_k^2}{N}\ d\mathcal{V}_k\ \mathbf{n} + \mu_k \iiint_{\mathcal{V}_k} N\nabla^2 w_k\ d\mathcal{V}_k\ \mathbf{e}_s && (\downarrow)\\
&- \mu_k\kappa^2 \iiint_{\mathcal{V}_k} \frac{w_k}{N}\ d\mathcal{V}_k\ \mathbf{e}_s && (\downarrow)\\
&- \rho_k g\left(\sin\phi\ \mathbf{e}_s + \cos\phi\ \mathbf{b}\right)\int_s^{s+\triangle s} \mathcal{A}_k(s)\ ds && (.)
\end{aligned}$$

The gradient terms can be evaluated in general, using the integral formula of Gauss. This integral formula is the volume analog to the fundamental theorem of

calculus. In short, this theorem states: if F is an antiderivative the continuous function f, which is contained in the closed interval $[a, b]$, than the integral of f is equivalent to the antiderivative evaluated at the limits of the inerval, i.e. $F(b)-F(a)$. This theorem is extendable to any piecewise smooth surface containing the gradient of a scalar or vector field.

$$\iiint_{\mathcal{V}_k} \nabla \cdot \mathbf{f}\ d\mathcal{V}_k = \iint_{\mathcal{A}_k^e} \mathbf{f}_k \cdot \mathbf{n}_k\ d\mathcal{A}_k^e + \iint_{\mathcal{A}_k^i} \mathbf{f}_k \cdot \mathbf{n}_k\ d\mathcal{A}_k^i \tag{3.21}$$

$$+ \iint_{\mathcal{A}_k^{s+\triangle s}} \mathbf{f}_k^{s+\triangle s} \cdot \mathbf{n}_k^{s+\triangle s}\ d\mathcal{A}_k^{s+\triangle s} + \iint_{\mathcal{A}_k^s} \mathbf{f}_k \cdot \mathbf{n}^s\ d\mathcal{A}_k^s \tag{.}$$

Since the flow areas at the upstream and downstream sides of the control volume are always opposite each other, $\mathbf{n}^s = -\mathbf{n}^{s+\triangle s}$. The line integrals of the external and interface boundaries are modeled assuming a constant pipe diameter and a variable liquid interface height. In general, the differential area at the liquid-liquid interface follows the relationship $dA_k^i = (\mathbf{n}_k^i \cdot \mathbf{n}_{S_k})\, dS_k^i ds$. Where $\mathbf{n}_k^i$ is the unit normal of the liquid surface, and $\mathbf{n}_{S_k}$ is the unit normal to the parameter located in the cross-sectional plane. This is simply taking the projection of the differential area in the axial and cross-stream directions. Applying these concepts, and considering the area average defined in Eq. 3.15, Eq. 3.21 becomes Eq. 3.22

$$\iiint_{\mathcal{V}_k} \nabla \cdot \mathbf{f}_k\ d\mathcal{V}_k = \int_s^{s+\triangle s} \int_{S_k^e} \mathbf{f}_k \cdot \mathbf{n}_k^e\ dS_k^e ds \tag{3.22}$$

$$+ \int_s^{s+\triangle s} \int_{S_k^i} \left(\mathbf{f}_k \cdot \mathbf{n}_k^i\right) \left(\mathbf{n}_k^i \cdot \mathbf{n}_{S_k}\right) dS_k^i ds \tag{$^{\downarrow}$}$$

$$+ \iint_{\mathcal{A}_k^{s+\triangle s}} \mathbf{f}_k^{s+\triangle s} \cdot \mathbf{n}_k^s\ d\mathcal{A}_k^{s+\triangle s} - \iint_{\mathcal{A}_k^s} \mathbf{f}_k \cdot \mathbf{n}_k^s\ d\mathcal{A}_k^s \tag{$^{\downarrow}$}$$

$$= \int_s^{s+\triangle s} \int_{S_k^e} \mathbf{f}_k \cdot \mathbf{n}_k^e\ dS_k^e ds + \int_s^{s+\triangle s} \int_{S_k^i} \left(\mathbf{f}_k \cdot \mathbf{n}_k^i\right) \left(\mathbf{n}_k^i \cdot \mathbf{n}_{S_k}\right) dS_k^i ds \tag{$^{\downarrow}$}$$

$$+ \mathcal{A}_k^{s+\triangle s} \ll \mathbf{f}_k^{s+\triangle s} \cdot \mathbf{n}^{s+\triangle s} \gg - \mathcal{A}_k^s \ll \mathbf{f}_k^s \cdot \mathbf{n}^s \gg \tag{.}$$

The first three terms on the RHS of Eq. 3.22, contain integrals of either products

or fractions that are not able to be evaluated without a priori knowledge of the velocity distribution in the (r, θ) directions. This issue is resolved by defining coupling coefficients that represent the tendency of the term's components to exhibit a cause and effect relationship as a function of position, and the covariance of the square of the axial velocity that measures the magnitude to which the average square of the velocity varies with the square of the averaged velocity, and not necessarily the cause and effect relationship. The use of the covariance is typical in the study of fluid flows, and can be shown to have values that vary between 1.024 for single-phase turbulent flow and 1.33 for single-phase laminar flow. No information on the coupling coefficient for the toroidal flow was found by the author, but should also carry a value close to unity. This is correct due to N being a cyclic function that oscillates about unity, such that its integral from 0 to 2π is equal to unity. The coupling coefficients and covariance are defined in Eq. 3.23, Eq. 3.24, Eq. 3.25, and Eq. 3.26. The use of these objects for the first three terms of the RHS of Eq. 3.20, are given in Eq. 3.27, Eq. 3.28, and Eq. 3.29.

$$\mathcal{C}_1 \equiv \frac{\frac{1}{\mathcal{A}_k}\iint_{\mathcal{A}_k}\frac{w_k^2}{N}d\mathcal{A}_k}{\frac{\frac{1}{\mathcal{A}_k}\iint_{\mathcal{A}_k} w_k^2\ d\mathcal{A}_k}{\frac{1}{\mathcal{A}_k}\iint_{\mathcal{A}_k} N d\mathcal{A}_k}} = \frac{\iint_{\mathcal{A}_k}\left(\frac{w_k^2}{N}\right)d\mathcal{A}_k}{\iint_{\mathcal{A}_k} w_k^2 d\mathcal{A}_k} \tag{3.23}$$

$$\mathcal{C}_2 \equiv \frac{\frac{1}{\mathcal{A}_k}\iint_{\mathcal{A}_k}\frac{w_k}{N}\ d\mathcal{A}_k}{\frac{\frac{1}{\mathcal{A}_k}\iint_{\mathcal{A}_k} w_k d\mathcal{A}_k}{\frac{1}{\mathcal{A}_k}\iint_{\mathcal{A}_k} N d\mathcal{A}_k}} = \frac{\iint_{\mathcal{A}_k}\left(\frac{w_k}{N}\right)d\mathcal{A}_k}{\iint_{\mathcal{A}_k} w_k d\mathcal{A}_k} \tag{3.24}$$

$$\mathcal{C}_3 \equiv \frac{\frac{1}{\mathcal{A}_k}\iint_{\mathcal{A}_k} N\mu\nabla^2 w_k\ d\mathcal{A}_k}{\frac{1}{\mathcal{A}_k}\iint_{\mathcal{A}_k} N d\mathcal{A}_k \times \frac{1}{\mathcal{A}_k}\iint_{\mathcal{A}_k}\mu\nabla^2 w_k d\mathcal{A}_k} = \frac{\iint_{\mathcal{A}_k} N\mu\nabla^2 w_k\ d\mathcal{A}_k}{\iint_{\mathcal{A}_k}\mu\nabla^2 w_k d\mathcal{A}_k} \tag{3.25}$$

$$Cov(w^2) \equiv \frac{\frac{1}{\mathcal{A}_k}\iint_{\mathcal{A}_k}(w_k^2)\,d\mathcal{A}_k}{\left(\frac{1}{\mathcal{A}_k}\iint_{\mathcal{A}_k} w_k d\mathcal{A}_k\right)^2} \tag{3.26}$$

$$\rho_k\kappa\iiint_{\mathcal{V}_k}\frac{w_k^2}{N}\ d\mathcal{V}_k\ \mathbf{n} = \rho_k\kappa\int_s^{s+\triangle s}\iint_{\mathcal{A}_k}\frac{w_k^2}{N}\ d\mathcal{A}_k ds\ \mathbf{n} \tag{3.27}$$

$$= \rho_k\kappa\mathcal{C}_1\, Cov(w_k^2)\int_s^{s+\triangle s}\mathcal{A}_k \ll w_k \gg^2 ds\ \mathbf{n} \tag{.}$$

$$\iiint_{\mathcal{V}_k} N\mu\nabla^2 w_k \; d\mathcal{V}_k \; \mathbf{e}_s = \int_s^{s+\triangle s} \mathcal{C}_3 \iint_{\mathcal{A}_k} \mu\nabla^2 w_k d\mathcal{A}_k ds \; \mathbf{e}_s \tag{3.28}$$

$$= \mathcal{C}_3 \iiint_{\mathcal{V}_k} \mu\nabla^2 w_k d\mathcal{V}_k ds \; \mathbf{e}_s \tag{.}$$

$$\mu_k\kappa^2 \iiint_{\mathcal{V}_k} \frac{w_k}{N} \; d\mathcal{V}_k \; \mathbf{e}_s = \mu_k\kappa^2 \int_s^{s+\triangle s} \iint_{\mathcal{A}_k} \frac{w_k}{N} \; d\mathcal{A}_k ds \; \mathbf{e}_s \tag{3.29}$$

$$= \mu_k\kappa^2\mathcal{C}_2 \int_s^{s+\triangle s} \mathcal{A}_k \ll w_k \gg ds \; \mathbf{e}_s \tag{.}$$

Substituing Eq. 3.22, Eq. 3.27, Eq. 3.28, and Eq. 3.29 into Eq. 3.20 results in Eq. 3.30.

$$\int_s^{s+\triangle s} \int_{S_k^e} p_k^e \cdot \mathbf{n}_k^e \; dS_k^e ds + \int_s^{s+\triangle s} \int_{S_k^i} \left(p_k^i \cdot \mathbf{n}_k^i\right) \left(\mathbf{n}_k^i \cdot \mathbf{n}_{S_k}\right) \; dS_k^i ds \tag{3.30}$$

$$+ \mathcal{A}_k^{s+\triangle s} \ll p_k^{s+\triangle s} \cdot \mathbf{n}^s \gg - \mathcal{A}_k^s \ll p_k^s \cdot \mathbf{n}^s \gg \tag{$\downarrow$}$$

$$= -\rho_k\kappa\mathcal{C}_1 \, Cov(w_k^2) \int_s^{s+\triangle s} \mathcal{A}_k \ll w_k \gg^2 ds \; \mathbf{n} \tag{$\downarrow$}$$

$$+ \mu_k\mathcal{C}_3 \int_s^{s+\triangle s} \int_{S_k^e} \nabla w_k^e \cdot \mathbf{n}_k^e \; dS_k^e ds \tag{$\downarrow$}$$

$$+ \mu_k\mathcal{C}_3 \int_s^{s+\triangle s} \int_{S_k^i} \left(\nabla w_k^i \cdot \mathbf{n}_k^i\right) \left(\mathbf{n}_k^i \cdot \mathbf{n}_{S_k}\right) \; dS_k^i ds \tag{$\downarrow$}$$

$$+ \rho_k\mu_k\mathcal{C}_3\mathcal{A}_k^{s+\triangle s} \cancelto{0}{\ll \nabla w_k^{s+\triangle s} \cdot \mathbf{n}^s \gg} - \rho_k\mu_k\mathcal{C}_3\mathcal{A}_k^s \cancelto{0}{\ll \nabla w_k^s \cdot \mathbf{n}^s \gg} \tag{$\downarrow$}$$

$$- \mu_k\kappa^2\mathcal{C}_2 \int_s^{s+\triangle s} \mathcal{A}_k \ll w_k \gg ds \; \mathbf{e}_s \tag{$\downarrow$}$$

$$- \rho_k g \left(\sin\phi \; \mathbf{e}_s + \cos\phi \; \mathbf{b}\right) \int_s^{s+\triangle s} \mathcal{A}_k \; ds \tag{.}$$

The axial direction integrals in Eq. 3.30 are evaluated by considering the mean

value theorem for the integrals, $\int_s^{s+\triangle s} f ds = \triangle s f$.

$$\frac{\int_{S_k^e} p_k^e \mathbf{n}_k^e \, dS_k^e}{A_{total}} + \frac{\int_{S_k^i} p_k^i \mathbf{n}_k^i \left(\mathbf{n}_k^i \cdot \mathbf{n}_{S_k}\right) dS_k^i}{A_{total}} \tag{3.31}$$

$$+ \frac{\mathcal{A}_k^{s+\triangle s} \ll p_k^{s+\triangle s} \gg - \mathcal{A}_k^s \ll p_k^s \gg}{\triangle s \mathcal{A}_{total}} \mathbf{e}_s \tag{$\downarrow$}$$

$$= -\rho_k \kappa \mathcal{C}_1 \, Cov(w_k^2) \frac{\mathcal{A}_k \ll w_k \gg^2}{A_{total}} \, \mathbf{n} \tag{$\downarrow$}$$

$$+ \mu_k \mathcal{C}_3 \frac{\int_{S_k^e} \nabla w_k^e \cdot \mathbf{n}_k^e \, dS_k^e}{A_{total}} + \mu_k \mathcal{C}_3 \frac{\int_{S_k^i} \left(\nabla w_k^i \cdot \mathbf{n}_k^i\right) \left(\mathbf{n}_k^i \cdot \mathbf{n}_{S_k}\right) \, dS_k^i}{A_{total}} \tag{$\downarrow$}$$

$$- \mu_k \kappa^2 \mathcal{C}_2 \frac{\mathcal{A}_k \ll w_k \gg}{A_{total}} \, \mathbf{e}_s - \rho_k g \left(\sin\phi \, \mathbf{e}_s + \cos\phi \, \mathbf{b}\right) \frac{\mathcal{A}_k}{A_{total}} \tag{.}$$

When the limit of $\triangle s \to 0$ is taken, it produces the general averaged balance equation for the individual phases. Given by Eq. 3.32.

$$\frac{\int_{S_k^e} p_k^e \mathbf{n}_k^e \, dS_k^e}{A_{total}} + \frac{\int_{S_k^i} p_k^i \mathbf{n}_k^i \left(\mathbf{n}_k^i \cdot \mathbf{n}_{S_k}\right) dS_k^i}{A_{total}} + \frac{\partial \alpha_k \ll p_k \gg}{ds} \mathbf{e}_s \tag{3.32}$$

$$= -\rho_k \kappa \mathcal{C}_1 \, Cov(w_k^2) \alpha_k \ll w_k \gg^2 \mathbf{n} \tag{$\downarrow$}$$

$$+ \mu_k \mathcal{C}_3 \frac{\int_{S_k^e} \nabla w_k^e \cdot \mathbf{n}_k^e \, dS_k^e}{A_{total}} + \mu_k \mathcal{C}_3 \frac{\int_{S_k^i} \left(\nabla w_k^i \cdot \mathbf{n}_k^i\right) \left(\mathbf{n}_k^i \cdot \mathbf{n}_{S_k}\right) dS_k^i}{A_{total}} \tag{$\downarrow$}$$

$$- \mu_k \kappa^2 \mathcal{C}_2 \alpha_k \ll w_k \gg \, \mathbf{e}_s - \rho_k g \left(\sin\phi \, \mathbf{e}_s + \cos\phi \, \mathbf{b}\right) \alpha_k \tag{.}$$

The above equation is the three-dimensional vector equation, representing the momentum balance for toroidal flow with zero-valued cross-stream velocities. To find the axial momentum equation used in the equilibrium stratified calculation, the interface is first assumed flat, i.e. $\alpha \neq f(s)$, then the scalar product of Eq. 3.32 is taken with the axial unit vector $\mathbf{e}_s$. This results in the projection of the forces in the axial direction.

$$\frac{\int_{S_k^e} p_k^e \mathbf{n}_k^e dS_k^e}{A_{total}} \cdot \mathbf{e}_s + \frac{\int_{S_k^i} p_k^i \mathbf{n}_k^i \left(\mathbf{n}_k^i \cdot \mathbf{n}_{S_k}\right) dS_k^i}{A_{total}} \cdot \mathbf{e}_s + \frac{\partial \alpha_k \ll p_k \gg}{ds} \mathbf{e}_s \cdot \mathbf{e}_s \tag{3.33}$$

$$= -\rho_k \kappa \mathcal{C}_1 \, Cov(w_k^2) \alpha_k \ll w_k \gg^2 \mathbf{n} \cdot \mathbf{e}_s \tag{$\downarrow$}$$

$$+ \mu_k \mathcal{C}_3 \frac{\int_{S_k^e} \nabla w_k^e \cdot \mathbf{n}_k^e \, dS_k^e}{A_{total}} \cdot \mathbf{e}_s + \mu_k \mathcal{C}_3 \frac{\int_{S_k^i} (\nabla w_k^i \cdot \mathbf{n}_k^i) (\mathbf{n}_k^i \cdot \mathbf{n}_{S_k}) \, dS_k^i}{A_{total}} \cdot \mathbf{e}_s \qquad (^{\downarrow})$$

$$- \mu_k \kappa^2 \mathcal{C}_2 \alpha_k \ll w_k \gg \mathbf{e}_s \cdot \mathbf{e}_s - \rho_k g \left(\sin\phi \, \mathbf{e}_s + \cos\phi \, \mathbf{b} \right) \alpha_k \cdot \mathbf{e}_s \qquad (.)$$

Inspecting Eq. 3.33, reveals the first, second, and fourth terms to be perpendicular to the axial direction at all locations, and hence do not contribute to the axial momentum equation. Additionally, the perimetrical unit normal is parallel with the k^{th}-phase liquid surface normal, i.e. $(\mathbf{n}_k^i \cdot \mathbf{n}_{S_k}) = 1$. The remaining terms compose the area averaged momentum equation used for the helical model development.

$$\alpha_k \frac{\partial \ll p_k \gg}{ds} = - \mathcal{C}_3 \frac{\int_{S_k^e} \tau_k^e dS_k^e}{A_{total}} - \mathcal{C}_3 \frac{\int_{S_k^i} \tau_k^i dS_k^i}{A_{total}} \qquad (3.34)$$

$$- \mu_k \kappa^2 \mathcal{C}_2 \alpha_k \ll w_k \gg - \rho_k g \alpha_k \sin\phi \qquad (.)$$

The product of the gradient of velocity and dynamic viscosity is replaced by the shear stress. Shear stress terms are written as functions of the mean axial velocity, and the final axial momentum equation used for the void fraction calculation is given by Eq. 3.35. This step is consistent with the use of the wall shear correlations that are to be applied.

$$\alpha_k \frac{\partial \ll p_k \gg}{ds} = - \mathcal{C}_3 \frac{\tau_k^e S_k^e}{A_{total}} - \mathcal{C}_3 \frac{\tau_k^i S_k^i}{A_{total}} - \mu_k \kappa^2 \mathcal{C}_2 \alpha_k \ll w_k \gg - \rho_k g \alpha_k \sin\phi \qquad (3.35)$$

3.4 Equilibrium Stratified Liquid Height

The equations developed in the previous section, are drawn upon for developing the helical flow map, based on the pioneering analysis of Taitel & Dukler (1976). Their two step analysis was discussed in the literature review, and was shown to be accurate for prediction of the flow regimes in a linear inclined geometry. A model that is appropriate for prediction of the flow regimes in a helical geometry can be developed by building upon the proven techniques of these authors, providing that proper inclusion of the differences in curved flow friction factor and cross-stream centrifugal force effects are addressed. The basis for the method of including these forces in the current model is as follows.

The characteristic of the centrifugal and gravity body forces to act perpendicularly to the direction of flow removes them from the axial momentum equation and the

resulting calculation of the equilibrium liquid height. This seems contradictory to the observation that the axial flow rate and liquid hold-up are clearly dependent on the curvature, see Sec. 2.1. However, the reason for increase in friction losses in the curved geometry is the steeper axial velocity gradient at the outside of the bend compared to linear systems, not because of secondary flow velocities. The secondary flow presence is just another effect of the curvature, not necessarily the origin of the flow losses. Given this reasoning, the one-dimensional simplification is valid as long as the effects of axial velocity distribution is retained in the axial equation. As found in the previous section, the axial equation integration removes the position dependence, and transfers the wall veloctiy gradient effects into the shear stresses, which is the important effect of the axial velocity distribution. Provided that the correlations for shear stress are accurate for the helical flow that is being modeled, the one-dimensional axial equation can be considered quite appropriate.

The incorporation of the appropriate friction forms is only done after a single equation is gotten that represents the two-phase flow field. One first considers a single axial momentum equation, Eq. 3.37, developed by equating the pressure gradients of the individual phases, Eq. 3.36. Eq. 3.37 allows for the interface shear stress to retard phase 2 and accelerate phase 1, if phase 2 is traveling at a greater velocity than phase 1, and vis versa if phase 1 has a greater velocity than phase 2, Eq 3.38b. Standard convention is used for friction factor and shear stress.

$$\frac{\partial \ll p_2 \gg}{ds} = \frac{\partial \ll p_1 \gg}{ds} \tag{3.36}$$

$$\frac{\mathcal{C}_3}{\mathcal{A}_{total}} \left(\frac{\tau_2^e S_2^e}{\alpha} - \frac{\tau_1^e S_1^e}{(1-\alpha)} \right) + \frac{\mathcal{C}_3 \tau^i S^i}{\mathcal{A}_{total}} \left(\frac{1}{\alpha} + \frac{1}{(1-\alpha)} \right) \tag{3.37}$$

$$+ \kappa^2 \mathcal{C}_2 \left(\mu_2 \ll w_2 \gg - \mu_1 \ll w_1 \gg \right) + g \sin\phi \left(\rho_2 - \rho_1 \right) = 0 \tag{.}$$

$$\tau_k^e = f_k^j \frac{\rho_k \ll w_k \gg^2}{2} \quad \text{where } k = (1,2) \text{ for } (liquid, gas) \tag{3.38a}$$

$$\tau^i = f_2^j \frac{\rho_2 \left(\ll w_2 \gg - \ll w_1 \gg \right) | \ll w_2 \gg - \ll w_1 \gg |}{2} \tag{3.38b}$$

where $j = (l,t)$ for $(laminar, turbulent)$

It can be shown to simplify the analysis if the void fraction is written as phasic areas. Considering the above friction factor forms, the combined axial momentum equation becomes,

$$\mathcal{C}_3\left(f_2^j\frac{\rho_2 \ll w_2 \gg^2}{2}\frac{S_2^e}{\mathcal{A}_2}-f_1^j\frac{\rho_1 \ll w_1 \gg^2}{2}\frac{S_1^e}{\mathcal{A}_1}\right) \tag{3.39}$$

$$+\mathcal{C}_3 f_2^j\frac{\rho_2\left(\ll w_2 \gg - \ll w_1 \gg\right)|\ll w_2 \gg - \ll w_1 \gg|}{2}S^i\left(\frac{1}{\mathcal{A}_2}+\frac{1}{\mathcal{A}_1}\right) \tag{$^{\downarrow}$}$$

$$+\kappa^2\mathcal{C}_2\left(\mu_2 \ll w_2 \gg -\mu_1 \ll w_1 \gg\right)+g\sin\phi\left(\rho_2-\rho_1\right)=0 \tag{.}$$

Closure of the problem requires that forms for the friction factors be defined, which in the curved cases are functions of the Dean number (De). As pointed out in the liturature review, multiple forms of De have been put forward by different researchers. Where discussed in the current study, the De is the form shown in Eq. 3.40. This is the same form recommended by Van Dyke (1978) and Berger et. al. (1983).

Comparing the different laminar fricition factor correlations published for helical flow, shows good agreement for both the published theoretical and empirical equations. Specifically, the equations developed by Ito (1969) are widely used, and have shown to be accurate over a wide range of laminar De numbers. Professor Ito additionally developed theoretical and empirical correlations for the turbulent flow friction factor (Ito 1959). Ito's 1959 investigation was the only published theoretical investigation of turbulent curved flow, at the time, and includes a correlation for his own data along with all other reported data on turbulent pressure losses in curved flows. Ito's correlations have the undesirable characteristic that they do not asymptotically approach a linear friction factor; and as shown in Fig. 3.6, underestimates the laminar friction factor for all published curvatures with Reynolds numbers less than 100. Also shown in the figure is the most current recommendation, by Ju et. al. (2001), for the single-phase curvature corrected laminar friction factor. The method of applying a correction factor to the linear friction coefficient is a conventional approach in curved flow modeling, and is akin to the two-phase friction corrections used in linear flows. The method of Ju et. al. has the desired attribute of asymptotically approaching the linear friction factor for large radii of curvature, while also matching the empirical correlations for coiled flows. Ju et. al. also recommends a correlation for the turbulent friction factor correction factor, which also asymptotically approaches the linear

turbulent friction factor. The current work uses the Blasius form for the gas-phase linear friction factor, and the liquid-phase superficial friction factor, as recommended by Taitel & Dukler (1976), Barnea (1987), and Petalas & Aziz (2000), and includes the empirical friction factor corrections for curved flows of Ju et. al. (2001). The Ju et. al. correction factor and the linear friction factor of Taitel & Dukler, are given in Eq. 3.41 and Eq. 3.42. Values for the friction coefficients used for the friction factors are $C_{fric1} = 0.04$, $C_{fric2} = 0.11$, $n = 0.2$, $m = 0.23$, $p = 0.14$ for turbulent flow, and $C_{fric1} = 16$, $C_{fric2} = 0.015$, $n = 1$, $m = 0.75$, $p = 0.4$ for laminar flow.

The actual average phasic velocities, and the curvature corrected critical Reynolds number of Miropolskiy (1963), are used to determine whether or not the phasic flow is turbulent or laminar, which is inline with the discussions of Sec. 2.

$$De = \left(\frac{r_0}{a}\right)^{1/2} \left(\frac{2r_0 \ll w \gg}{\nu}\right) = \frac{r_0}{a}^{1/2} Re \tag{3.40}$$

$$f = f_{linear} \left(1 + C_{fric2} Re^m \left(\frac{r_0}{a}\right)^p\right) \tag{3.41}$$

$$f_{linear} = C_{fric1} Re^{-n} \tag{3.42}$$

$$Re_{crit} = 2100 \left(1 + 12 \left(\frac{r_0}{a}\right)^{\frac{1}{2}}\right) \qquad \text{Miropolskiy (1963)} \tag{3.43}$$

$$\text{where} \quad Re_{s1} = \frac{2r_0 \rho_1 j_1}{\mu_1}$$

Review of Eq. 3.39 and the above friction correlations, shows 7 parameters: area average phase-1 axial velocity, area average phase-2 axial velocity, phase-1 area, phase-2 area, phase-1 external wetted parameter, phase-2 wetted parameter, and interface length. This list is reduced to 3 parameters by considering the liquid-liquid interface to be flat and the cross-section to be circular. As shown in Fig. 3.7, a flat interface between the phases produces a symmetry line, on which the mass centers of the area averaged fluids lie. This is a result of the area average velocity giving equal weight to all cross-section locations, placing the mass center at the geometric center lying on the symmetry line. With these considerations, all the geometric parameters can be shown as functions of equilibrium height alone, where the equilibrium height is

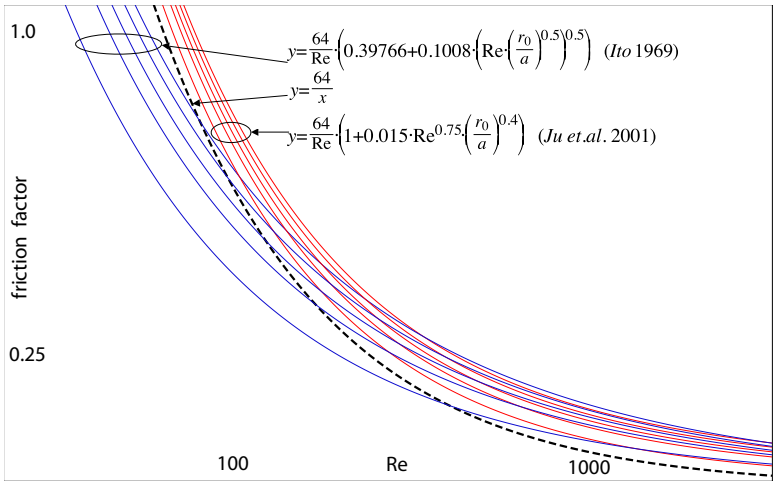

Figure 3.6: Comparison of the Ju et. al. (2001) and Ito (1969) friction factor correlations for toroidal and helical flows. Both Ju et. al. and Ito's correlations produce curves from the right to left with decreasing curvature (i.e. linear asymptote), showing Ito's correlation to diverge from, rather than asymptotically approach, the linear condition.

perpendicular to the liquid surface, and measured as the chord length splitting the phase-1 area. The equations describing the wetted parameters and phasic areas, along with calculated values for two different radii pipes, are shown in Fig. 3.8 and Fig. 3.9.

The majority of the published studies on flow regime transitions utilize a non-dimensional form of the momentum equation, where the equilibrium height can be correlated to the Lockhart-Martinelli parameter and a term representing the body forces. A similar momentum equation for the curved case, is found by using $2r^0$ for lengths, $4r^{0^2}$ for areas, and j_1 & j_2 for velocities, to non-dimensionalize Eq. 3.39, Eq. 3.41, Eq. 3.43, Fig. 3.8, and Fig. 3.9. The non-dimensional curved flow momentum equation is given in Eq. 3.44, where non-dimensional objects carry an asterisk accent in the hat position (i.e. $\overset{*}{f}$ is the non-dimensional form of the object f). Note that the curved friction multiplier accounts for the increased phasic velocity gradient at the wall, and as such, is not applied to the interfacial friction term; this can be seen in Eq. 3.44 as the B_2 gas curved friction multipliers are divided out of the term in the balance equation that represents the friction force at the interface, i.e. the S_i term. More specifically, the friction losses in the curved flows increase not because of secondary flows, but from the shift of the maximum axial velocity towards the

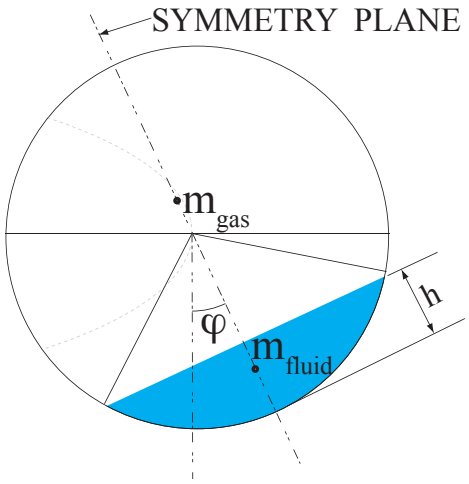

Figure 3.7: Depiction of the ideal stratified condition in toroidal or helical flows.

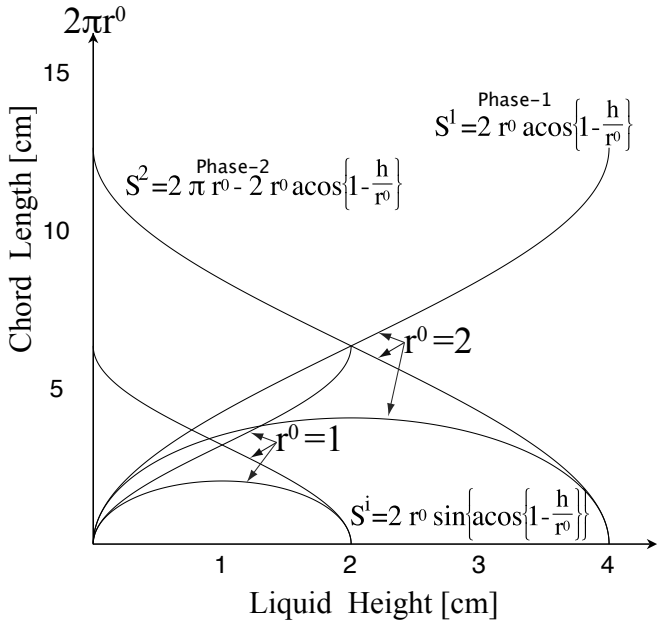

Figure 3.8: Graph of phasic wetted parameters as a function of the equilibrium liquid height, and ideal stratified condition.

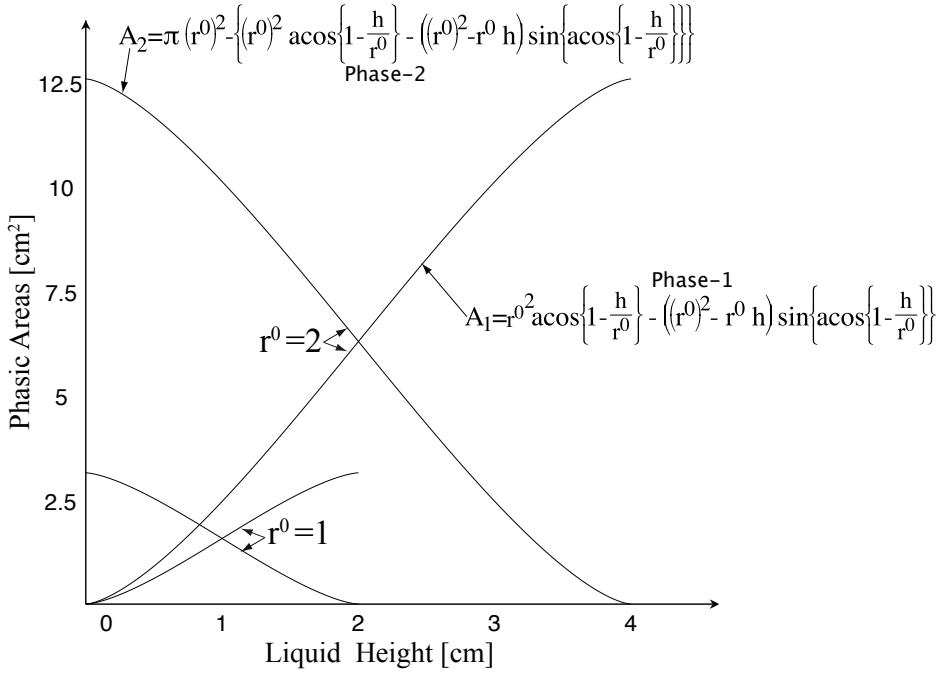

Figure 3.9: Graph of phasic areas as a function of the equilibrium liquid height, and ideal stratified condition.

solid interface. This increases the velocity gradient at the wall, resulting in greater friction losses. Since the maximum axial velocity of each phase do not necessarily move towards each other due to curvature, the interface friction does not experience the same increase that the wall friction does. This is in agreement with advancements in multi-phase flow modeling made by the Stanford University Petroleum Engineering department professors Petalas & Aziz. Petalas & Aziz have analyzed the largest multi-phase flow data base to determine the most accurate linear friction correlation forms for flow regime transition modeling. They have concluded that the interface friction factor is not necessarily the same as the gas-phase friction factor in all conditions, and as detailed above, is not assumed exactly equivalent to the gas phase friction in the curved condition. Also note that Eq. 3.44 does not use the simplifying assumption that the difference between the gas and liquid phase velocities must be always equal to the gas phase velocity, a modification recommended by most new analyses (for example see Petalas & Aziz 1998).

$$\overset{*}{w}_2^2 \left(\overset{*}{w}_2 \overset{*}{D}_2^h\right)^{-n} \frac{\overset{*}{S}_2}{\overset{*}{A}_2} - X^2 \frac{B_1}{B_2} \overset{*}{w}_1^2 \frac{\overset{*}{S}_1}{\overset{*}{A}_1} \left(\overset{*}{w}_1 \overset{*}{D}_1^h\right)^{-n}$$

$$+\frac{W}{B_2}\overset{*}{S}_i\left(\frac{1}{\overset{*}{A}_1}+\frac{1}{\overset{*}{A}_2}\right)\left(\overset{*}{w}_2\overset{*}{D}_2^h\right)^{-n}+4\frac{Z}{B_2}-4\frac{Y}{B_2}=0 \tag{3.44}$$

$$X^2=\frac{\frac{\rho_1 j_1^2}{2}\left(\frac{\rho_1 j_1 D}{\mu_1}\right)^{-n}\frac{4C_{fric1}}{D}}{\frac{\rho_2 j_2^2}{2}\left(\frac{\rho_2 j_2 D}{\mu_2}\right)^{-n}\frac{4C_{fric1}}{D}} \tag{3.45a}$$

$$Y=\frac{g\left(\rho_1-\rho_2\right)\sin\phi}{\frac{\rho_2 j_2^2}{2}\left(\frac{\rho_2 j_2 D}{\mu_2}\right)^{-n}\frac{4C_{fric1}}{D}} \tag{3.45b}$$

$$W=\frac{\left|j_2\overset{*}{w}_2-j_1\overset{*}{w}_1\right|\left(j_2\overset{*}{w}_2-j_1\overset{*}{w}_1\right)}{j_2^2} \tag{3.45c}$$

$$Z=\frac{4\frac{\overset{*}{\kappa}^2}{D^2}\left(\mu_2 j_2\overset{*}{w}_2-\mu_1 j_1\overset{*}{w}_1\right)}{\frac{\rho_2 j_2^2}{2}\left(\frac{\rho_2 j_2 D}{\mu_2}\right)^{-n}\frac{4C_{fric1}}{D}} \tag{3.45d}$$

$$B_1=1+C_{fric2}\left(\frac{\rho_1\overset{*}{w}_1 j_1 4\overset{*}{A}_1 D}{\mu_1\overset{*}{S}_1}\right)^m\left(\frac{r^0}{a}\right)^p \tag{3.45e}$$

$$B_2=1+C_{fric2}\left(\frac{\rho_2\overset{*}{w}_2 j_2 4\overset{*}{A}_2 D}{\mu_2\overset{*}{S}_2}\right)^m\left(\frac{r^0}{a}\right)^p \tag{3.45f}$$

The set of objects consisting of Eq. 3.44, Eq. 3.45, Eq. 3.41, Eq. 3.42, Fig. 3.8, and Fig. 3.9 provide the framework that can be solved for a unique relationship between the phasic velocities and the equilibrium liquid height. For the case of negligible curvature, $\frac{r^0}{a}\rightarrow 0$, $B_1\rightarrow 1$, $B_2\rightarrow 1$, $Z\rightarrow 0$, and Eq. 3.44, and when considering the same approximation as Taitel & Dukler (1976) (i.e. $w_2-w_1\approx w_2$), Eq. 3.44 is identical to the momentum equation developed by Taital & Dukler (1976).

For the equilibrium liquid height calculation, the actual curvature of the helix is used. This follows recommendation of Truesdell & Adler (1970), who concluded the major effect of pitch was the influence on curvature and the effective radius of the helix. The curvature of a helix is given by Eq. 3.46, where p is the pitch and a the helical radius, i.e. the inverse of curvature ($r^0_{helix}=\frac{1}{\kappa_{helix}}$). The solutions for

equilibrium liquid height are given in Sec. 4.

$$\kappa_{helix} = \frac{a}{a^2 + \left(\frac{p}{2\pi}\right)^2} \tag{3.46}$$

3.5 Transition Mechanisms From The Stratified Condition

Determination of the transition from the equilibrium stratified condition has been shown (Taitel & Dukler 1976 and 1978, Barnea 1987, Petalas & Aziz 2000) to be well predicted by the Kelvin-Helmholtz stability criteria for wave growth. The theory is as follows. For an equilibrium stratified condition, an individual wave on the liquid surface causes a change in the gas flow area, which affects the pressure of the gas flowing over the wave due to the Bernoulli effect. In the case that the change in pressure is greater than the increase in the body forces from gravity and centrifugal forces, the wave will experience a net force that supports wave grow. Wave growth under this force imbalance will continue until the wave crest reaches the top of the pipe, and blocks the gas flow path. If sufficient liquid inventory is present, the blockage forms into a liquid slug; if insufficient liquid is present, the blockage is swept along the walls of the pipe in an annular flow regime. Taitel & Dukler (1976, 1978) showed this condition to be satisfactorily modeled by $\overset{*}{h}_l < 0.5$ for the annular condition, and $\overset{*}{h}_l >= 0.5$ for the intermittent condition. It is clear that the stability criteria depends directly on the stabilizing effect of the gravity body force. In a curved flow, this body force includes the centrifugal acceleration. The integration of this force is now considered.

Due to the similarities between helical and linear flows, the mechanism of transition from the stratified regime in helical coils is assumed to be similar to that in the linear flow. The crux of this assumption, is the inclusion of the direction and magnitude of the body forces, acting on a wave that forms from this smooth interface equilibrium condition. For these forces to be included, the orientation of the surface must be calculated. Banerjee (1967) and Whalley (1980) have shown that this orientation is calculable from a simple force balance, where the centrifugal force on the gas and liquid phases is treated similar to the buoyancy force of gravity. The buoyancy of the centrifugal force is perpendicular to the action of gravity, and the centrifugal buoyancy can be combined with gravity vectorially. This condition is shown in Fig. 3.10. Since the surface orientation adjusts to a zero net buoyancy force, the vari-

ation in surface height due to the presence of a solitary wave can either experience added stability, a reduction in stability, or no change in stability, from the centrifugal force on the wave mass. It all depends on the projection of the wave growth direction along the centrifugal force vector. This mechanism is explained as follows. If the equilibrium stratification is that of a linear configuration, the wave growth is perpendicular to the centrifugal force, and does not experience any contribution to the growth from the centrifugal force. This is the case if the centrifugal force on the liquid and gas is exactly equal. If the flow is orientated with the higher density fluid on the outside of the bend, wave growth is opposite to the action of centrifugal forces, and is attenuated by centrifugal forces. If the flow has undergone film-inversion, the wave growth is in the same direction as the action of the centrifugal force on the wave, and wave growth is promoted by the centrifugal force on the wave mass.

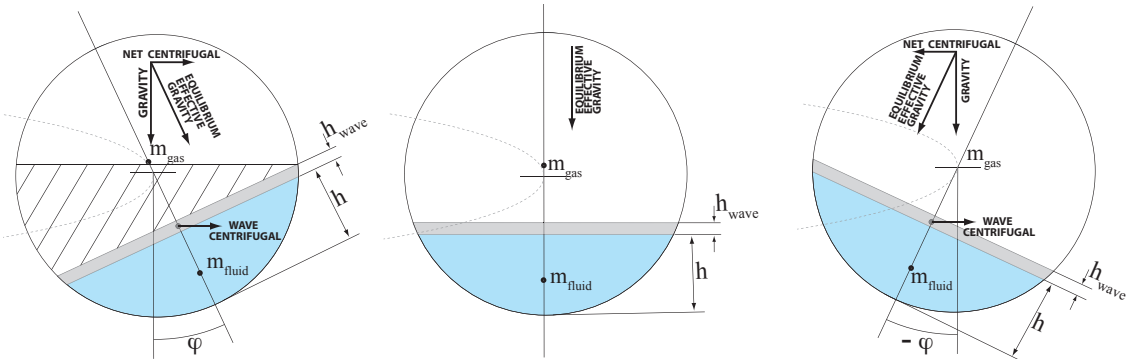

Figure 3.10: Diagram of the buoyancy forces of gravity and centrifugal forces, for standard, neutral, and inverted conditions.

It is obvious that the wave effective gravity, and the effective gravity determining the interface orientation, are not necessarily the same. This increase may or may not contribute to the stability of the wave. Review of Fig. 3.10 shows that in the inverted condition, any additional centrifugal force in the gas phase is expressed against the pipe wall, and does not attenuate the wave centrifugal force due to wave formation. Because of this, the inverted case is always destabilized by the wave centrifugal force, and stabilized by the equilibrium effective gravity. It is not the same for the standard condition, as additional centrifugal force experienced by the gas is only partially conveyed to the pipe wall(shown as the cross-hatched area in the left image of Fig. 3.10), and partially presented to the wave crest. Because of this, the standard condition is always stabilized by both the equilibrium centrifugal

force and wave centrifugal force. The phasic velocities at the wave are functions of the equilibrium condition velocities, equilibrium liquid height, and wave height, by Eqs. 3.47; the interface orientation angle and wave effective gravity are given by Eq. 3.48 and Eq. 3.49. Primed values are located at the wave, as depicted in Fig. 3.11, subscript 2 denotes the less dense phase, and subscript 1 denotes the more dense phase.

$$\ll w_2' \gg = \frac{\ll w_2 \gg}{1 + \frac{\triangle A_2}{A_2}} \tag{3.47a}$$

$$\ll w_1' \gg = \frac{\ll w_1 \gg}{1 - \frac{\triangle A_2}{A_1}} \tag{3.47b}$$

$$\varphi = atan\left(\frac{\rho_1 \ll w_1 \gg^2 - \rho_2 \ll w_2 \gg^2}{ag\left(\rho_1 - \rho_2\right)}\right) \tag{3.48}$$

$$g_{eff}^{wave} = \left(\frac{\ll w_1 \gg^2}{a} \sin\varphi + g\cos\varphi\cos\phi\right) \tag{3.49}$$

Calculating an effective gravity and interface orientation previous to evaluating the stability criteria has the benefit of allowing the use of a similar analysis as completed in the linear case, by simply applying the effective gravity to the linear stability criteria. The Taitel & Dukler approach is utilized here, for the case of curved flows, and is as follows. The original Kelvin-Helmholtz stability criteria for growth of a solitary, infinitesimal plane wave, on the surface of a liquid sheet, due to gas flow over the liquid, and bound in the vertical direction by two horizontal parallel planes, is given by Eq. 3.50a (Milne-Thomson 1960, Chandrasekhar 1961). The same criteria for a circular inclined pipe with a finite wave is given by Eq. 3.50b. As discussed in the literature review, the extension of this criteria to the enclosed pipe flow has proven accurate for flow regime transition of multi-phase flow.

$$w_2 > \left(\frac{\left(\rho_1 - \rho_2\right) g h_{gas}}{\rho_2}\right)^{\frac{1}{2}} \tag{3.50a}$$

$$w_2 > \left(1 - \frac{h}{2r_0}\right)\left(\frac{\left(\rho_1 - \rho_2\right) g_{eff}^{wave}\cos\phi A_2}{\rho_2 \frac{dA_1}{dh}}\right)^{\frac{1}{2}} \tag{3.50b}$$

The extension of the above criteria is found by comparing the force balance for the solitary infinitesimal wave to a solitary finite wave in curved flow. Since the criteria

ignores surface tension and wave motion, and the centrifugal forces are included in the gravity term, the forces determining wave growth are: effective gravity buoyancy force, and Bernoulli effect. A schematic of the co-current flow case is given in Fig. 3.11. The Taitel & Dukler form of the Kelvin-Helmholtz stability criteria for an inclined circular cross-section pipe, is simply extended by inserting Eq. 3.49 into Eq. 3.50a, to the form of Eq. 3.51.

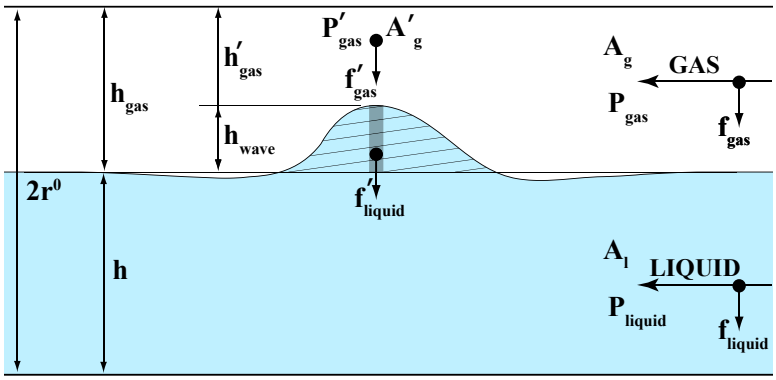

Figure 3.11: Diagram of the configuration for the Kelvin-Helmholtz instability formation of growing wave height.

$$\ll w_2 \gg \quad > \tag{3.51}$$

$$\left(1-\frac{h}{2r_0}\right)\left(\frac{(\rho_1-\rho_2)\left(\frac{\ll w_1 \gg^2}{a}\sin\varphi + g\cos\varphi\cos\phi\right)A_2}{\rho_2 2r_0\left(1-\left(\frac{h}{r_0}-1\right)^2\right)^{\frac{1}{2}}}\right)^{\frac{1}{2}}$$

The discussion of the current section, and a review of Eq. 3.51, shows that all the required parameters are calculable. From these objects, the flow regime transition for the helical geometry is solved for and presented in the results section.

4 RESULTS

4.1 Introduction

The equations developed in Sec. 3 are solved numerically for the area averaged phasic velocities and equilibrium liquid height, for specific phasic mass flux. The accuracy of the momentum balance is checked for the linear asymptote by comparing with the solutions for gas and liquid hold-up, by Barnea & Taitel (1992), the most current publication by one of the authors of the original work of Taitel & Dukler (1976). For checking of the linear asymptote, the radius of curvature is set to a very large value (a >500,000 [m]), which approximates the linear flow condition used in the original published works. Additionally, for the comparison, digitized values from the actual published graph are utilized to eliminate the possibility of bias introduction from the author.

4.2 Linear Asymptote Check

Seven comparisons are carried out to check the accuracy of the current equations for the linear asymptote. Figure 4.1 shows the variation in equilibrium height due to changes in the inclination angle. Figure 4.1 also indicates the region of small upward inclined flows where multiple solutions to the equilibrium height are found. The difficulty in determining which one of the multiple solutions is correct has been discussed in current publications with no clear solution as to which root is correct (Barnea 1992, Xiao et. al. 1990, Petalas & Aziz 1998). Barnea (1992) completed an analysis to determine which of the multiple roots were stable solutions, and determined that when 3 roots existed, only the smallest valued one was both linearly and non-linearly stable, the middle value never stable, and the largest valued non-dimensional height linearly stable under certain conditions. In other words, it is found that the largest value is appropriate for calculating the equilibrium liquid height used in determining the transition to intermittent flow conditions in that it represents the liquid hold-up regardless of the structural stability of the flow, but is not always appropriate for determining the actual liquid hold-up. Comparisons for the horizontal and various inclinations of linear pipe are shown in Figures 4.2 through 4.8. The current equation's solutions are found to match the Barnea & Taitel (1992) predictions very well,

and provided that their methods have proven accurate, the current equations are equally appropriate for linear predictions.

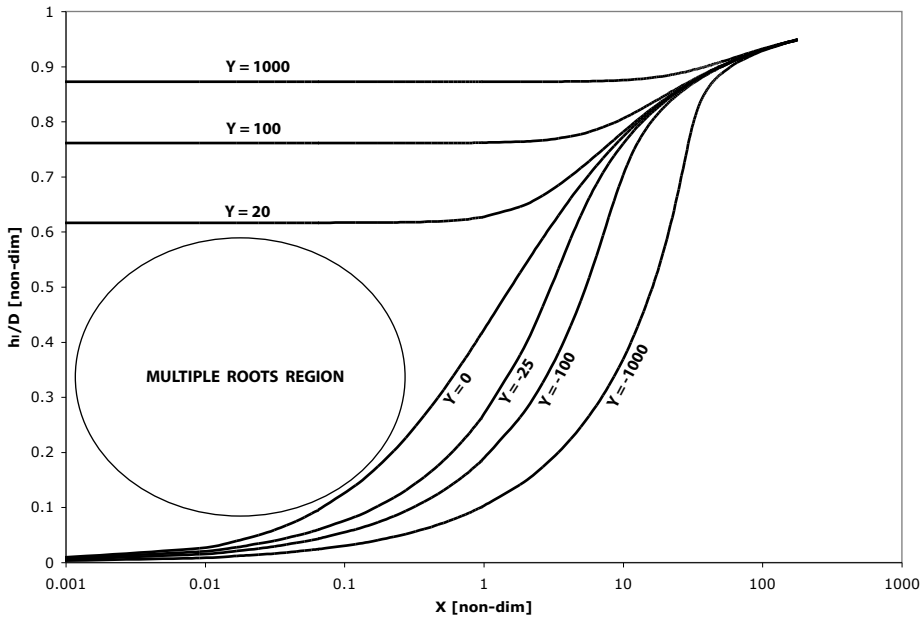

Figure 4.1: Calculation of the equilibrium liquid height in a linear flow at various inclination angles.

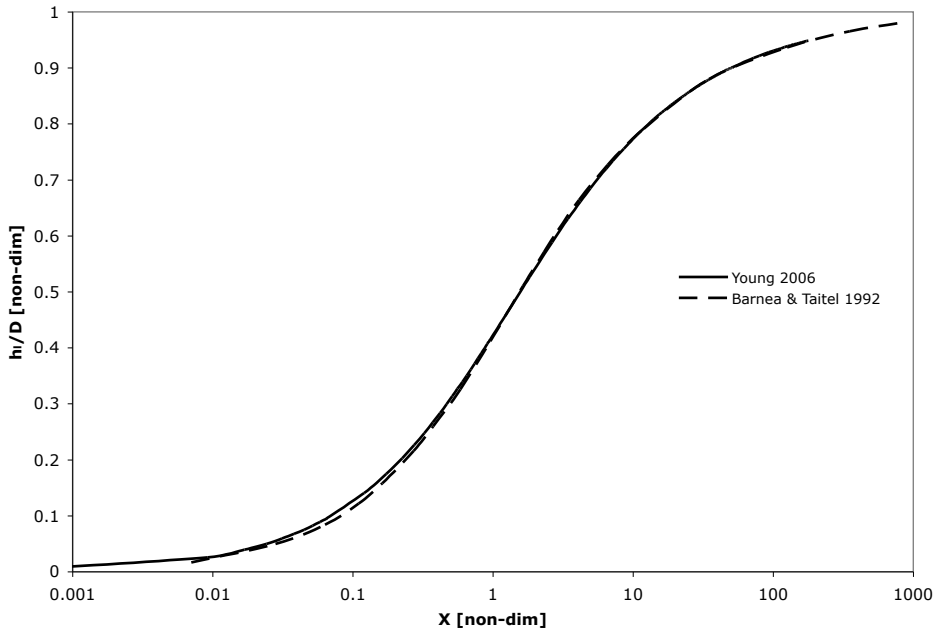

Figure 4.2: Comparison of equilibrium height predictions of Young with Barnea & Taitel 1992, for horizontal linear asymptote.

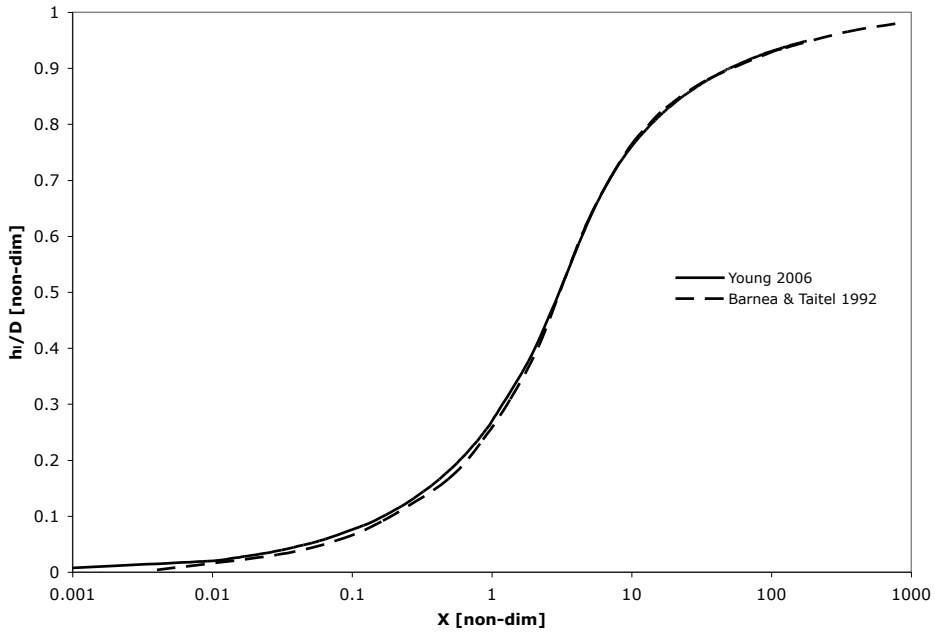

Figure 4.3: Comparison of equilibrium height predictions of Young with Barnea & Taitel 1992, for Y = -25 (0.49°downward inclination) linear asymptote.

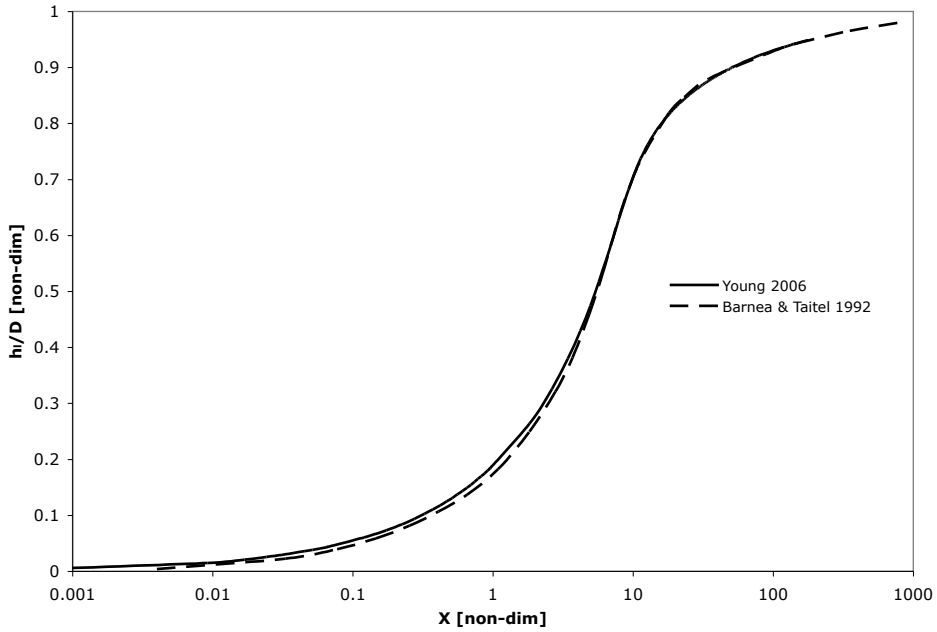

Figure 4.4: Comparison of equilibrium height predictions of Young with Barnea & Taitel 1992, for Y = -100 (1.96°downward inclination) linear asymptote.

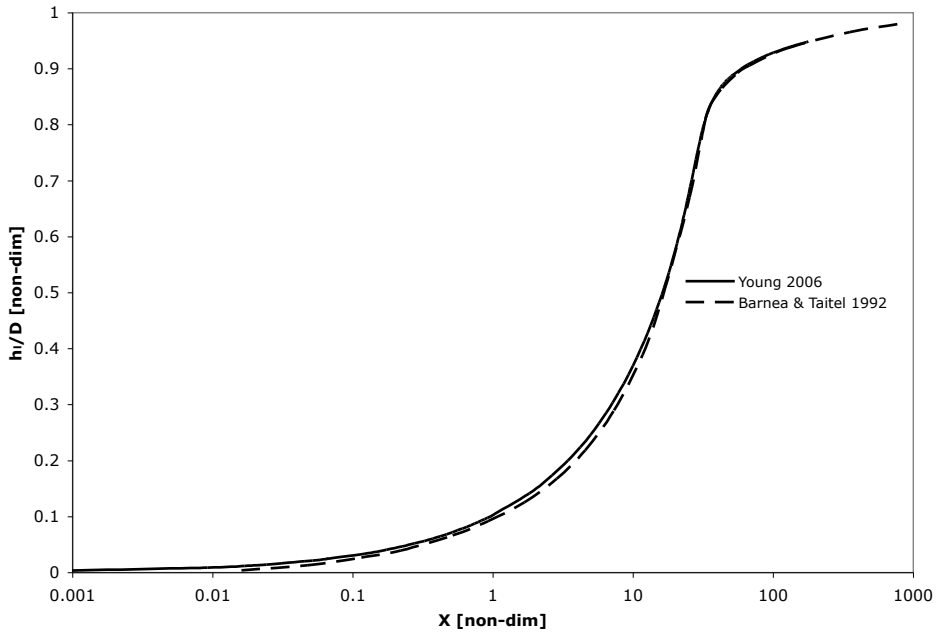

Figure 4.5: Comparison of equilibrium height predictions of Young with Barnea & Taitel 1992, for Y = -1000 (20.00°downward inclination) linear asymptote.

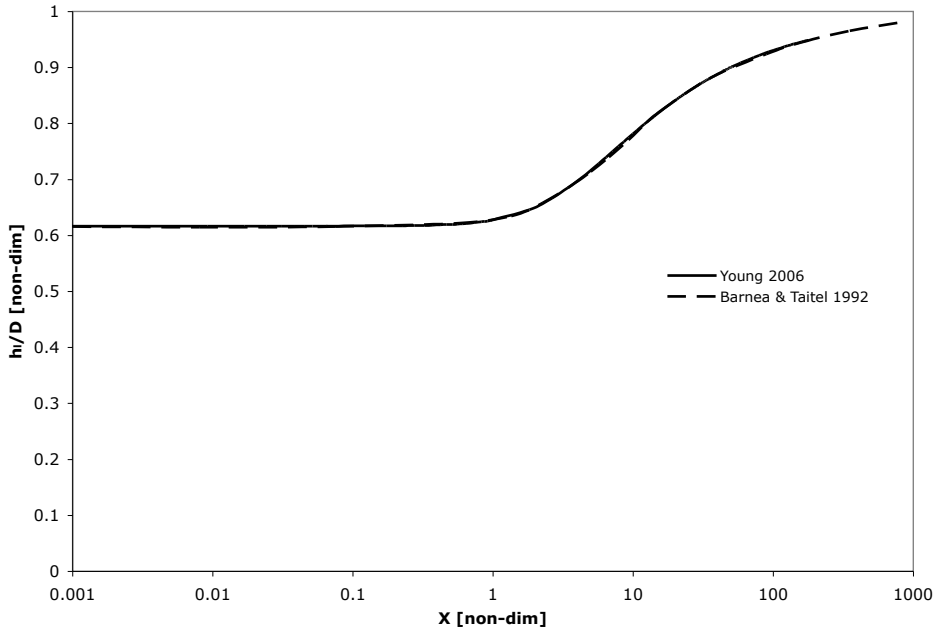

Figure 4.6: Comparison of equilibrium height predictions of Young with Barnea & Taitel 1992, for Y = 20 (0.39°upward inclination) linear asymptote.

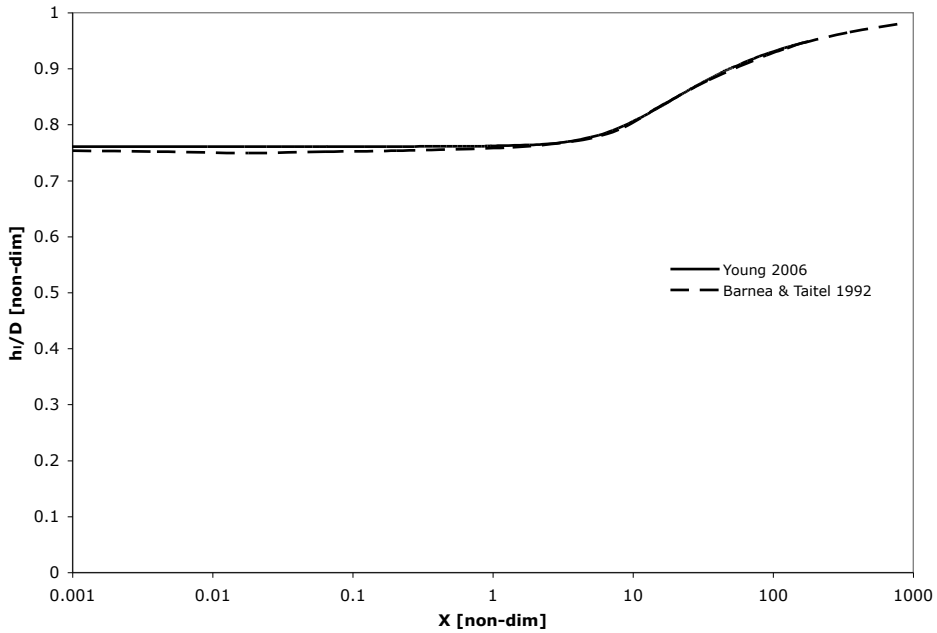

Figure 4.7: Comparison of equilibrium height predictions of Young with Barnea & Taitel 1992, for Y = 100 (1.96°upward inclination) linear asymptote.

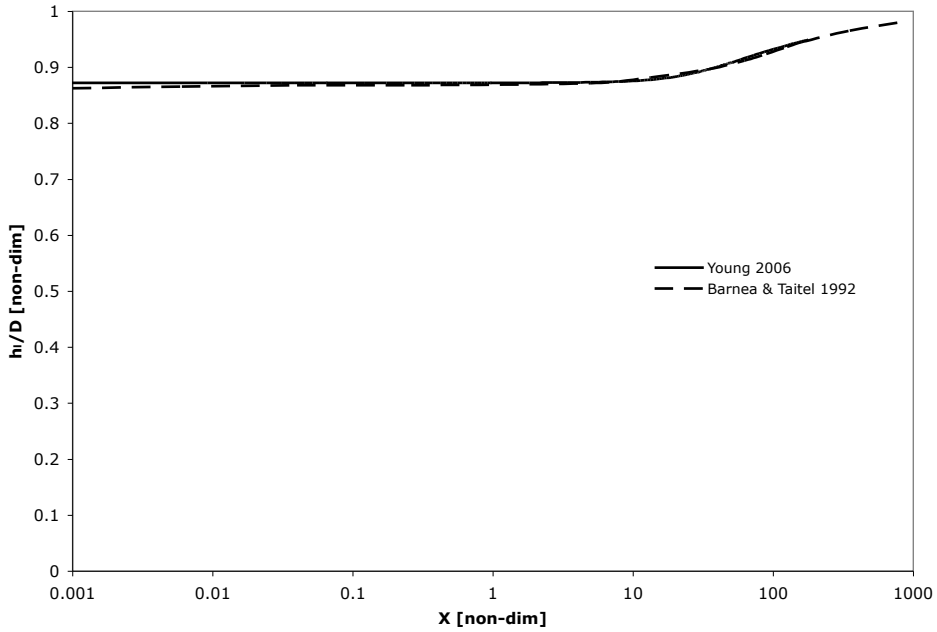

Figure 4.8: Comparison of equilibrium height predictions of Young with Barnea & Taitel 1992, for Y = 1000 (20.00°upward inclination) linear asymptote.

4.3 Helical Liquid Hold-Up Calculations

This section looks at the trends in the calculated liquid hold-up in the stratified equilibrium condition helical flow. The published data set and reported observations about upward helical flow are consistent, in that every experimental observation has reported the increase in liquid hold-up and reduction in the stratified flow regime, with increasing curvature. So it is the match of these trends that form the basis for comparison of the current approach. Note that these observations are obviously only applicable to the ranges in which the tests were carried out, and as such, the new methods predictions are compared for the range of parameters that match the published observations.

Reviewing Fig. 4.9, Fig. 4.10, and Fig. 4.12 demonstrates the current modeling characteristics for variations in the curvature, of horizontal and inclined flows. The three figures show the calculated variation in the liquid equilibrium height (i.e. liquid hold-up) for changes in the curvature, a close up of the region where the calculations change from showing looser coils as the case presenting greater liquid hold-up, and the calculated equilibrium liquid height after the curved friction factor modification,

respectively. This modification is discussed in more detail below.

In support of the conditional trends noted in the figures, Saxena et. al. (1990) experimentally determined that liquid hold-up in helical coils depended on a coefficient a, which was found to depend on curvature and liquid superficial velocity, independent of small inclinations of a tightly wrapped helix. However, when the helices were loosely wrapped (curvature ratios greater than 51.6) inclination effects were found to be dominant, and the curvature had negligible effect compared with the gravity force introduced by inclining the pipe. The condition was possibly explained by Mandal & Das (2002 & 2003) by considering the slip between the phases. Their experiments showed decreased two-phase pressure drop and increased liquid hold-up with increasing curvature, for the case where overall gas volumetric flow rate was 10 times that of the liquid. Under their conditions, the centrifugal force was always greater for the liquid phase, and the acceleration of the liquid phase due to interfacial drag is inversely related to the coil diameter. So a decrease in coil diameter presented a relative decrease in two-phase pressure drop. Additionally, the increasing curvature is accompanied by an increase in number of coils for a length of pipe; so that the effects of slip and gravity act in opposition to each other. Mandal & Das concluded that the combined effect was that of greater liquid hold-up with increasing curvature.

Another method for calculating the equilibrium height, is to use the the actual laminar or turbulent phasic friction coefficients pointwise calculated at the actual Lockhart Martinelli values for which the transition from laminar to turbulent phasic flow occurs. This would most accurately correspond to reality, and match what is recommended in the original publication by Taitel & Dukler (1976) (and many of the studies published since 1976). However, the most often taken approach is to apply either the laminar or the turbulent coefficients for the entire range of Lockhart Martinelli values, for this produces the most consistent calculation results. It is often not considered whether or not the superficial velocities could actually yield both laminar and turbulent phasic flows. Reviewing the form of the equilibrium calculation, and noting that the only method of producing a range of LM values by modifying the base parameters, is to hold the gas volumetric flow constant and varying the liquid volumetric flow. This is due to that fact that a constant Y value requires a constant gas volumetric flow rate for a given inclination angle. Simply specifying Y and X values while not considering the resulting set of liquid and gas velocities and resulting appropriate friction forms, is artificially imposing the friction

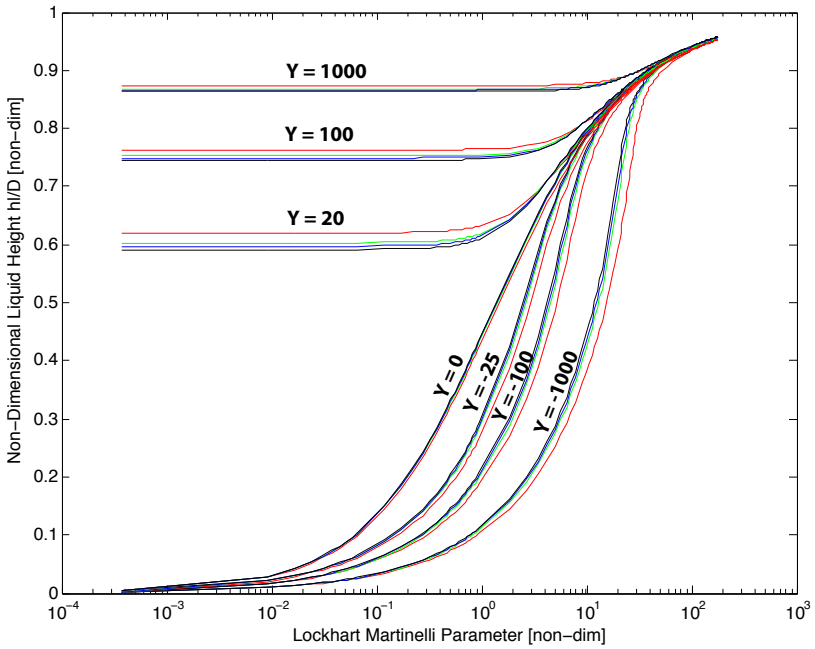

Figure 4.9: Calculation of liquid hold-up for different curvature ratios and different inclinations, using the turbulent gas and turbulent liquid conditions. Pipe diameter is 0.0254 [m], red line curvature ratio = 1E6, green line curvature ratio = 100, blue line curvature ratio = 20, black line curvature ratio = 5.

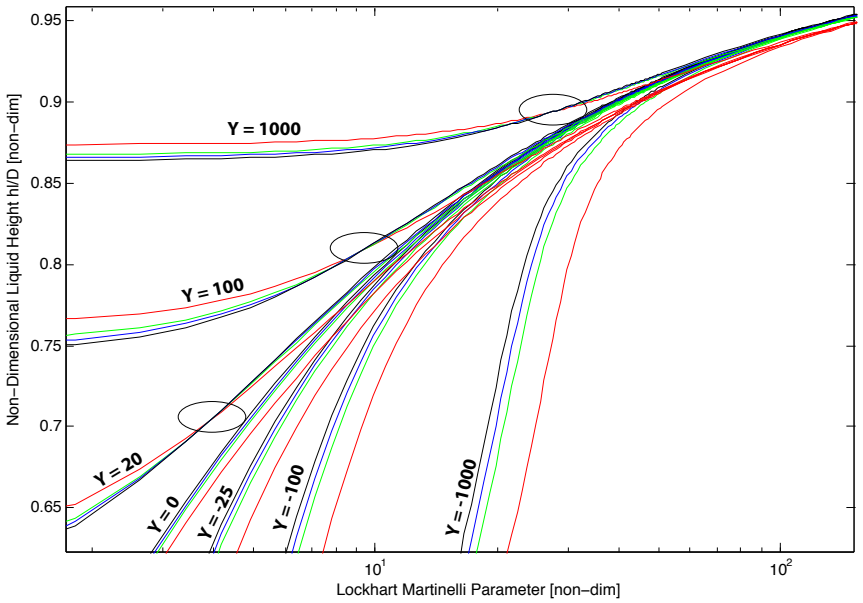

Figure 4.10: Close up of the calculation of liquid hold-up for different curvature ratios and different inclinations, using the turbulent gas and turbulent liquid conditions. Pipe diameter is 0.0254 [m], red line curvature ratio = 1E6, green line curvature ratio = 100, blue line curvature ratio = 20, black line curvature ratio = 5. Inversions of the calculation of looser vs. tighter coiling as the greater predicted liquid heights are marked with ellipses.

forms. This could introduce the condition where the application of only the laminar or turbulent coefficients over the entire calculation would result in somewhat artificial calculated values. However, this effect on the equilibrium height calculation for all possible conditions in a linear flow are well modeled by the gas-turbulent/liquid-turbulent friction factors, as shown in the works of Taitel & Dukler (1976), Taitel (1977), Petalas & Aziz (1998), and Barnea (1987). The effects of applying the actual friction coefficients into the linear flow terms of the equilibrium calculation can be seen in the obscure behavior depicted in Fig. 4.11. This strange sudden behavior is a direct result of the discontinuity between the turbulent and laminar friction factor values, and as discussed above, and is not a necessary inclusion since the vast majority of transitions take place in air-water systems where both phases are turbulent flows. As such, it is proposed that the differences between turbulent and laminar friction forms only be introduced when considering the curvature effects of the liquid phase. Per the above discussion, the curved flow friction component is modified by using liquid curved friction multiplier friction coefficients of $C_{_{fric2}} = 0.015$, $m = 0.75$, $p = 0.4$, as recommended by Ju. et. al. (2001). The results of this modification are shown for the up-flow inclinations of 0°, 1°, 3°, and 5° in Figure 4.12. Also depicted in Fig. 4.12 are the ranges of Lockhart Martinelli parameter values for the available published flow regime and liquid hold-up observations. Current calculations are for the lower roots, when multiple roots exist.

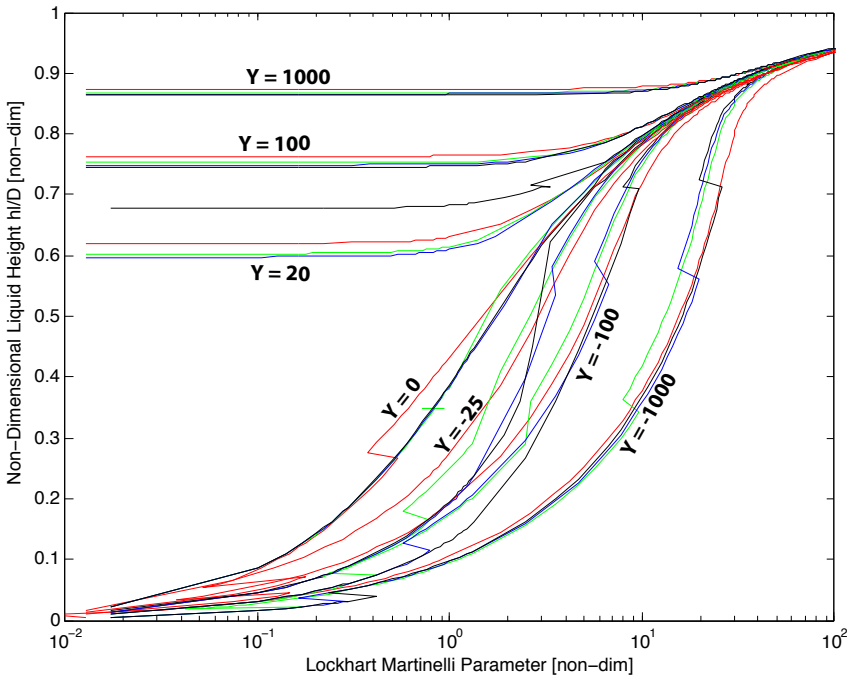

Figure 4.11: Calculation of liquid hold-up for different curvature ratios and different inclinations, using the actual friction conditions for both gas and liquid (Reynolds numbers and friction factors are based on actual velocities, not superficial velocities.) Pipe diameter is 0.0254 [m], red line curvature ratio = 1E6, green line curvature ratio = 100, blue line curvature ratio = 20, black line curvature ratio = 5.

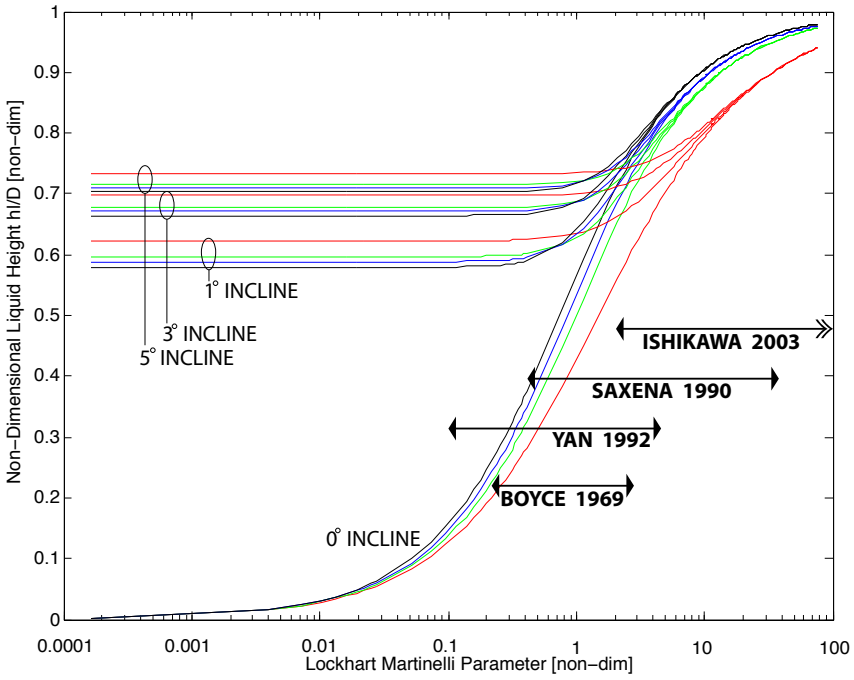

Figure 4.12: Calculation of liquid hold-up for different curvature ratios and different upward inclinations, for the case where linear components and gas phase curved friction multiplier are considered turbulent, and the liquid phase curved friction multiplier is considered laminar. Pipe diameter is 0.0254 [m], red line curvature ratio = 1E6, green line curvature ratio = 100, blue line curvature ratio = 20, black line curvature ratio = 5. Upper roots are shown.

4.4 Surface Inversion Calculations

The dependence of centrifugal body forces on surface orientation, on determining whether this force retards or promotes wave growth, is discussed in Sec. 3.5 and its influence is given by Eq. 3.49 and Eq. 3.50b. It was shown that the orientation of the interface between the phases is given by Eq. 3.48, which is dependent on the actual phasic velocities. These velocities are only known after the equilibrium height has been calculated, which causes each pair of superficial velocities to have a unique surface inversion angle. The surface inversion angle is represented in Fig. 3.10, and is positive for the case when the heavier fluid flows along the outside of the curve. The calculated inversion angles, as functions of the superficial liquid and gas velocities, for the experimental conditions of the four author's works presented in this results section, are represented using the surface graphs shown in Fig. 4.13, Fig. 4.15, Fig. 4.17, and Fig. 4.19. The calculated inversion angle iso-lines, as functions of the superficial liquid and gas velocities, for the experimental conditions of the four author's works presented in this results section, are represented using the line graphs shown in Fig. 4.14, Fig. 4.16, Fig. 4.18, and Fig. 4.20.

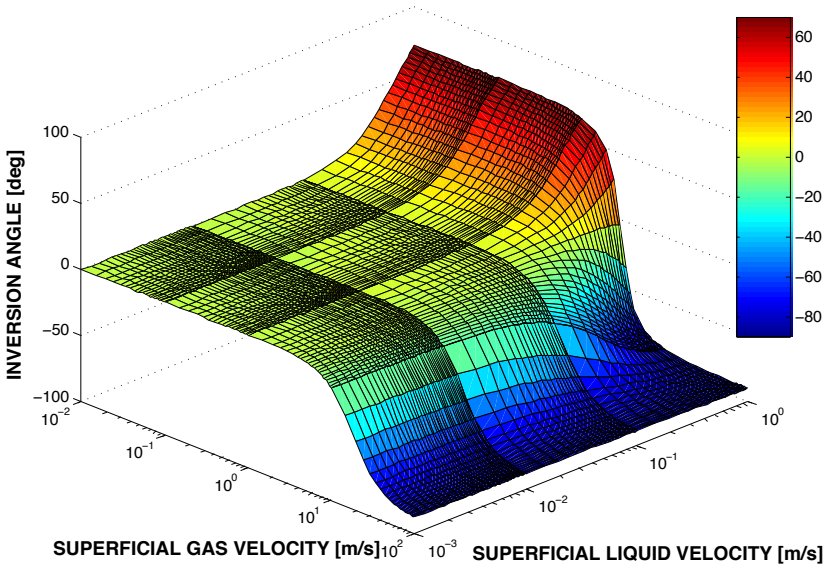

Figure 4.13: Surface describing inversion angle as a function of superficial velocities for Yan 1992 data. Pipe diameter is 0.0083 [m], Coil to Tube Diameter Ratio = 9.

Fig. 4.13, Fig. 4.15, Fig. 4.17, and Fig. 4.19 agree with the mechanism describing inversion angle. Specifically, as the relative actual velocity of the less dense

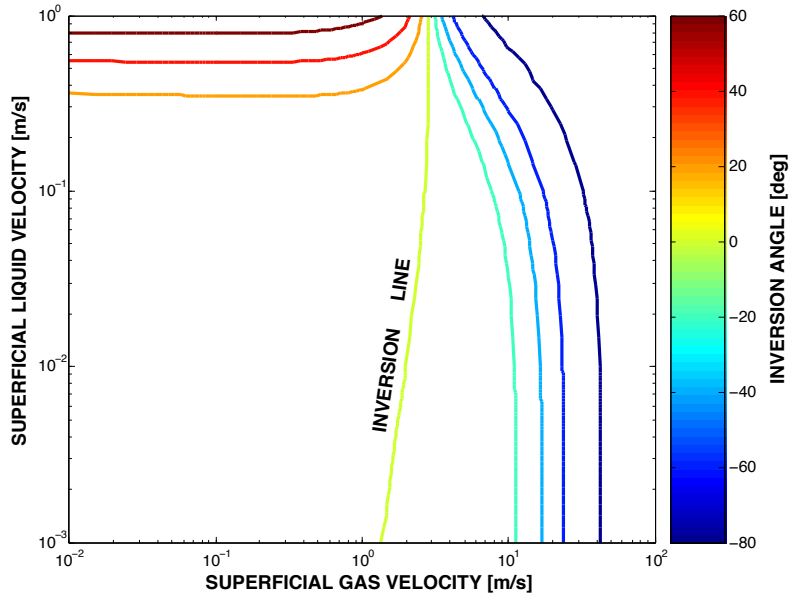

Figure 4.14: Iso-lines describing specific inversion angles as a function of superficial velocities for Yan 1992 data. Pipe diameter is 0.0083 [m], Coil to Tube Diameter Ratio = 9.

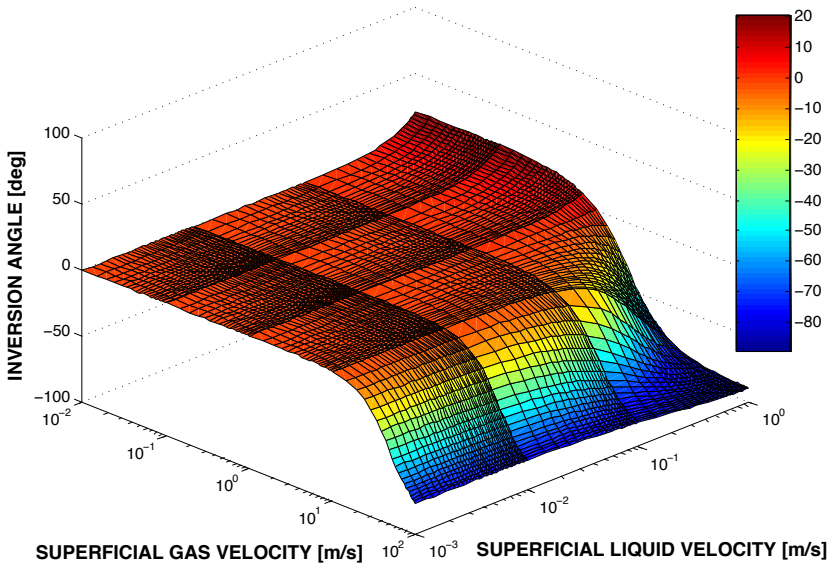

Figure 4.15: Surface describing inversion angle as a function of superficial velocities for Ishikawa 2003 data. Pipe diameter is 0.02 [m], Coil to Tube Diameter Ratio = 27.

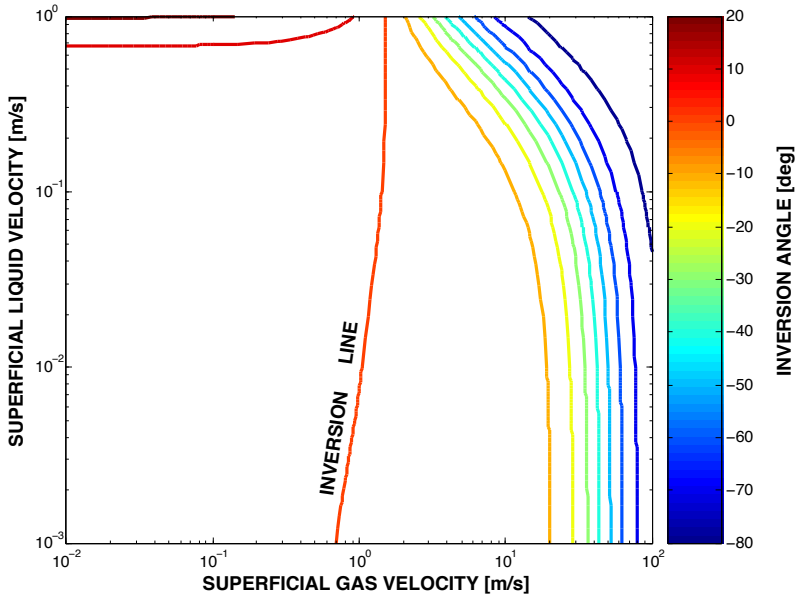

Figure 4.16: Iso-lines describing specific inversion angles as a function of superficial velocities for Ishikawa 2003 data. Pipe diameter is 0.02 [m], Coil to Tube Diameter Ratio = 27.

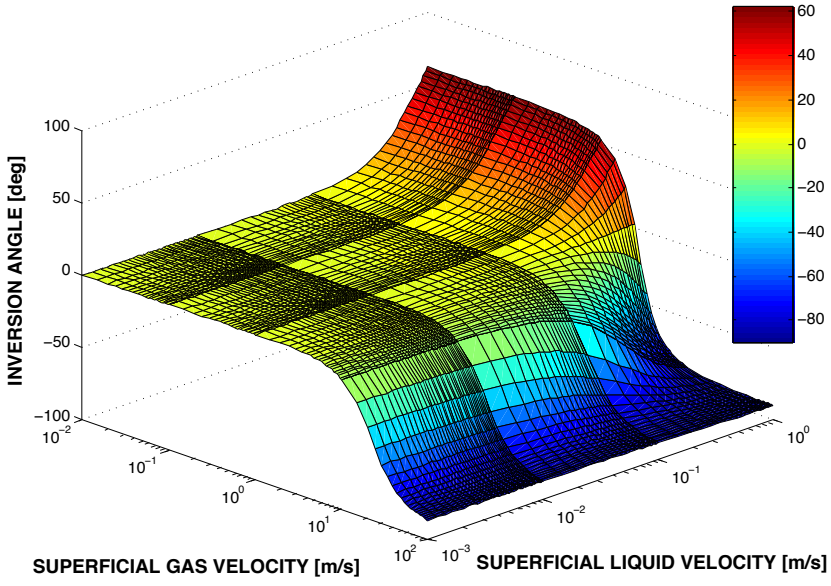

Figure 4.17: Surface describing inversion angle as a function of superficial velocities for Saxena 1990 data. Pipe diameter is 0.01 [m], Coil to Tube Diameter Ratio = 11.

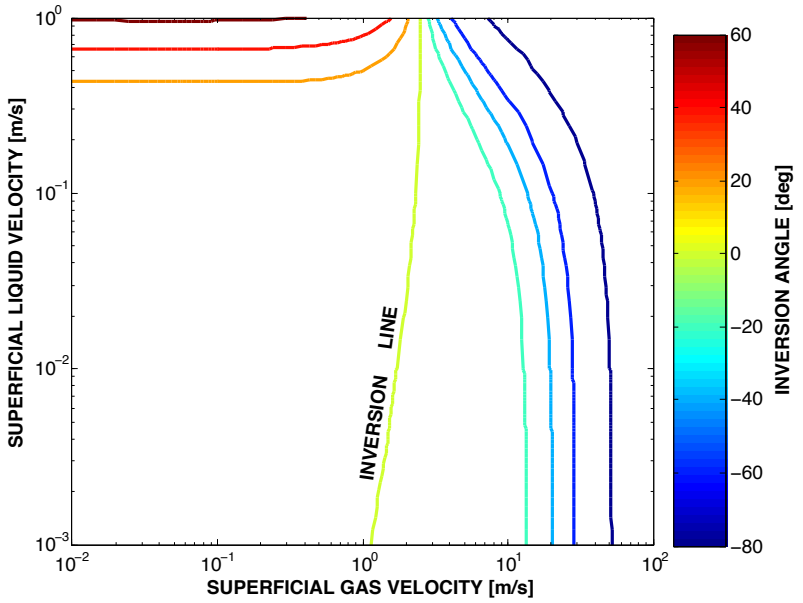

Figure 4.18: Iso-lines describing specific inversion angles as a function of superficial velocities for Saxena 1990 data. Pipe diameter is 0.01 [m], Coil to Tube Diameter Ratio = 11.

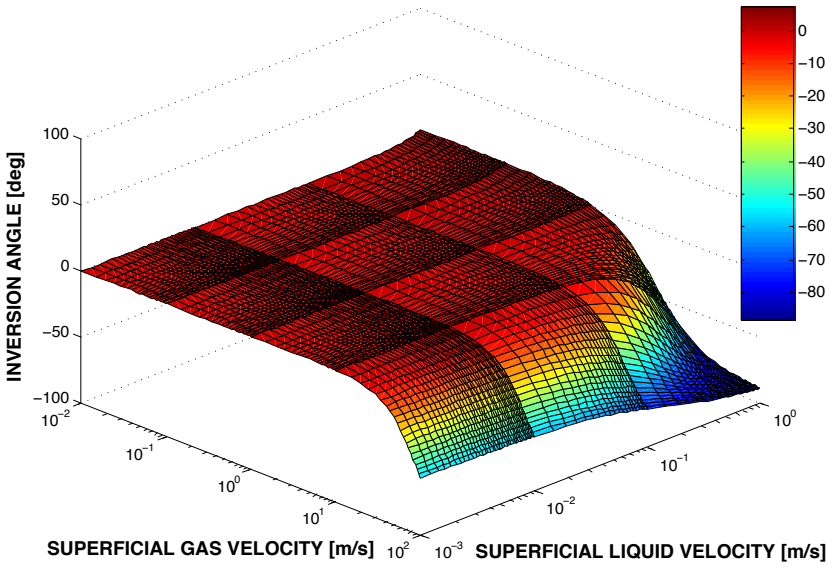

Figure 4.19: Surface describing inversion angle as a function of superficial velocities for Boyce 1969 data. Pipe diameter is 0.0318 [m], Coil to Tube Diameter Ratio = 48.

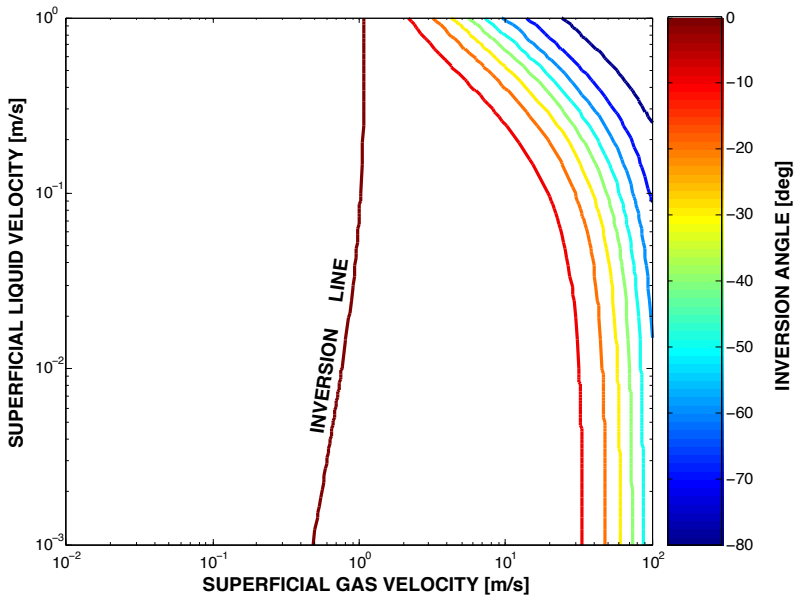

Figure 4.20: Iso-lines describing specific inversion angles as a function of superficial velocities for Boyce 1969 data. Pipe diameter is 0.0318 [m], Coil to Tube Diameter Ratio = 48.

phase increases to a sufficient velocity such that the centrifugal force on the lighter phase is greater than that affecting the denser phase, negative inversion is calculated. Fig. 4.14, Fig. 4.16, Fig. 4.18, and Fig. 4.20 all show the film-inversion line, where the area left of the line represents the denser fluid flowing along the bottom or outside of the bend, and the area to the right representing the film-inversion phenomena of Banerjee (1967). The scale of these plots are similar to those in Sec. 4.5, and the regions of positive and negative inversion can be related to the stratified transitions presented in that section.

4.5 Helical Transition Calculations

The presentation of the comparisons in this section depend on the justification of the use of a horizontal condition in prediction of the stratified transitions for helical coils. Justification is based on, or at least supported by, the published observations of liquid hold-up and the presence of the stratified flow regime in both linear and helical upward flow of slightly inclined pipes. Specifically, it is proposed that the change in the stratified transition boundary location is only weakly dependent on inclination angles when they are less than 5°, even though the inclusion of small inclination angles in the equilibrium height calculation can be in contrast to this. In fact, the predictions of stratified regimes in linear inclined flows often use the horizontal map, for slightly inclined conditions, because the strong dependence of liquid hold-up on inclination basically eliminates the prediction of ANY stratified regime for an inclined pipe. Provided that stratification is present in slightly inclined flows, it is appropriate to use the horizontal map for the slightly inclined pipe flow stratification prediction.

Lun et al. (2004) found that slightly inclined ($\phi \lesssim 5°$) two-phase (oil-water) flows exhibited similar flow patterns to the horizontal cases. Importantly, Lun noted the presence of the stratified regime at these inclinations. Petalas & Aziz (1998) provide comparisons of flow regime maps for both air-water and oil-gas systems. Inspection of the Petalas & Aziz maps show that the two systems experience similar transition boundaries, with the oil-gas system expressing a reduction in the stratified regimes due to fluid property differences. Hence, if stratification is present in a similar oil flow, than it is definitely expected in a water flow. The stratified regime is reported in flow regime observations of both linear and helical upward flowing systems with small inclination angles ($\phi \lesssim 5°$) (Boyce 1969, Saxena 1990, Lun et. al. 2004, Petalas & Aziz 1998).

Barnea & Taitel (1992) and Petalas & Aziz (1998) concluded that huge differences exist in the solution for equilibrium height calculation at small inclination angles, due to the multiple root problem. As an example, Petalas & Aziz (1998) determined that the calculated non-dimensional liquid height varied between $h_l/D \approx 0.05$ and $h_l/D \approx 0.7$ for a 2° inclination case. Petalas & Aziz (1998) recommend the use of the lowest roots, which are near the horizontal calculated values for slightly inclined flows. The issue of accurately predicting the stratified transition can be seen to arise from the initial liquid hold-up calculation used in determining the transition boundary.

For the case of even 1° inclination, the hold-up calculation effectively eliminates the stratified region from being present on the flow map. Yet the stratified flow is reported to exist in these flows. Additionally, reported observations for helical flow indicate a very weak dependence of liquid hold-up on helix angle, see Banerjee et. al. (1969), Xin et. al. (1996), and Mandal & Das (2002 & 2003). All of these studies concluded that liquid hold-up is independent of helix angle for small inclination angle values ($\phi \lesssim 3°$). Based on the recommendation of the use of the lowest root, that this value accurately corresponds to the horizontal values, and the conclusions of Banerjee et. al. (1969), Xin et. al. (1996), and Mandal & Das (2002 & 2003) that inclination angle has negligible effect on liquid hold-up of tightly wrapped helices, it is recommended to use the horizontal condition in calculating the equilibrium heights used in the stratified transition predictions of small inclination tightly wrapped helices.

A comparison of the stratified transition boundary for an example 0.0254 [m] I.D. helical flow with varying coil to tube diameter ratios is shown in Fig. 4.21. The general trend of a reduction in the stratified region in curved upward flows is depicted in the figure. Figures 4.22, 4.23, 4.24, and 4.25 show comparisons of the the current model's prediction of the stratified to non-stratified transition, using the linear and the curvature effects, and the published regime observations of Yan 1992, Ishikawa 2003, Saxena 1990, and Boyce 1969 respectively. Even though the authors of the above mentioned studies are consistent in concluding that the intermittent regime dominates more of the map than the stratified condition, as the curvature increases, only Saxena (1990) reports actual stratified data. All studies, even those that did not publish their data, concluded that the intermittent to annular transition changes so that intermittent dominates more of the map. Reviewing Fig. 4.21, Fig. 4.22, Fig. 4.23, Fig. 4.24, and Fig. 4.25, we see that the current model is in agreement with both of these observations. The intermittent to annular transition moves in favor of the intermittent regime, and the intermittent to stratified transition moves also to favor the intermittent regime. These general trends are shown in Fig. 4.21 with black arrows indicating increasing curvature. Since no new modeling was contributed with respect to the annular-intermittent transition, no credit is taken and individual comparisons are not made.

Review of the surface maps of the inversion angle, and the maps for the stratified transitions, indicates that the stratified transition line would traverse along the region of the inversion surface map where the inversion angle is approximately zero, i.e. no

reinforcement and no stabilization of the stratified condition due to surface orientation. However, with increasing gas superficial velocity, the transition line traverses along the region of the inversion surface where the inversion angle is negative. Specifically, it is found that the surface orientation only has the opportunity to affect the higher gas flow rate region by destabilizing the interface, while the destabilization of the lower gas flow rates occurs due to the increased liquid hold-up. The combination of these two effects is that for the entire range of flows, less of the stratified regime is observed. This is in agreement with all the authors of previous works reported in the literature review.

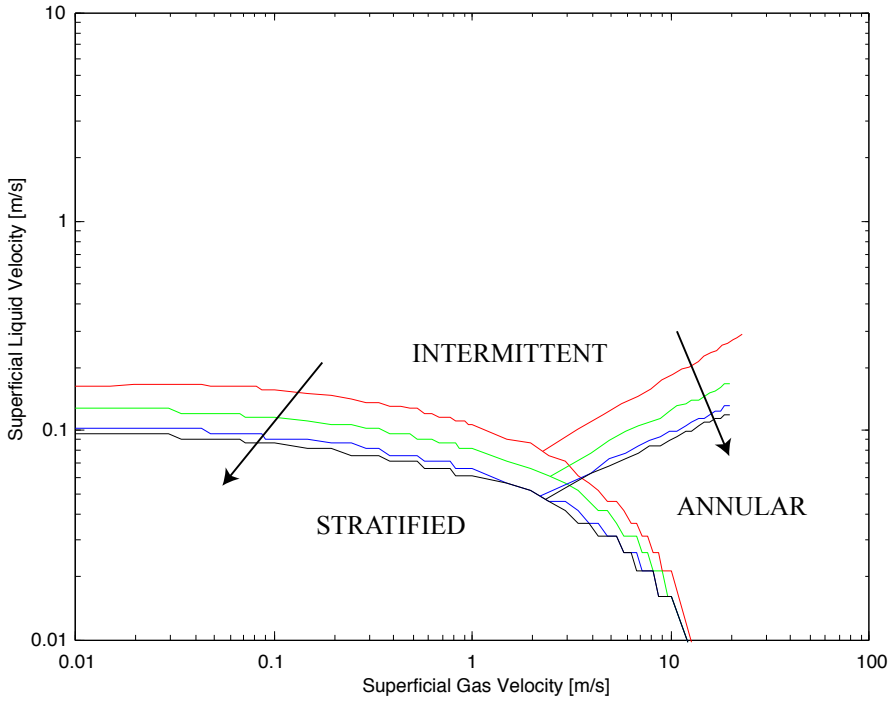

Figure 4.21: Calculation of the stratified transition boundary for different curvature ratios, for the case where linear components and gas phase curved friction multiplier are considered turbulent, and the liquid phase curved friction multiplier is considered laminar. Pipe diameter is 0.0254 [m], red line curvature ratio = 1E6, green line curvature ratio = 100, blue line curvature ratio = 10, black line curvature ratio = 5. Arrows indicate the trend of the transition line with increasing curvature.

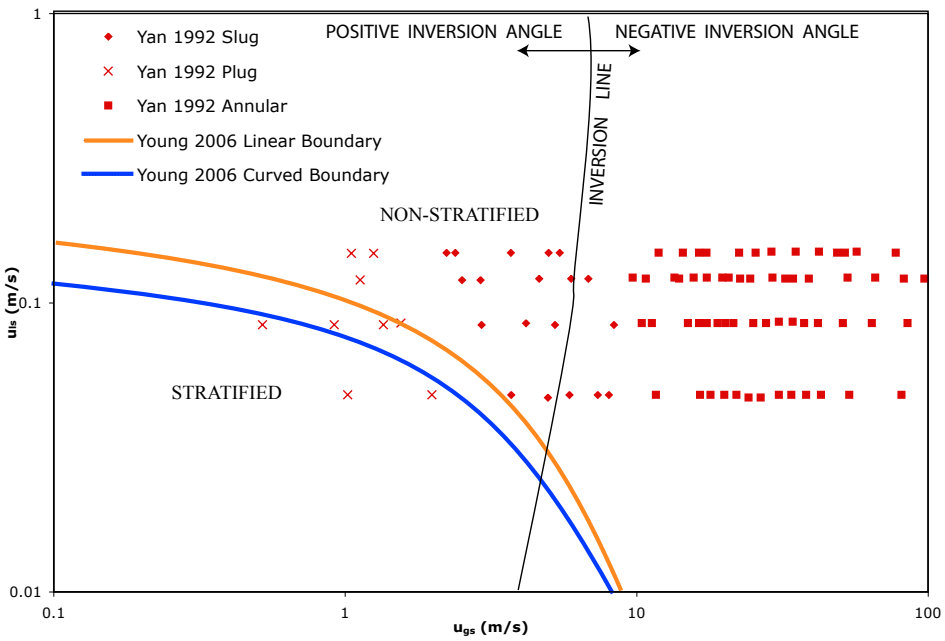

Figure 4.22: Calculation of the stratified transition boundary for Yan 1992 data. Pipe diameter is 0.0083 [m], Coil to Tube Diameter Ratio = 9.

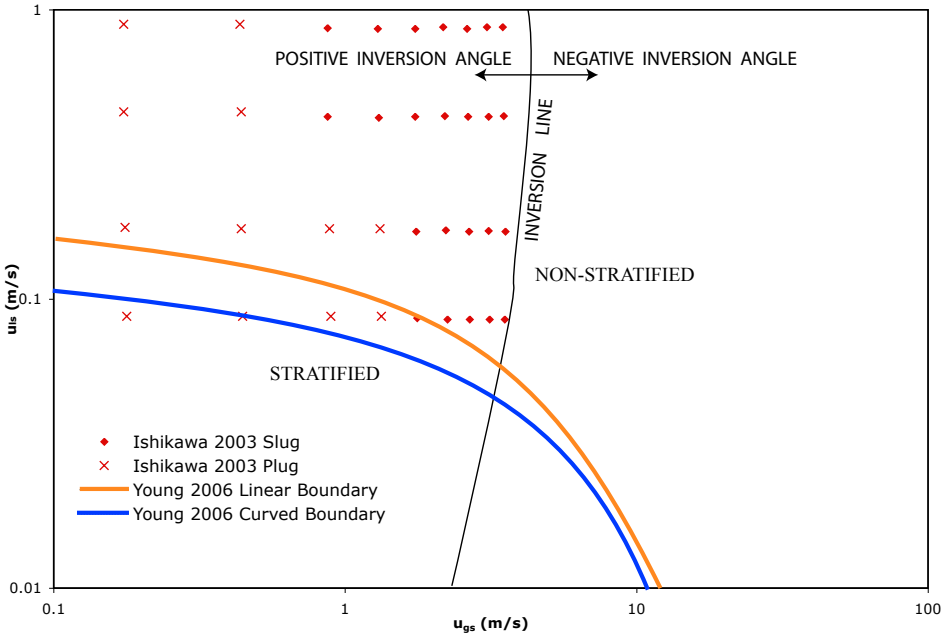

Figure 4.23: Calculation of the stratified transition boundary for Ishikawa 2003 data. Pipe diameter is 0.02 [m], Coil to Tube Diameter Ratio = 27.

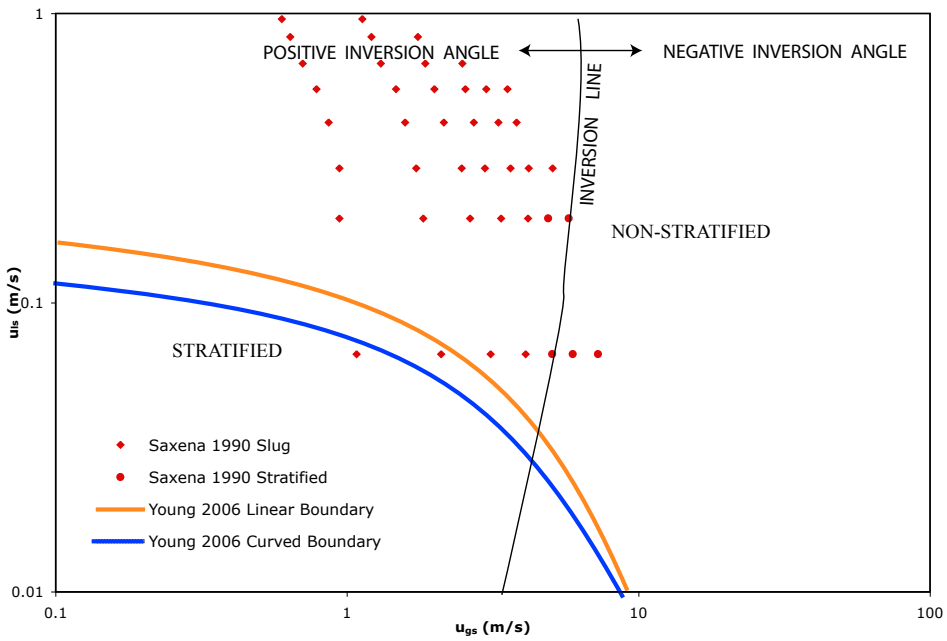

Figure 4.24: Calculation of the stratified transition boundary for Saxena 1990 data. Pipe diameter is 0.01 [m], Coil to Tube Diameter Ratio = 11.

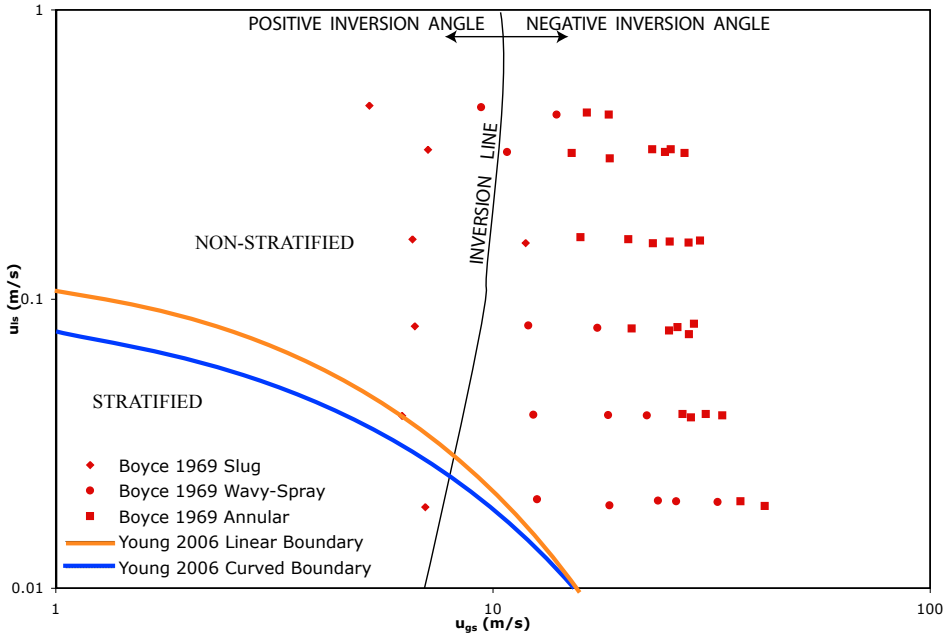

Figure 4.25: Calculation of the stratified transition boundary for Boyce 1969 data. Pipe diameter is 0.0318 [m], Coil to Tube Diameter Ratio = 48.

5 CONCLUSIONS

5.1 Current Model

An extensive literature review was completed of the published works on fluid flows in helical geometries. This has provided much insight into the characteristics of both single and two-phase helical flows, and provided a foundation for the creation of fluid models for this system. A general model was developed to treat centrifugal force effects on the liquid hold-up, interface orientation, and transition between stratified-intermittent/annular. All published helical flow studies are consistent in their observations that a stratified flow condition exists in slightly inclined helical flows, that the intermittent regime dominates a greater range of flows than the stratified regime as curvature effects are introduced, that the intermittent regime dominates a greater range of flows than the annular regime as curvature effects are introduced, and that liquid hold-up increases with increasing curvature. The current model is in agreement with all observations and is an improvement over the previous approaches. The current model provides additional insight into two-phase flow regime transitions of helical coils and an improved method for predicting the major flow regimes observed in helical flow, i.e. intermittent, annular, and stratified.

Specifically, it was found that the current calculated liquid hold-up values:

1. Agree with all published observations for the entire range of Lockhart/Martinelli values for the downflow case.
2. Agree with published observations for the entire range of Lockhart/Martinelli values in the case where pitch is negligible.
3. Agree with published observations for Lockhart/Martinelli values greater than approximately 1 for all upwards inclinations of helix angles, when the liquid curved friction factor is modified.
4. Agree with published observations for Lockhart/Martinelli values greater than approximately 4 in the case where the helical angle results in a Y value of 20, for an unmodified liquid curved friction factor.
5. Agree with published observations for Lockhart/Martinelli values greater than approximately 9 in the case where the helical angle results in a Y value of 100,

for an unmodified liquid curved friction factor.

6. Agree with published observations for Lockhart/Martinelli values greater than approximately 30 in the case where the helical angle results in a Y value of 1000, for an unmodified liquid curved friction factor.

Specifically, it was found that the current calculated flow regime transitions:

1. Agree with all published observations that the stratified regime is suppressed by intermittent flow for two-phase upflow in helices.
2. Agree with all published observations that the annular regime is suppressed by intermittent flow for two-phase upflow in helices.
3. Correctly predicts additional non-stratified data points in comparison to the linear model, for the data reported by all published data that was identified in the literature review.

5.2 Future Work

A major handicap in evaluating the current model is the lack of experimental observation. Where linear methods have a data base of approximately 20,000 laboratory measurements to compare to, only a few hundred are currently published for helical flows. Though work in this area has seen an increase in interest due to the use of helical heat exchangers in the HTR-10 and the HTTR reactor designs, additional flow regime observations are needed to evaluate available methods of predicting flow regime transitions. Specifically, additional experimental observations at lower liquid superficial velocities ($j_g < 0.1$) for a range of curvatures should be studied to determine the actual stratified transition location as a function of flow and geometric parameters.

The current approach utilized a general formulation style for an orthogonal coordinate system, such that the extension to a geometry which includes torsion is possible. Section 2 showed that the study of helical two-phase flow is not at a very mature point in its evolution. Detailed computational modeling of a helical two-phase system could greatly benefit the understanding of how a given flow pattern may arise.

NOMENCLATURE

English Letters

a coil radius $[m]$

A_0 a/r_0, coil to tube radius ratio [non-dimensional]

d_0 tube diameter $[m]$

De Dean number

e internal energy

E^3 Euclidean 3-space

f friction factor

Fr Froude number

H helicity

He helical number [non-dimensional]

j superficial velocity $[m/s]$

J Jacobian operation

k $\frac{2r_0<w>}{\nu}\left(\frac{r_0}{a}\right)^{1/2}$ Dean number as defined by White (1929)

m Mass $[kg]$

p coil pitch $[m]$

R r/a, non-dimensional radius

R_c $r_0/r_c = R_0/\left(1+(p^*/2\pi)^2\right)$

R_0 r_0/a, tube to coil radius ratio [non-dimensional]

r radial distance from the duct centerline $[m]$

r_c $a\left(1+(p/2\pi)^2\right)$, radius of curvature $[m]$

r_0 tube radius $[m]$

s distance along centerline of tube $[m]$

S The surface of a volume region in an integral, or the wetted perimeter.

u radial component of velocity $[m/s]$

v azimuthal component of velocity $[m/s]$

V Volume $[m^3]$

w axial component of velocity, $[m/s]$

$<>$ area average

Greek Letters

Γ_{ijk} Christoffel symbol of the first kind
Γ^{i}_{jk} Christoffel symbol of the second kind
δ differential value, or boundary layer thickness
ν kinematic viscosity
κ curvature of a smooth curve
ρ density $[kg/m^3]$
τ shear stress or torsion
ϕ source term
ψ arbitrary quantity
Ψ stream function

Subscripts

$,i$ The index comma denotes differentiation w/ respect to i, i.e. $F_{,i} = \partial F/\partial x^i$
c coil
g gas
i indicates a coordinate direction or the interface, determined by context. In tensor form this is often a superscript.
j index of the interfaces between phases
k phase index, either liquid or gas phase
l liquid
m mixture
s straight flow
TP two phase
w wall

Superscripts

$\bar{}$ (overbar) time averaged value, or denotes a new coordinate frame
$\bar{\bar{}}$ (double overbar) phase averaged value
$\tilde{}$ (tilde) mass weighted mean value, or non-dimensional parameter
$\dot{}$ (dot) flow rate of value or derivative with respect to a natural parameter, e.g. $\dot{m}$ would be mass flow rate in $[kg/s]$ or $\frac{d\mathbf{x}}{ds}$
$'$ (single prime) a linear flux or derivative, e.g. m' would be linear mass flux in $[kg/ms]$ or $\frac{d\mathbf{m}}{dx}$

$''$ (double prime) an area flux, e.g. m'' would be mass flux in $[kg/m^2s]$

$'''$ (triple prime) a volume flux, e.g. m''' would be mass flux in $[kg/m^3s]$

* non-dimensional quantity

$^\rightarrow$ vector

BIBLIOGRAPHY

1. Abram, J. *Tensor Calculus, Through Differential Geometry*, Butterworths Publishing, 1965.

2. Agrawal, S. S., G. A. Gregory, G. W. Govier, *An Analysis of Horizontal Stratified Two Phase Flow in Pipes*, Can. J. of Chem. Eng., Vol. 51, p. 280, 1973.

3. Akagawa, K., T. Sadaguche, M. Ueda, *Study on a Gas-Liquid Two-Phase flow in Helically Coiled Tubes*, Bulletin of the JSME, Vol. 14, p. 564, 1971.

4. Aris, R. *Vectors, Tensors, and the Basic Equations of Fluid Mechanics*, Dover Publications, 1962.

5. Awwad, A., R. C. Xin, Z. F. Dong, M. A. Ebadian, H. M. Soliman, *Measurement and Correlation of the Pressure Drop in Air-Water Two-Phase Flow in Horizontal Helicoidal Pipes*, International Journal Multiphase Flow, Vol. 21, p. 607, 1995.

6. Baker, O., *Design of Pipeline for Simultaneous Flow of Oil and Gas*, Oil & Gas Journal, July 1954.

7. Banerjee, S. E., A. M. Chan, *Separated Flow Models I. Analysis of the Averaged and Local Instantaneous Formulations*, Int. Journal Multiphase Flow, Vol. 6, p. , 1980.

8. Banerjee, S., E. Rhodes, D. S. Scott, *Film Inversion of Cocurrent Two-Phase Flow in Helical Coils* , AIChE Journal, Vol. 13, p. 189, 1967.

9. Banerjee, S., E. Rhodes, D. S. Scott, *Studies on Co-Current Gas-Liquid Flow in Helically Coiled Tubes, I. Flow Pattern Pressure Drop and Hold-Up*, Can. J. of Chem. Eng., Vol. 47, p. 445, 1969.

10. Barnea, D., *A Unified Model for Predicting Flow-Pattern Transitions for the Whole Range of Pipe Inclinations*, International Journal of Multiphase Flow, Vol. 13, p. 1, 1987.

11. Barnea, D., Y. Taital, *Structural and Interfacial Stability of Multiple Solutions for Stratified Flow*, Int. J. of Multiphase Flow, Vol. 18, p. 821, 1992.

12. Barua, S. N., *On Secondary Flow in Stationary Curved pipes*, Q. J. Mech. & Appl. Math, Vol. 16, p. 61, 1963.

13. Berger, S. A., L. Talbot, S. S. Yao, *Flow in Curved Pipes*, Annual Review of Fluid Mechanics, Vol. 15, p. 461, 1983.

14. Bonnecaze, R. H., W. Erskine, E. J. Greskovich, *Holdup and Pressure Drop for Two-Phase Flow Slug Flow in Inclined Pipes*, AIChE Journal, Vol. 17, p. 1109, 1971.

15. Boyce, B. E., J. G. Collier, J. Levy,*Hold-Up and Pressure Drop Measurements in the Two-Phase Flow of Air-Water Mixtures in Helical Coils*, Proc. Int. Symp. On Research in Cocurrent Gas-Liquid Flow, University of Waterloo, p. 203, 1969.

16. Brodkey, R. S., *The Phenomena of Fluid Motion*, Addison-Wesley Publishing Commpany, p. 466, 1967.

17. Carter, J. A., *A Turbannular Flow Process for the Continuous Polymerisation of 6.6 Nylon*, AIChE, I. Chem. E Symposium Series No.3, p. 29, 1965.

18. Chandrasekhar, S., *Hydrodynamic and Hydromagnetic Stability*, Oxford University Press, 1961.

19. Chen, X., L. Guo, *Flow Patterns and Pressure Drop in Oil-Air-Water Three-Phase Flow Through Helically Coiled Tubes*, International Journal of Multiphase Flow, Vol. 25, p. 1053, 1999.

20. Chen, Y., *Modeling Two-Phase Flow in Pipes: Flow Pattern Transitions and Drift Flux Modeling*, M.S. Thesis, Stanford University, 2001.

21. Collins, W. M., S. C. R. Dennis, *The Steady Motion of Viscous Fluid in a Curved Tube*, Quarterly Journal of Mechanics and Applied Mathematics, Vol. 28, p. 133, 1975.

22. Dean, W. R., *Note on the Motion of Fluid in a Curved Pipe*, Phil. Mag., Vol. 4, 1927.

23. Dean, W. R., *The Stream-Line Motion of Fluid in a Curved Pipe*, Phil. Mag., Vol. 5, 1928.

24. Delhaye, J. M., *Equations Fondamentales des Ecoulements Diphasique*, CEA-R-3429, (1) et (2), 1968.

25. Delhaye, J. M., *General Equations of Two-Phase Systems and Their Application to Air-Water Bubble Flow and to Steam-Water Flashing Flow*, ASME Paper 69-HT-63, 11th Heat Transfer Conference, Minneapolis, 1969.

26. Delhaye, J. M., P. Vernier, *General Two-Phase Flow Equations Applied to Thermodynamics of Boiling Water Reactors*, Energie Primaire, Vol. 4. No. 1, 1968.

27. Delhaye, J. M., *Local Time Averaged Equations*, Proceedings of NATO Advanced Study Institute, Two-Phase Flows and Heat Transfer, Vol. 1, p. 91, 1976.

28. Dennis, S. C. R., M. Ng, *Dual Solutions for Steady Laminar Flow Through a Curved Tube*, Quarterly Journal of Mechanics and Applied Mathematics, Vol. 35, p. 305, 1982.

29. Dukler, A. E., M. Wicks, *Gas-Liquid Flow in Conduits*, in Modern Chemical Engineering, (A. Acrivos ed.), Vol. 1, p. 345, Rheinhold, New York, 1963.

30. Dukler, A. E., J. A. Fabre, J. B. McQuillen, R. Vernon, *Gas-Liquid Flow at Microgravity Conditions: Flow Patterns and Their Transitions*, Int. J. Multiphase Flow, vol. 14, p.389, 1988.

31. Etchells, A. W., *Stratified Horizontal Two Phase Flow in Pipe*, Ph.D. Thesis, University of Delaware, 1970.

32. Eustice, J., *Experiments on Stream-line Motion in Curved Pipes*, Proc. Roy. Soc. A, Vol. 85, p. 119, 1911.

33. Germano, M. *The Dean Equations Extended to a Helical pipe Flow*, Journal Fluid Mechanics, Vol. 203, p. 289, 1988.

34. Germano, M., *On the Effect of Torsion on a Helical Pipe Flow*, Journal of Fluid Mechanics, Vol. 125, p. 1, 1982.

35. Gilli, P. V., *Heat Transfer Characteristics of Helical Tube Bundles as used in Steam Generators of Gas-Cooled Reactors*, 3rd Int. Conf. On Peaceful Uses of Atomic Energy, Geneva Paper A/CONF.28/P/519, 1964.

36. Goering, D. J., *The Influence of Curvature and Buoyancy in Three-Dimensional Pipe Flows*, Ph.D. Dissertation, University of California at Berkeley, 1989.

37. Gouse, S. W., *An Introduction to Two-Phase Flow*, MIT Report DSR873-3, June 1964.

38. Govier, G. W., K. Aziz, *Flow of Complex Mixtures in Pipes*, Text by Van Nostrand-Reinhold, New York, 1972.

39. Gratton, M., *The Effects of Torsion on Anomalous Diffusion in Helical Pipe Flow*, Masters Thesis, Harvey Mudd College, 2002.

40. Grindley, J. H., A. H. Gibson, *On the Frictional Resistance to the Flow of Air through a Pipe*, Proc. Roy. Soc., Vol. 80, p. 114, 1908.

41. Hamersma, P. J., J. Hart, *A pressure Drop Correlation for Gas/Liquid Pipe Flow With a Small Liquid Holdup*, Chem. Engng. Sci., Vol. 42, p. 1187, 1987.

42. Hart, J., J. Ellenberger, P. J. Hamersma, *Single and Two-Phase flow Through Helically Coiled Tubes*, Chemical Engineering Science, Vol. 43, p. 775, 1988.

43. Hart, J., J. Ellenberger, P. J. Hammersma, *Single and Two Phase Flow Through Helically Coiled Tubes*, Chem. Eng. Sci., Vol. 43, p. 775, 1988.

44. Hayashi, T., *Comparison of Heat Transport Capability of a Steam Generator (SG) in a High-Temperature-Gas-Cooled Reactor With That of an SG in Other Types of Reactors*, Nuclear Technology, Vol. 78, 1987.

45. Hefferon, J., *Linear Algebra*, Free e-book, archived at http://joshua.smcvt.edu/linearalgebra/, 2003.

46. Hoogendoorn, C. J., *Gas-Liquid Flow in Horizontal Pipes*, Chem. Eng. Sci., Vol. 9, p. 205, 1959.

47. Huang, W., D. Gu, *A Study of Secondary Flow and Fluid Resistance in Rectangular, Helical coiled Channel*, Int. Chem. Eng., Vol. 29, p. 480, 1989.

48. Hsu, Y.Y., R. W. Graham, *Transport Processes in Boiling and Two-Phase Systems*, American Nuclear Society publication. 1986.

49. Isbin, H. S., Y. S. Su, *Use of Mechanical Energy Balance for Two-Phase Flow*, Journal of American Institute of Chemical Engineers, Vol. 7, p. 174, 1961.

50. Ishii, M., *Thermo-Fluid Dynamic Theory of Two-Phase Flow*, Text - Eryolles Paris, 1975.

51. Ishii, M., *Drift Flux Model and Derivation of Kinematic Constitutive Laws*, Proceedings of NATO Advanced Study Institute, Two-Phase Flows and Heat Transfer, Vol. 1, p. 91, 1976.

52. Ishikawa, M., H. Oiwa, K. Sakai, Y. Murai, S. Toda, K. Tamayama, F. Yamamoto, *Flow Structure and Pressure Loss of Two-Phase flow in Helically coiled Tubes*, Proceedings of 4th Joint ASME / JSME Fluids Engineering Conference, p. 1453, 2003.

53. Ito, H., *Friction Factors for Turbulent Flow in Curved Pipes*, Trans. ASME D81, p. 123, 1959.

54. Ito, H., *Laminar Flow in Curved Pipes*, Z. Angew. Math Mech., Vol. 49, p. 653, 1969.

55. Jenkins, R., M.Ch.E. Thesis, Univ. of Del., 1947 (As referenced in [30]).

56. Joseph, B., E. P. Smith, R. J. Adler, *Numerical Treatment of Laminar Flow in Helically Coiled Tubes of Square Cross Section*, AIChE Journal, Vol. 21, p. 965, 1975.

57. Ju, H., Y. Zhang, Z. Huang, Z. Liu, J. Li, Y. Yu, *Experimental and Operational Verification of the HTR-10 Once-Through Steam Generator*, Journal of Nuclear Science and Technology, Vol. 41, p. 765, 2004.

58. Ju, H., Z. Huang, Y. Xu, B. Duan, Y. Yu, *Hydraulic Performance of Small Bending Radius Helical Coil-Pipe*, Journal of Nuclear Science and Technology, Vol. 38, p. 826, 2001.

59. Kao, H. C., *Torsion Effect on Fully Developed Flow in a Helical Pipe*, Journal Fluid Mechanics, Vol. 184, p. 335, 1987.

60. Kasturi, G., J. B. Stepanek, *Two Phase Flow I & II. Pressure Drop and Void Fraction Measurements in Cocurrent Gas-Liquid Flow in a Coil,*, Chemical Engineering Science, Vol. 27, p. 1871, 1972.

61. Keshock, E. G., C. S. Lin, M. E. Harrison, L. G. Edwards, J. Knapp, X. Zhang, *Measurement of Two-Phase Flow Characteristics Under Microgravity Conditions*, 4th Microgravity Fluid Physics & Transport Phenomena Conference, 1998.

62. Kocamustafaogullari, G., *Thermo-Fluid Dynamics of Separated Two-Phase Flow*, Ph. D. Dissertation, Georgia Institute of Technology, 1971.

63. Koutsky, J. A., R. J. Adler, *Minimization of Axial Dispersion by Use of Secondary Flow in Helical Tubes*, Canadian Journal of Chemical Engineering, Vol. 42, p. 239, 1964.

64. Kutaleladze, S. S., *Heat Transfer in Condensation and Boiling*, Moscow, AEC-TR-3770, USAEC Technical Information Service, 1952.

65. Lamb, D. E., J. L. White, *Use of Momentum and Energy Equation in Two-Phase Flow*, Journal of American Institute of Chemical Engineers, Vol. 8, p. 281 1962.

66. Lavine, A. G., *A Three-Dimensional Analysis of Natural Convection in a Toroidal Loop*, Ph.D. Dissertation, University of California, Berkeley, 1984.

67. Linehan, J. H., *The Interaction of Two-Dimensional, Stratified, Turbulent Air-Water and Steam-Water Flows*, Argonne National Laboratory Report ANL-7444, Argonne Illinois, 1968.

68. Lipschultz, M., *Differential Geometry*, Schaum's Outline Series, McGraw-Hill, 1969.

69. Liu, S., A. Afacan, H. A. Nasr-El-Din, J. H. Masliyah, *An Experimental Study of Pressure Drop in Helical Pipes*, Proceedings of the Royal Society of London. Series A, Vol. 444, p. 307, 1994

70. Lockhart, R. W., R. C. Martinelli, *Proposed Correlation of Data for Isothermal two-Phase, Two-Component Flow in Pipes*, Chemical Engineering Progress, Vol. 45, p. 39, 1949.

71. Lum, Y. L., J. Lovick, P. Angeli, *Low Inclination Oil-Water Flows*, Canadian Journal of Chemical Engineering, Vol. 82, p. 303, 2004

72. Mandal, S. N., S. K. Das, *Gas-Liquid Flow Through Coils*, Proceedings of the 9^{th} APCChE Congress & CHEMECA 2002, p. 198, 2002.

73. Mandal, S. N., S. K. Das, *Gas-Liquid Flow Through Helical Coils in Vertical Orientation*, Ind. Eng. Chem. Res., Vol. 42, p. 3487, 2003.

74. Mandal, S. N., S. K. Das, *Gas-Liquid Flow Through Helical Coils in Horizontal Orientation*, Canadian Hournal of Chemical Engineering, Vol. 80, p. 979, 2002.

75. Mandhane, J. M., G. A. Gregory, K. Aziz, *A Flow Pattern Map for Gas-Liquid Flow in Horizontal Pipes*, International Journal Multiphase Flow, Vol. 1, p. 537, 1974.

76. Manlapaz, R. L., S. W. Churchill, *Fully Developed Laminar Convection From a Helical Coil*, Chem. Eng. Communications, Vol. 9, p. 185, 1981.

77. Manlapaz, R. L., S. W. Churchill, *Fully Developed Laminar Flow in a Helically Coiled Tube of Finite Pitch*, Chemical Engineering Communications, Vol. 7, p. 57, 1980.

78. Martinelli, R.C., D. B. Nelson, *Prediction of pressure drop during forced circulation boiling of water*, Transactions, American Society of Mechanical Engineers, Vol. 70, p. 695, 1948.

79. Matteo, C., *Mechanistic Modeling of Slug Dissipation in Helical Pipes,*, Masters Thesis, University of Tulsa, 2003.

80. McConalogue, D. J., R. S. Srivastava, *Motion of a fluid in a curved tube*, Proceedings of the Royal Society of London. Series A, Vol. 307, p. 37, 1968.

81. Milne-Thomson, L. M., *Theoretical Hydrodynamics*, Macmillan Company, New York, 1960.

82. Minton, P. E., *Designing spiral-Tube Heat Exchangers*, Chemical Engineering, p. 145, 1970.

83. Mishra, P., S. N. Gupta, *Momentum transfer in curved pipes. 1. Newtonian Fluids*, Int. J. Heat Mass Transfer, Vol. 8, p. 67, 1979.

84. Mori, Y., W. Nakayama, *Study on Forced Convection Heat Transfer in Curved Pipes*, International Journal Heat and Mass Transfer, Vol. 8, p. 67, 1965 .

85. Morton, F., P. J. King, A. McLaughlin, *Helical Coil Distillation Columns Parts I-II*, Trans. Instn. Chem. Engrs., Vol. 42, p. 285, 1964.

86. Mujawar, B. A., M. Raja Rao, *Gas-Non-Newtonian Liquid Two-Phase Flow in Helical Coils*, Ind. Eng. Chem. Process Des. Dev., Vol. 20, p. 391, 1981.

87. Murata, S., Y. Miyake, T. Inaba, H. Ogawa, *Laminar Flow in a Helically Coiled Pipe*, Bulletin JSME, Vol. 24, p. 355, 1981.

88. Nandakumar, K., J. H. Masliyah, *Bifurcation in Steady Laminar flow Through Curved Tubes*, Journal of Fluid Mechanics, Vol. 119, p. 475, 1982.

89. Oiwa, H., Y. Murai, M. Ishikawa, Y. Yamamoto, *Numerical Analysis of Bubbly Flow in Helical Tubes*, Proceedings of the 15th Symposium on CFD, C14-3, p. 1, 2001.

90. Peebles, F. N., H. J. Garber, *Studies on the Motion of Gas Bubbles in Liquids*,Chemical Engineering Progress, Vol. 49, p. 88, 1953.

91. Petalas, N., Aziz, K., *A Mechanistic Model for Stabilized Multiphase Flow in Pipes,*, CIM 98-39, Proceedings, 49th Annual Technical Meeting of the Petroleum Society of the CIM, Calgary, Alberta, Canada, June 8-10, 1998.

92. Petalas, N., Aziz, K., *A Mechanistic Model for Multiphase Flow in Pipes*, Journal of Canadian Petroleum Technology, Vol. 39, p. 43, 2000.

93. Quanping, Y., G. H. Hu, *Development of a Helical Coordinate System and its Application to Analysis of Polymer Flow in Screw Extruders. Part I. The Balance Equations in a Helical Coordinate System*, Journal of Non-Newtonian Fluid Mechanics, Vol. 69, p. 155, 1997.

94. Rangacharyulu, K., G. S. Davies, *Pressure Drop and holdup Studies of Air-Liquid Flow in Helical Coils*, The Chemical Engineering Journal, Vol. 29, p. 41, 1984.

95. Rippel, G. R., C. M. Eidt, H. B. Jordan, *Two Phase Flow in Coiled Tube*, Ind. Eng. Chem. Proc. Des. Dev., Vol. 5, p. 32, 1966.

96. Ros, N. C. J., *Simultaneous Flow of Gas and Liquid as Encountered in Well Tubing*, Journal of Petroleum Technology, Vol. 13, p. 1037, 1961.

97. Saxena, A. K., A. Schumpe, K. D. P. Nigam, W. D. Deckwer, *Flow Regimes, Hold-up and Pressure Drop for Two Phase Flow in Helical Coils*, The Canadian Journal of Chemical Engineering, Vol. 68, 1990.

98. Scott, D. S., *Properties of Concurrent Gas-Liquid Flow*, Advances in Chemical Engineering, Vol. 4, p. 199, Academic Press, 1963.

99. Sharipov, R. A., *Quick Introduction to Tensor Analysis*, Online Distributed Notes, Online archive http://uk.arxiv.org/, 2004.

100. Soeberg, H., *Viscous Flow in Curved Tubes: I. Velocity Profiles*, Chemical Engineering Science, Vol. 43, p. 855, 1988.

101. Sokolnikoff, L. S., *Tensor Analysis: Theory and Applications to Geometry and Mechanics of Continua*, John Wiley & Sons, 1964.

102. Spedding, P. L., J. J. J. Chen, V. T. Nguyen, *Pressure Drop in Two Phase Gas-Liquid Flow in Inclined Pipes*, Int. J. Multiphase Flow, Vol. 8, p. 407, 1981.

103. Spiegel, M. R., *Vector Analysis - And an Introduction to Tensor Analysis*, Schaum's Outline Series, McGraw-Hill, 1959.

104. Taitel, Y., A. E. Dukler, *A Model for Predicting Flow Regime Transitions in Horizontal and Near Horizontal Gas-Liquid Flow*, AIChE Journal, Vol. 22, p. 47, 1976.

105. Taitel, Y., N. Lee, A. E. Dukler, *Transient Gas-Liquid Flow in Horizontal Pipes: Modeling the Flow Pattern Transitions*, AIChE, Vol. 24, p. 920, 1978.

106. Taylor, G. I., *The Criterion for Turbulence in Curved Pipes*, Proceedings of the Royal Society of London. Series A, Vol. 124, p. 243, 1929

107. Thome, J. R., J. E. Hajal, *Two-Phase Flow Pattern Map for Evaporation in Horizontal Tubes: Latest Version*, Heat Transfer Engineering, Vol. 24, p. 3, 2003.

108. Thomson, J., LL. D., F. R. S. E., *On the Origin of Windings of Rivers in Alluvial Plains, with Remarks on the Flow of Water Round Bends in Pipes,*, Proceedings of the Royal Society of London. Series A, Vol. 25, p. 5, 1876.

109. Todreas, N. E., M. S. Kazimi, *Nuclear Systems I: Thermal Hydraulic Fundamentals*, Hemisphere Publishing text, 1989.

110. Truesdell, C., *Mechanical Basis of Diffusion*, Journal of Chemical Physics, Vol. 37, p. 2336, 1962.

111. Truesdell, L. C., R. J. Adler, *Numerical Treatment of Fully Developed Laminar Flow in Helically Coiled Tubes*, AIChE Journal, Vol.16, p. 1010, 1970.

112. Tung, T. T., R. L. Laurence, *A Coordinate Frame for Helical Flows*, Polymer Engineering and Science, Vol. 15, p. 401, 1975.

113. Tuttle, E. R., *Laminar Flow in Twisted Pipes*, Journal of Fluid Mechanics, Vol. 219, p. 545, 1990.

114. Uddin, A. K. *A Model To Predict Two-Phase Flow Patterns in Helically Coiled Tubes*, Miami International Symposium on Multiphase Transport and Particulate Phenomena, p. 219, 1988.

115. Van Dyke, M. *Extended Stokes Series: Laminar Flow Through a Loosely Coiled Pipe*, Journal of Fluid Mechanics, Vol. 86, p. 129, 1978.

116. Vohr, J., *The Energy Equation for Two-Phase Flow*, Journal of American Institute of Chemical Engineers, Vol. 8, p. 280, 1962.

117. Wallis, G. B., *One Dimensional Two-Phase Flow*, McGraw-Hill, New York, 1969.

118. Wang, C. Y., *On the Low-Reynolds-Number Flow in a Helical Pipe*, Journal Fluid Mechanics, Vol. 108, p. 185, 1981.

119. Wang, J. W., J. R. G. Andrews, *Numerical simulation of flow in Helical Ducts*, AIChE Journal, Vol. 41, p. 1071, 1995.

120. Webster, D. R., J. A. C. Humphrey, *Traveling Wave Instability in Helical Coil Flow*, Phys. Fluids, Vol. 9, p. 407, 1997.

121. Whalley, P. B., *Air-Water Two-Phase Flow in a Helically Coiled Tube*, Journal of Multiphase Flow, Vol. 6, p. 345, 1980.

122. White, C. M., *Streamline Flow Through Curved Pipes*, Proc. Royal Soc., A123, p. 645, 1929.

123. Wu, Q., M. Ishii, *Interfacial Wave Stability of Concurrent Two-Phase Flow in a Horizontal Channel*, Int. J. Heat Mass Transfer, Vol. 39, p. 2067, 1996.

124. Xiao, J. J., O. Shoham, J. P. Brill, *A Comprehensive Mechanistic Model for Two-Phase Flow in Pipelines*, Paper SPE 20631, 65^{th} ATC&E of SPE, New Orleans, 1990.

125. Yan, A., *Study of Two-Phase Flow Patterns and Frictional Pressure Drop in Helical and Spiral Coils*, Masters Thesis, University of Tennessee, Knoxville, 1992.

126. Zabielski, L., A. J. Mestel, *Steady Flow in a Helically Symmetric Pipe*, Journal Fluid Mechanics, Vol. 370, p. 297, 1998.

127. Zuber, N., *The Effects of Non-uniform Flow and Concentration Distributions and the Effect of the Local Relative Velocity on the Average Volumetric Concentration in Two-Phase Flow*, GEAP-4542, General Electric Co., 1964.

128. Zürcher, O., D. Favrat, J. R. Thome, *Development of a Diabatic Two-Phase Flow Pattern Map for Horizontal Flow Boiling*, Int. Journal of Heat and Mass Transfer, Vol. 45, p. 291, 2002.

APPENDIX

A – Coordinate Formulation Background

The review of literature on helical flow modeling (Sec. 2.6) exposed contention with respect to what is the *correct* helical coordinate system, and each author has their own opinion as to the answer. It is in the mathematics and models that the opinions of the different authors play out. For the most part the statements are understandable and the ideas easily followed. However, when the the works of Sec. 2.6 were first read by the author of this dissertation, some objects were not fully understood. In hopes of fostering better understanding, some background concepts are discussed here. Information for this subsection is derived from Aris (1962), Abram (1965), Tung & Laurence (1975), Hefferon (2003), and Sharipov (2004). Since the concepts are general and the merger of ideas from all the sources, individual references are not given in this subsection. The concepts covered are:

- The need for coordinate systems which match the geometry of the flow.
- Curvilinear coordinate systems, as the helical system is curvilinear.
- The basis and dual basis coordinate systems.
- The definition and physical importance of the Jacobian.
- Contravariant and covariant objects.
- Metric tensors.
- Christoffel symbols.

The discussion in Section 2.6 is concerned with the proper description of a curved flow field. This flow lives in the same 3-space as the rest of us, but has the distinction that its path is shaped to follow a symmetrically advancing curve through 3-space. Since it exists within this confinement, it is advantageous to describe its motion by a locally concise system. An example would be using a polar coordinate system instead of a Cartesian system, for describing the velocity distribution of a circular pipe, see Fig A.1. In this example, the Cartesian cross-stream velocity gradient is not always aligned with one of the coordinate directions, which introduces difficulty in formulating things like the shear stress at the wall. For this reason, circular pipe

flow is often formulated in polar cylindrical coordinates. For similar reasons, helical flow is most often formulated in toroidal coordinates.

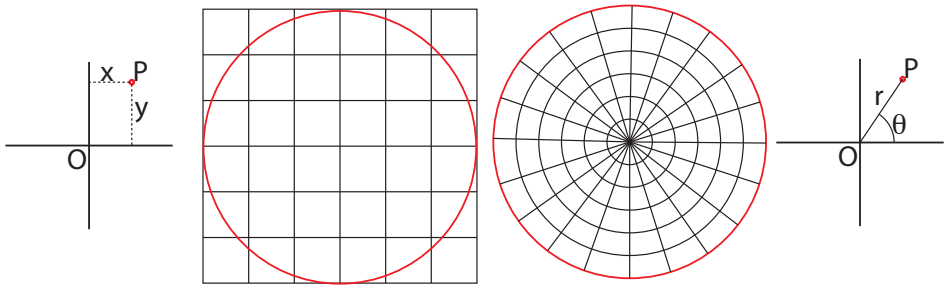

Figure A.1: Example of using Cartesian and Polar coordinate systems for describing the cross-section of a pipe. The pipe wall is shown in red.

What makes a given system curvilinear or not has to do with what are called coordinate curves or lines. These are the curves in space generated by holding two of the three coordinates constant, and varying the third. The Cartesian description of space creates straight coordinate lines for each of the three coordinates, where the cylindrical and spherical coordinate systems both produce at least one coordinate curve that is not a straight line. For this reason, the latter two are what we call curvilinear systems. Extending this idea, coordinate planes can be created by holding one coordinate constant and varying the other two. This creates surfaces in space that are flat and parallel to the coordinate direction for a rectilinear system and surfaces with curvature in a curvilinear system. Coordinate curves for Cartesian and polar spherical systems are shown in Fig. A.2. It is found that all systems describing helical flow are curvilinear, and that the same vector entity placed at two different locations in a curvilinear system will have different vector components, which motivates the description of these objects.

Aris (1962) justifies developing tensor analysis, when he states "... *tensor calculus is the natural language of continuum or field theories* ... (hence also) *fluid mechanics*". And in the case of helical flow, tensor methods are found to be indispensable. Tensor analysis is based on linear algebra, vector spaces, the explicit consideration of the basis, and centered on identification of an object's behavior under transformation. Vector space is an extension of the simpler scalar space, which is the geometric space that we live in, and can be developed by first looking at scalar space. The model of scalar space was originally formalized in the work *Elements* by Euclid in the 3^{rd}

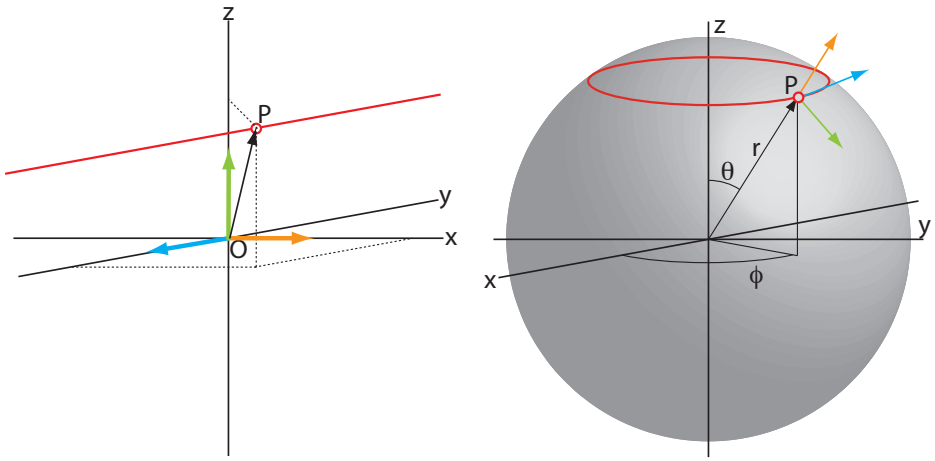

Figure A.2: Example of Cartesian and Polar Spherical coordinate curves, shown in red. Cartesian curve is generated by varying the y coordinate, and the spherical curve is for varying the ϕ coordinate.

century B.C. For this reason, you will often hear reference to Euclidean 3-space (E^3) when reading physics or math texts. The elements to which Euclid spoke are the point, line, and plane, and the definition of E^3 was formed by compliance to 5 axioms that describe the relations of belonging, betweeness, and congruence of these elements. An interesting point on Euclid's work is that the original postulates did not hold up under all tests it has underwent, and over the past 2000 years the axioms have been increased in number to 20.

Vital to using a particular system is the definite description of all the positions residing within the system. Identification of positions within space begins with first choosing an origin as a reference location, then giving the position in relation to this origin. The choice of the origin is quite arbitrary, and can be placed at the whim of the researcher (though some placements obviously have advantages). Referencing the location of a point in space to this origin is easily carried out by introducing the concept of vectors, and vector space. Vector space is a necessary framework for vectors to exist logically, and is defined by two operations. The operations are *vector summation* and/or *scalar multiplication*, and result in an object who is also a member of the set. The gist of these rules can be stated mathematically by Eqs. A.1, for the set of vectors V. These are referred to as the vector space closure rules.

$$\mathbf{u} \in V \quad \text{for all} \quad \mathbf{u} = \mathbf{v} + \mathbf{w} \tag{A.1a}$$

$$\mathbf{u} \in V \quad \text{for all} \quad \mathbf{u} = \mathbf{r} \cdot \mathbf{v} \quad \text{where} \quad r \in R \tag{A.1b}$$

The addition rule is defined in such a way that the combination of any three non-coplanar vectors can definitely describe a general vector in space. When non-coplanar vectors are used for describing vectors they are referred to as the basis of the system. It is usual that the basis are unit length vectors aligned with the coordinate axes. Then the vector components of the displacement vector are simply scaler multiples of these base vectors. In Figure A.2, the origin is labeled point (O), the point in space as (P), and the base vectors are colored line segments with arrowheads. Figure A.3 depicts the components of the displacement vector (d_x, and d_y), the base components of a velocity vector located at point P (v_x, and v_y), and the basis vectors of the x and y coordinate axes (e_x, and e_y). As shown in the figure, the vector components are parallel to the basis vectors and differ only in length. The length is described by a scalar multiplication factor. When the basis vectors are constructed in a rectilinear system like the Cartesian system, they transform simply and vector functions can be described by parallel translation to the origin then compared to the system basis. This translation of the velocity vector to the origin is visualized in Fig. A.3, and the equations for the position and velocity vectors are given in Eqs. A.2. Items in boldface ($\mathbf{x}$) or with an overarrow ($\vec{x}$) are vector quantities, and those without are scalar quantities. Note that the basis vectors (e_i) can be functions of position, and are required to be independent. Independence is quickly described as the case that any one of the bases cannot be expressed in terms of the other bases.

$$\mathbf{d} = \mathbf{d}_x + \mathbf{d}_y = d_x\mathbf{e}_x + d_y\mathbf{e}_y \tag{A.2a}$$

$$\mathbf{v} = \mathbf{v}_x + \mathbf{v}_y = v_x\mathbf{e}_x + v_y\mathbf{e}_y \tag{A.2b}$$

The example is extended to three dimensions, and a simplifying convention is introduced that is an indispensable part of tensorial methods. This convention is simply a rule that repeated Latin indices (i, j, k) on one side of the equality, one in the upper and one in the lower index position, are summed over the values of 1, 2, and 3; repeated Greek (α, β, γ), with one in the upper and one in the lower index position, are summed over the values of 1 and 2. It should be said that in rectilinear systems, the summation convention is used loosely, and summation is often carried out over two lower, two upper, or upper and lower positioned indices. When an index is not repeated on one side of the equation, it is not summed and can take on any of the

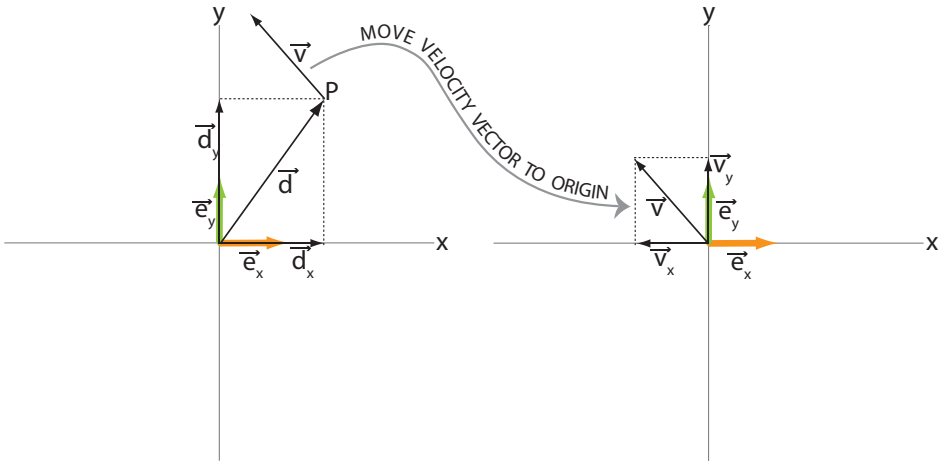

Figure A.3: A nice attribute of the Cartesian coordinate system, transformation of basis vectors does not change them, i.e. they are not dependent on position.

available values. These two types of indices are referred to as dummy and free indices, respectively. The exclusion of the explicit summation symbol and use of repetition to indicate the free and dummy indices was first proposed by Einstein, and is referred to as Einstein notation. The use of this convention is shown in Equation A.3, which, when applied to Eqs. A.2, simplifies the form greatly. Here a general vector $\mathbf{r}$ is also used.

$$\mathbf{r} = \mathbf{r}_x + \mathbf{r}_y + \mathbf{r}_z = r^x\mathbf{e}_x + r^y\mathbf{e}_y + r^z\mathbf{e}_z = \sum_{i=1}^{3} r^i\mathbf{e}_i = r^i\mathbf{e}_i \tag{A.3}$$

It is not necessary to use mutually orthogonal base vectors for describing space, and any triad that is non-coplanar can be setup as the basis. The non-coplanar character is ensured when the result of taking the triple scalar product is non-zero (this is discussed in more detail below). In addition, when working in a general system that is not restricted to an orthogonal Cartesian basis, a second *different* basis can be be created. This new basis is defined with the orthogonality of Eq. A.4, where the individual bases would be giren by Eqs. A.5. In Eqs. A.4 & A.5, E is the triple scalar product and δ^i_j is the Kronecker delta that is unity when $i = j$ and zero when $i \neq j$.

$$\mathbf{e}^i \cdot \mathbf{e}_j = \delta^i_j \tag{A.4}$$

$$\mathbf{e}^1 = \frac{\mathbf{e}_2 \times \mathbf{e}_3}{E} \tag{A.5a}$$

$$\mathbf{e}^2 = \frac{\mathbf{e}_3 \times \mathbf{e}_1}{E} \tag{A.5b}$$

$$\mathbf{e}^3 = \frac{\mathbf{e}_1 \times \mathbf{e}_2}{E} \tag{A.5c}$$

To ask the question as to why go through the trouble of defining an extra basis is natural, and Abram (1965) offers the explanation that many reasons exist, but the only obvious ones are that it provides a second method of expressing any given vector and that it simplifies the form of the scalar products of vectors in non-orthogonal systems to one that is similar to that found in orthogonal systems. When one moves to using a dual basis system, the customary Cartesian habit of only placing indices in the lower positions is found to be insufficient. This custom is based on the fact that the difference between the two bases does not exist in the Cartesian system. Operating in a curvilinear system requires more attention to ensure that a proper transformation of objects takes place. Why this is the case is easily visualized by comparing the basis for the Cartesian and spherical polar coordinates of Fig. A.2. The figure makes it obvious that any rotation in ϕ or θ would create completely different basis in the curvilinear system; and using the parallel transformation, like that done for the velocity vector in the Cartesian system example, would produce nonsensical results (see Fig. A.4).

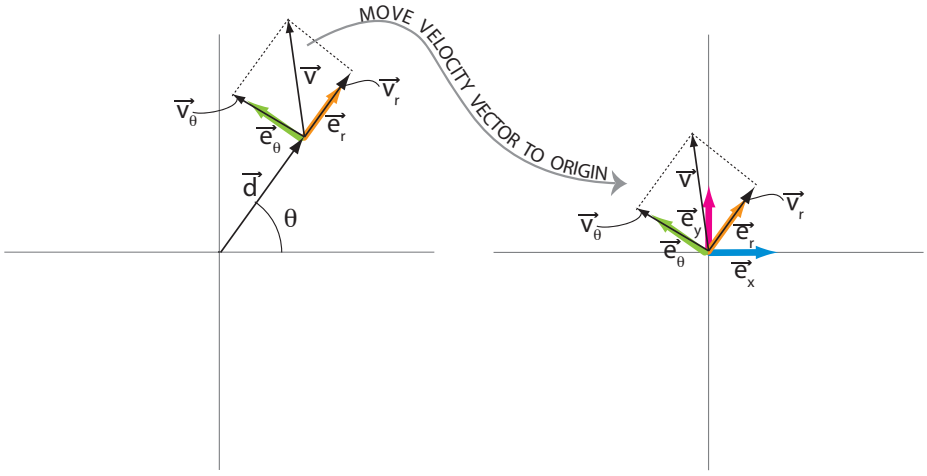

Figure A.4: Translation of basis vectors in a curvilinear system does not produce sensible results without proper transformation.

Proper transformations are defined as those that can be inverted to return to the original coordinate system, i.e. a change from x, y, z to $\bar{x}, \bar{y}, \bar{z}$, by the relation

$\bar{x}^i = \bar{x}^i(x, y, z)$, does not inhibit the change from $\bar{x}, \bar{y}, \bar{z}$ to x, y, z, by the relation $x^i = x^i(\bar{x}, \bar{y}, \bar{z})$. This is ensured if the Jacobian between the systems exists and is non-zero. To describe what this means in layman terms, one looks to the physical interpretation of the Jacobian as the ratio of the volume elements in the two systems $(d\bar{V}/dV)$. This not only makes clear the requirement that it have a non-zero value, i.e. that a finite volume of one system will not collapse to a point in the other system, but also implies its relationship to dilation and compressibility of fluids. This physical interpretation of the Jacobian, and definition of its mathematical form, is motivated by asking the following question: what is the differential volume at some new coordinates, given a differential volume at the original coordinates? To answer this question, take the original differential volume as $dV = dxdydz$, and the new differential volume as $d\bar{V} = d\bar{x}d\bar{y}d\bar{z}$. Then the chain rule of differentiation, the scalar product, vector product, and scalar triple products are defined. These definitions are written out in Eqs. A.6.

$$d\bar{x}^i = \frac{\partial \bar{x}^i}{\partial x^j} dx^j \qquad \text{differentiation chain rule} \tag{A.6a}$$

$$\mathbf{u} \cdot \mathbf{v} = u^i v_i \qquad \text{scalar product} \tag{A.6b}$$

$$\mathbf{u} \times \mathbf{v} = \epsilon^{ijk} u_j v_k \qquad \text{vector product} \tag{A.6c}$$

$$\mathbf{u} \cdot (\mathbf{v} \times \mathbf{g}) = \epsilon^{ijk} u_i v_j g_k \qquad \text{scalar triple product} \tag{A.6d}$$

The vector product of two vectors $(\mathbf{v}, \mathbf{g})$ is physically a parallelogram surface constructed of the two vectors; where the normal is perpendicular to both vectors and its magnitude is equal to the area of the surface. The scalar product of third vector $(\mathbf{u})$ with this surface's normal gives the projection of the normal onto the third vector, i.e. the height of a parallelopiped volume whose sides are constructed with the three vectors. This provides the physical interpretation of the scalar triple product, which can be used for calculating the differential volume after the change to new coordinates. This is done by using Eq. A.6d to interpret the volume $d\bar{V} = d\bar{x}d\bar{y}d\bar{z}$, and noting $\bar{x}^i = \bar{x}, \bar{y}, \bar{z}$ for $(i = 1, 2, 3)$. Then Eq. A.6a is substituted into that result to yield the Jacobian of the transformation of variables (see Eqs. A.7). Note that $\bar{x}^3$ is not x cubed, as the upper index is indicating the component and not the exponent, etc.

$$d\bar{V} = d\bar{x} \cdot (d\bar{y} \times d\bar{z}) = d\bar{x}^1 \cdot \left(d\bar{x}^2 \times d\bar{x}^3\right) = \epsilon_{ijk} d\bar{x}^i d\bar{x}^j d\bar{x}^k \tag{A.7a}$$

$$d\bar{V} = \epsilon_{ijk}\frac{\partial \bar{x}^i}{\partial x^1}dx^1\frac{\partial \bar{x}^j}{\partial x^2}dx^2\frac{\partial \bar{x}^k}{\partial x^3}dx^3 = \mathsf{J}dx^1dx^2dx^3 = \mathsf{J}dV \tag{A.7b}$$

$$\mathsf{J} = \epsilon_{ijk}\frac{\partial \bar{x}^i}{\partial x^1}\frac{\partial \bar{x}^j}{\partial x^2}\frac{\partial \bar{x}^k}{\partial x^3} = \frac{d\bar{V}}{dV} \tag{A.7c}$$

As pointed out earlier, objects in a general system can behave in one of two ways, and the distinction is made between these two classes of objects by how they transform. The first class are the contravariant objects and their components transform according to Eq. A.8; the second class are the Covariant objects and their components transform with coordinates according to Eq. A.9. Here, x^i are the independent parameters (coordinates) and v^i the vector components. It is important to note that the terms contravariant and covariant are terms that refer strictly to ***components of tensors***. The contravariance was simply defined as the rule of partial differentiation of coordinates whose indices were ***arbitrarily*** always taken to be superscripts. Considering this rule and the contravariant definition, Eq. A.6a & Eq. A.8 respectively, makes clear that the coordinates x^i are themselves ***only components of a contravariant vector when transformations between*** x^i ***and*** $\bar{x}^i$ ***are linear***, i.e. $\bar{x}^i = a^i_j x^j$ where $a^i_j = \frac{\partial \bar{x}^i}{\partial x^j}$ is a constant. Since it is only in the linear transformation case that this is true, for all other cases the fact that the coordinates are written with a superscript index can cause confusion, and it must be remembered that they are not components of contravariant vectors. However, the differentials of the coordinates are comply with Eq. A.8, and as such are contravariant object, i.e. the higher derivatives of the coordinates (e.g. velocity & acceleration) are contravariants. Also, in the notation of all other objects with superscript indices, the objects ***are*** considered components of contravariant tensors. This is not made clearly in most texts on tensor analysis, so one must think about it a little before ploughing ahead calling space coordinates contravariant objects. Detailed information on the transformations and their requirements are given in the second and seventh chapters of Abram (1965) and Aris (1962), respectively.

$$\bar{v}^i = \frac{\partial \bar{x}^i}{\partial x^j}v^j \tag{A.8}$$

$$\bar{v}_i = \frac{\partial x^j}{\partial \bar{x}^i}v_j \tag{A.9}$$

With a little thought, it comes to light that quantities that are differentials and derivatives fit as contravariance and covariance objects; more to the point, objects

that are ***gradients OF spatial position*** are contravariant objects (dx^i in the numerator; like position differential, velocity, and acceleration), and objects that are ***gradients IN spatial position*** are covariant objects (dx^i in the denominator; like a concentration gradient & temperature gradient). Additionally, these objects are defined for higher order tensors, and for mixed types. The transformation rules for 2^{nd} order contravariant, covariant, and mixed contravariant/covariant tensors are given in Eq. A.10, Eq. A.11, and Eq. A.12 respectively. An example of a mixed vector is the Kronecker delta; as seen by thinking about the way the definition of this object with respect to the independent coordinates would transform, $\bar{\delta}^i_j = \frac{\partial \bar{x}^i}{\partial \bar{x}^j} = \frac{\partial \bar{x}^i}{\partial x^l}\frac{\partial x^m}{\partial \bar{x}^j}\delta^l_m$.

$$\bar{v}^{ij} = \frac{\partial \bar{x}^i}{\partial x^l}\frac{\partial \bar{x}^j}{\partial x^k}v^{lk} \tag{A.10}$$

$$\bar{v}_{ij} = \frac{\partial x^l}{\partial \bar{x}^i}\frac{\partial x^k}{\partial \bar{x}^j}v_{lk} \tag{A.11}$$

$$\bar{v}^i_j = \frac{\partial \bar{x}^i}{\partial x^l}\frac{\partial x^k}{\partial \bar{x}^j}v^l_k \tag{A.12}$$

The reader should be getting the feeling that tensorial mathematics is heavily concerned with transformations and their effects on the description of objcts in space. This impression is correct and actually leads into the last two related concepts: the metric tensor and Christoffel symbols. The word metric is defined as a form of measurement within space, be it flat or curved, and the metric tensor is based on the concept of length or distance, using a specific representation of space. A terse introduction of this object is achieved by considering the distance ds between a point with coordinates u^j and a neighboring point at the location $u^j + du^j$, in the E^3 Cartesian space. Then the distance is given by the Pythagorean rule $ds^2 = \sum_{j=1}^{3} dy^j dy^j$. Since we are entering into more rigorous tensorial territory, we apply strictly the tensorial summation rule such that it is only affected for repeated indices in the upper to lower (or vis versa) locations, and an explicit summation symbol is used. The differentation chain rule of Eq. A.6a is used to affect a transformation to the general curvilinear coordinates u^j. This results in Eq. A.13, and is an example of transformation methods in tensor analysis. One should note that i of u^i is a free index, so the first differentiation is put with respect to i and the second with respect to k. The result is the form of Eq. A.14 for a curve's path length due to infinitesimal coordinate increments, and

Eq. A.15 for the metric tensor.

$$d\bar{y}^i = \frac{\partial \bar{y}^j}{\partial u^i} du^i \quad \text{into} \quad ds^2 = \sum_{j=1}^{3} dy^j dy^j \quad \text{results in} \quad ds^2 = \sum_{j=1}^{3} \frac{\partial \bar{y}^j}{\partial u^i} du^i \frac{\partial \bar{y}^j}{\partial u^k} du^k \tag{A.13}$$

$$ds^2 = g_{ik} du^i dk^k \tag{A.14}$$

$$g_{ik} = \sum_{j=1}^{3} \frac{\partial \bar{y}^j}{\partial u^i} \frac{\partial \bar{y}^j}{\partial u^k} = \frac{\partial \bar{y}^j}{\partial u^i} \frac{\partial \bar{y}^j}{\partial u^k} \tag{A.15}$$

As was found with all the Cartesian methods discusssed so far, it is also found that the normal differentiation method is insufficient for general tensor analysis. All the references listed at the beginning of this Appendix give examples of this situation. To handle the general case of differentiation, especially in curvilinear coordinates, a set of objects called the Christoffel symbols of the first and second kind are defined. These definitions are given in Eq. A.16 and Eq. A.17, respectively.

$$\Gamma_{ijk} = \frac{1}{2} \left(\frac{\partial g_{ik}}{\partial x^j} + \frac{\partial g_{jk}}{\partial x^i} - \frac{\partial g_{ij}}{\partial x^k} \right) \tag{A.16}$$

$$\Gamma^i_{jk} = g^{ir} \Gamma_{jkr} \tag{A.17}$$

where $g_{ij} g^{jk} = \delta^i_k$

B – Vector Operator Development

The forms for the vector operations required to evaluate Eq. 3.11 for the current coordinate system, and defined by the scale factors developed in Sec. 3, are developed in this section. The scalar factors are repeated in Eq. B.1. A short development of the gradient operator is provided as background for the concepts applying to curvilinear coordinates, and the general forms for the inner product of a vector with the gradient of a vector, and the Laplacian of a vector, are taken from *Schaum's Outline - Vector Analysis (1959)*, as their development is standard. They are also readily found in many standard vector analysis texts. These operators are then made specific to the current system by application of the current scalar factors.

$$h_i = \begin{bmatrix} 1 \\ r \\ N \end{bmatrix} \tag{B.1}$$

where $N = \frac{(a+r\cos\theta)}{a} = (1 + r\kappa\cos\theta)$

The relationship of the vector operators can be defined as functions of the scalar factors by considering the definition of the scalar factors given by Eqs. B.2, and the definition of a unit tangent vector along the general curve $\mathbf{x}$ in the coordinate directions as given by Eqs. B.3. These concepts lead to the differential of the position vector for curvilinear orthogonal coordinates given by Eq. B.4, and the differential arc length ds^2 given by Eq. B.5, which is simply the orthogonal version of the more general tensor form used to find the metric tensor in Sec. 3. This is also the form that provides the relationship between the metric tensor and the scalar factors used in that section to justify the use of the vector form of the Navier-Stokes equations in the current development.

$$h_r = \left|\frac{\partial \mathbf{x}}{\partial r}\right|; \qquad h_\theta = \left|\frac{\partial \mathbf{x}}{\partial \theta}\right|; \qquad h_s = \left|\frac{\partial \mathbf{x}}{\partial s}\right| \tag{B.2}$$

$$\mathbf{e}_r = \frac{\frac{\partial \mathbf{x}}{\partial r}}{\left|\frac{\partial \mathbf{x}}{\partial r}\right|}; \qquad \mathbf{e}_\theta = \frac{\frac{\partial \mathbf{x}}{\partial \theta}}{\left|\frac{\partial \mathbf{x}}{\partial \theta}\right|}; \qquad \mathbf{e}_s = \frac{\frac{\partial \mathbf{x}}{\partial s}}{\left|\frac{\partial \mathbf{x}}{\partial s}\right|} \tag{B.3}$$

$$d\mathbf{x} = \frac{\partial \mathbf{x}}{\partial r}dr + \frac{\partial \mathbf{x}}{\partial \theta}d\theta + \frac{\partial \mathbf{x}}{\partial s}ds \tag{B.4}$$

$$= h_r dr \mathbf{e}_r + h_\theta d\theta \mathbf{e}_\theta + h_s ds \mathbf{e}_s \qquad (.)$$

$$ds^2 = d\mathbf{x} \cdot d\mathbf{x} = h_r^2 dr^2 + h_\theta^2 d\theta^2 + h_s^2 ds^2 \qquad \text{(B.5)}$$

The gradient operator is written for any scalar, vector, or tensor function (Φ, Φ_i, or Φ_{ij}), as Eqs. B.6. Here the functions are taken to be of the current system (r, θ, s). It is obvious from the forms that the gradient operator increases the rank of the object it operates on. Review of the general vector form of the Navier-Stokes equations, Eq. 3.11, shows that the gradient of a scalar (∇p), the inner product of a vector with the gradient of a vector ($\mathbf{v} \cdot \nabla \mathbf{v}$), and the Laplacian of a vector ($\nabla^2 \mathbf{v}$) are required. Considering the gradient of a scalar (∇p), Eq. B.6a is expanded for curvilinear coordinates.

$$\nabla \Phi = \partial_k \Phi(r, \theta, s) = f_r \mathbf{e}_r + f_\theta \mathbf{e}_\theta + f_s \mathbf{e}_s \qquad \text{(B.6a)}$$

$$\nabla \Phi_i = \partial_k \Phi_i(r, \theta, s) = \sum_{i=r,\theta,s} f_{i_r} \mathbf{e}_r + f_{\theta_r} \mathbf{e}_\theta + f_{s_r} \mathbf{e}_s \qquad \text{(B.6b)}$$

$$\nabla \Phi_{ij} = \partial_k \Phi_{ij}(r, \theta, s) = \sum_{j=r,\theta,s} \sum_{i=r,\theta,s} f_{ij_r} \mathbf{e}_r + f_{ij_\theta} \mathbf{e}_\theta + f_{ij_s} \mathbf{e}_s \qquad \text{(B.6c)}$$

The functions in the (r, θ, s) directions can be found by writing the total derivative of a scalar as $\nabla \Phi \cdot d\mathbf{x}$, where $d\mathbf{x}$ is defined by Eq. B.4, see Eq. B.7.

$$d\Phi = \nabla \Phi \cdot d\mathbf{x} = (f_r \mathbf{e}_r + f_\theta \mathbf{e}_\theta + f_s \mathbf{e}_s) \cdot (h_r dr \mathbf{e}_r + h_\theta d\theta \mathbf{e}_\theta + h_s ds \mathbf{e}_s)$$

$$= f_r h_r dr + f_\theta h_\theta d\theta + f_s h_s ds \qquad \text{(B.7)}$$

Since the total derivative of a scalar field is given by Eq. B.8, comparison of Eq. B.7 with Eq. B.8 indicates that $f_r = \frac{1}{h_r} \frac{\partial \Phi}{\partial r}$, $f_\theta = \frac{1}{h_\theta} \frac{\partial \Phi}{\partial \theta}$, and $f_s = \frac{1}{h_s} \frac{\partial \Phi}{\partial s}$, and Eq. B.6a can be written as Eq. B.9, where (h_r, h_θ, h_s) are the scalar factors given by Eq. B.1. The forms for the the inner product of a vector with the gradient of a vector and the Laplacian of a vector follow similar developments. The general forms for the Laplacian of a scalar, Laplacian of a vector, and vector-dot-gradient-vector are given in Eq. B.10, Eq. B.11, and Eq. B.12, respectively. See Schaum's Outline - Vector Analysis (1959) and Georing (1989) for examples. Note the form of the gradient of a scalar is also given on page 137 of the Schaum's Outline, and matches the form

developed here. Often, as is the case with the two references of this paragraph, not all components of the general forms are given, due to their length; however, all three coordinate direction components are shown here for verification. The $\mathbf{e}_r$ term of the $\nabla^2\Phi_i$ and $\Phi_i \cdot \nabla\Phi_i$ operators are provided by Goering (1989); the $\mathbf{e}_\theta$ and $\mathbf{e}_s$ terms are generated by cyclic permutation of the indices (shown in Eq. B.11 and Eq. B.12) and developed below.

$$d\Phi = \frac{\partial\Phi}{\partial r}dr + \frac{\partial\Phi}{\partial\theta}d\theta + \frac{\partial\Phi}{\partial s}ds \tag{B.8}$$

$$\nabla\Phi = \partial_k\Phi(r,\theta,s) = \frac{1}{h_r}\frac{\partial\Phi}{\partial r}\mathbf{e}_r + \frac{1}{h_\theta}\frac{\partial\Phi}{\partial\theta}\mathbf{e}_\theta + \frac{1}{h_s}\frac{\partial\Phi}{\partial s}\mathbf{e}_s \tag{B.9}$$

$$\nabla^2\Phi = \frac{1}{h_1h_2h_3}\left[\frac{\partial}{\partial x_1}\left(\frac{h_2h_3}{h_1}\frac{\partial\Phi}{\partial x_1}\right) + \frac{\partial}{\partial x_2}\left(\frac{h_3h_1}{h_2}\frac{\partial\Phi}{\partial x_2}\right) + \frac{\partial}{\partial x_3}\left(\frac{h_1h_2}{h_3}\frac{\partial\Phi}{\partial x_3}\right)\right] \tag{B.10}$$

$$\begin{aligned}\nabla^2\Phi_i =& \left\{\nabla^2\Phi_1 + \frac{1}{h_1h_2h_3}\left[2\left(\frac{h_3}{h_1}\frac{\partial h_1}{\partial x_2}\frac{\partial\Phi_2}{\partial x_1} + \frac{h_2}{h_1}\frac{\partial h_1}{\partial x_3}\frac{\partial\Phi_3}{\partial x_1} - \frac{h_3}{h_2}\frac{\partial h_2}{\partial x_1}\frac{\partial\Phi_2}{\partial x_2} - \frac{h_2}{h_3}\frac{\partial h_3}{\partial x_1}\frac{\partial\Phi_3}{\partial x_3}\right)\right.\right. \\ &+ \Phi_2\left(\frac{\partial}{\partial x_1}\left(\frac{h_3}{h_1}\frac{\partial h_1}{\partial x_2}\right) - \frac{\partial}{\partial x_2}\left(\frac{h_3}{h_2}\frac{\partial h_2}{\partial x_1}\right) - \frac{1}{h_3}\frac{\partial h_3}{\partial x_1}\frac{\partial h_3}{\partial x_2}\right) \qquad \text{(B.11)} \\ &+ \Phi_3\left(\frac{\partial}{\partial x_1}\left(\frac{h_2}{h_1}\frac{\partial h_1}{\partial x_3}\right) - \frac{\partial}{\partial x_3}\left(\frac{h_2}{h_3}\frac{\partial h_3}{\partial x_1}\right) - \frac{1}{h_2}\frac{\partial h_2}{\partial x_1}\frac{\partial h_2}{\partial x_3}\right) \qquad (^{\downarrow}) \\ &\left.\left. - \frac{\Phi_1}{h_1}\left(\frac{h_3}{h_2}\left(\left(\frac{\partial h_1}{\partial x_2}\right)^2 + \left(\frac{\partial h_2}{\partial x_1}\right)^2\right) + \frac{h_2}{h_3}\left(\left(\frac{\partial h_1}{\partial x_3}\right)^2 + \left(\frac{\partial h_3}{\partial x_1}\right)^2\right)\right)\right]\right\}\mathbf{e}_1 \qquad (^{\downarrow}) \\ &+ \left\{\nabla^2\Phi_2 + \frac{1}{h_2h_3h_1}\left[2\left(\frac{h_1}{h_2}\frac{\partial h_2}{\partial x_3}\frac{\partial\Phi_3}{\partial x_2} + \frac{h_3}{h_2}\frac{\partial h_2}{\partial x_1}\frac{\partial\Phi_1}{\partial x_2} - \frac{h_1}{h_3}\frac{\partial h_3}{\partial x_2}\frac{\partial\Phi_3}{\partial x_3} - \frac{h_3}{h_1}\frac{\partial h_1}{\partial x_2}\frac{\partial\Phi_1}{\partial x_1}\right)\right.\right. \\ &+ \Phi_3\left(\frac{\partial}{\partial x_2}\left(\frac{h_1}{h_2}\frac{\partial h_2}{\partial x_3}\right) - \frac{\partial}{\partial x_3}\left(\frac{h_1}{h_3}\frac{\partial h_3}{\partial x_2}\right) - \frac{1}{h_1}\frac{\partial h_1}{\partial x_2}\frac{\partial h_1}{\partial x_3}\right) \qquad (^{\downarrow}) \\ &+ \Phi_1\left(\frac{\partial}{\partial x_2}\left(\frac{h_3}{h_2}\frac{\partial h_2}{\partial x_1}\right) - \frac{\partial}{\partial x_1}\left(\frac{h_3}{h_1}\frac{\partial h_1}{\partial x_2}\right) - \frac{1}{h_3}\frac{\partial h_3}{\partial x_2}\frac{\partial h_3}{\partial x_1}\right) \qquad (^{\downarrow}) \\ &\left.\left. - \frac{\Phi_2}{h_2}\left(\frac{h_1}{h_3}\left(\left(\frac{\partial h_2}{\partial x_3}\right)^2 + \left(\frac{\partial h_3}{\partial x_2}\right)^2\right) + \frac{h_3}{h_1}\left(\left(\frac{\partial h_2}{\partial x_1}\right)^2 + \left(\frac{\partial h_1}{\partial x_2}\right)^2\right)\right)\right]\right\}\mathbf{e}_2 \qquad (^{\downarrow})\end{aligned}$$

$$+\Bigg\{\nabla^2\Phi_3+\frac{1}{h_3h_1h_2}\Bigg[2\left(\frac{h_2}{h_3}\frac{\partial h_3}{\partial x_1}\frac{\partial\Phi_1}{\partial x_3}+\frac{h_1}{h_3}\frac{\partial h_3}{\partial x_2}\frac{\partial\Phi_2}{\partial x_3}-\frac{h_2}{h_1}\frac{\partial h_1}{\partial x_3}\frac{\partial\Phi_1}{\partial x_1}-\frac{h_1}{h_2}\frac{\partial h_2}{\partial x_3}\frac{\partial\Phi_2}{\partial x_2}\right)$$

$$+\Phi_1\left(\frac{\partial}{\partial x_3}\left(\frac{h_2}{h_3}\frac{\partial h_3}{\partial x_1}\right)-\frac{\partial}{\partial x_1}\left(\frac{h_2}{h_1}\frac{\partial h_1}{\partial x_3}\right)-\frac{1}{h_2}\frac{\partial h_2}{\partial x_3}\frac{\partial h_2}{\partial x_1}\right) \qquad (^{\downarrow})$$

$$+\Phi_2\left(\frac{\partial}{\partial x_3}\left(\frac{h_1}{h_3}\frac{\partial h_3}{\partial x_2}\right)-\frac{\partial}{\partial x_2}\left(\frac{h_1}{h_2}\frac{\partial h_2}{\partial x_3}\right)-\frac{1}{h_1}\frac{\partial h_1}{\partial x_3}\frac{\partial h_1}{\partial x_2}\right) \qquad (^{\downarrow})$$

$$-\frac{\Phi_3}{h_3}\left(\frac{h_2}{h_1}\left(\left(\frac{\partial h_3}{\partial x_1}\right)^2+\left(\frac{\partial h_1}{\partial x_3}\right)^2\right)+\frac{h_1}{h_2}\left(\left(\frac{\partial h_3}{\partial x_2}\right)^2+\left(\frac{\partial h_2}{\partial x_3}\right)^2\right)\right)\Bigg]\Bigg\}\mathbf{e}_3 \qquad (.)$$

$$\Phi_i\cdot\nabla\Phi_j=\left[\Phi_i\cdot\nabla\Phi_1+\frac{\Phi_1}{h_1}\left(\frac{\Phi_2}{h_2}\frac{\partial h_1}{\partial x_2}+\frac{\Phi_3}{h_3}\frac{\partial h_1}{\partial x_3}\right)-\frac{\Phi_2^2}{h_1h_2}\frac{\partial h_2}{\partial x_1}-\frac{\Phi_3^2}{h_1h_3}\frac{\partial h_3}{\partial x_1}\right]\mathbf{e}_1 \qquad (B.12)$$

$$+\left[\Phi_i\cdot\nabla\Phi_2+\frac{\Phi_2}{h_2}\left(\frac{\Phi_3}{h_3}\frac{\partial h_2}{\partial x_3}+\frac{\Phi_1}{h_1}\frac{\partial h_2}{\partial x_1}\right)-\frac{\Phi_3^2}{h_2h_3}\frac{\partial h_3}{\partial x_2}-\frac{\Phi_1^2}{h_2h_1}\frac{\partial h_1}{\partial x_2}\right]\mathbf{e}_2 \qquad (^{\downarrow})$$

$$+\left[\Phi_i\cdot\nabla\Phi_3+\frac{\Phi_3}{h_3}\left(\frac{\Phi_1}{h_1}\frac{\partial h_3}{\partial x_1}+\frac{\Phi_2}{h_2}\frac{\partial h_3}{\partial x_2}\right)-\frac{\Phi_1^2}{h_3h_1}\frac{\partial h_1}{\partial x_3}-\frac{\Phi_2^2}{h_3h_2}\frac{\partial h_2}{\partial x_3}\right]\mathbf{e}_3 \qquad (.)$$

When the velocity vector ($\Phi_i=\mathbf{v}$), pressure ($\Phi=p$), and scalar factors ($h_1=1, h_2=r, h_3=N$) are substituted into Eq. B.9, Eq. B.11, and Eq. B.12, the system specific operations needed to produce the toroidal Navier Stokes equations are found. These are shown in Eqs. B.13 through B.15. Note: intermediate steps are shown for verification, and the gradient term developed above already has the appropriate unit vectors and coordinates in the equation due to it being developed for the current system.

$$\nabla p=\frac{1}{1}\frac{\partial p}{\partial r}\mathbf{e}_r+\frac{1}{r}\frac{\partial p}{\partial\theta}\mathbf{e}_\theta+\frac{1}{N}\frac{\partial p}{\partial s}\mathbf{e}_s \qquad (B.13)$$

$$=\frac{\partial p}{\partial r}\mathbf{e}_r+\frac{1}{r}\frac{\partial p}{\partial\theta}\mathbf{e}_\theta+\frac{1}{(1+r\kappa\cos\theta)}\frac{\partial p}{\partial s}\mathbf{e}_s \qquad (.)$$

$$\nabla^2\mathbf{v}=\Bigg\{\nabla^2u+\frac{1}{1rN}\Bigg[2\left(\frac{N}{1}\frac{\partial 1}{\partial\theta}\frac{\partial v}{\partial r}+\frac{r}{1}\frac{\partial 1}{\partial s}\frac{\partial w}{\partial r}-\frac{N}{r}\frac{\partial r}{\partial r}\frac{\partial v}{\partial\theta}-\frac{r}{N}\frac{\partial N}{\partial r}\frac{\partial w}{\partial s}\right) \qquad (B.14)$$

$$+v\left(\frac{\partial}{\partial r}\left(\frac{N}{1}\frac{\partial 1}{\partial\theta}\right)-\frac{\partial}{\partial\theta}\left(\frac{N}{r}\frac{\partial r}{\partial r}\right)-\frac{1}{N}\frac{\partial N}{\partial r}\frac{\partial N}{\partial\theta}\right) \tag{$\downarrow$}$$

$$+w\left(\frac{\partial}{\partial r}\left(\frac{r}{1}\frac{\partial 1}{\partial s}\right)-\frac{\partial}{\partial s}\left(\frac{r}{N}\frac{\partial N}{\partial r}\right)-\frac{1}{r}\frac{\partial r}{\partial r}\frac{\partial r}{\partial s}\right) \tag{$\downarrow$}$$

$$-\frac{u}{1}\left(\frac{N}{r}\left(\left(\frac{\partial 1}{\partial\theta}\right)^2+\left(\frac{\partial r}{\partial r}\right)^2\right)+\frac{r}{N}\left(\left(\frac{\partial 1}{\partial s}\right)^2+\left(\frac{\partial N}{\partial r}\right)^2\right)\right)\Bigg]\Bigg\}\mathbf{e}_r \tag{$\downarrow$}$$

$$+\Bigg\{\nabla^2 v+\frac{1}{rN1}\Bigg[2\left(\frac{1}{r}\frac{\partial r}{\partial s}\frac{\partial w}{\partial\theta}+\frac{N}{r}\frac{\partial r}{\partial r}\frac{\partial u}{\partial\theta}-\frac{1}{N}\frac{\partial N}{\partial\theta}\frac{\partial w}{\partial s}-\frac{N}{1}\frac{\partial 1}{\partial\theta}\frac{\partial u}{\partial r}\right) \tag{$\downarrow$}$$

$$+w\left(\frac{\partial}{\partial\theta}\left(\frac{1}{r}\frac{\partial r}{\partial s}\right)-\frac{\partial}{\partial s}\left(\frac{1}{N}\frac{\partial N}{\partial\theta}\right)-\frac{1}{1}\frac{\partial 1}{\partial\theta}\frac{\partial 1}{\partial s}\right) \tag{$\downarrow$}$$

$$+u\left(\frac{\partial}{\partial\theta}\left(\frac{N}{r}\frac{\partial r}{\partial r}\right)-\frac{\partial}{\partial r}\left(\frac{N}{1}\frac{\partial 1}{\partial\theta}\right)-\frac{1}{N}\frac{\partial N}{\partial\theta}\frac{\partial N}{\partial r}\right) \tag{$\downarrow$}$$

$$-\frac{v}{r}\left(\frac{1}{N}\left(\left(\frac{\partial r}{\partial s}\right)^2+\left(\frac{\partial N}{\partial\theta}\right)^2\right)+\frac{N}{1}\left(\left(\frac{\partial r}{\partial r}\right)^2+\left(\frac{\partial 1}{\partial\theta}\right)^2\right)\right)\Bigg]\Bigg\}\mathbf{e}_\theta \tag{$\downarrow$}$$

$$+\Bigg\{\nabla^2 w+\frac{1}{N1r}\Bigg[2\left(\frac{r}{N}\frac{\partial N}{\partial r}\frac{\partial u}{\partial s}+\frac{1}{N}\frac{\partial N}{\partial\theta}\frac{\partial v}{\partial s}-\frac{r}{1}\frac{\partial 1}{\partial s}\frac{\partial u}{\partial r}-\frac{1}{r}\frac{\partial r}{\partial s}\frac{\partial v}{\partial\theta}\right) \tag{$\downarrow$}$$

$$+u\left(\frac{\partial}{\partial s}\left(\frac{r}{N}\frac{\partial N}{\partial r}\right)-\frac{\partial}{\partial r}\left(\frac{r}{1}\frac{\partial 1}{\partial s}\right)-\frac{1}{r}\frac{\partial r}{\partial s}\frac{\partial r}{\partial r}\right) \tag{$\downarrow$}$$

$$+v\left(\frac{\partial}{\partial s}\left(\frac{1}{N}\frac{\partial N}{\partial\theta}\right)-\frac{\partial}{\partial\theta}\left(\frac{1}{r}\frac{\partial r}{\partial s}\right)-\frac{1}{1}\frac{\partial 1}{\partial s}\frac{\partial 1}{\partial\theta}\right) \tag{$\downarrow$}$$

$$-\frac{w}{N}\left(\frac{r}{1}\left(\left(\frac{\partial N}{\partial r}\right)^2+\left(\frac{\partial 1}{\partial s}\right)^2\right)+\frac{1}{r}\left(\left(\frac{\partial N}{\partial\theta}\right)^2+\left(\frac{\partial r}{\partial s}\right)^2\right)\right)\Bigg]\Bigg\}\mathbf{e}_s \tag{$\downarrow$}$$

$$=\Bigg\{\nabla^2 u+\frac{1}{r(1+r\kappa\cos\theta)}\Bigg[2\left(-\frac{(1+r\kappa\cos\theta)}{r}\frac{\partial v}{\partial\theta}-\frac{r\kappa\cos\theta}{(1+r\kappa\cos\theta)}\frac{\partial w}{\partial s}\right) \tag{$\downarrow$}$$

$$+v\left(\kappa\sin\theta+\frac{r\kappa^2\cos\theta\sin\theta}{(1+r\kappa\cos\theta)}\right) \tag{$\downarrow$}$$

$$- u\left(\frac{(1+r\kappa\cos\theta)}{r}+\frac{r\kappa^2\cos^2\theta}{(1+r\kappa\cos\theta)}\right)\Bigg]\Bigg\}\mathbf{e}_r \tag{$\downarrow$}$$

$$+\Bigg\{\nabla^2 v+\frac{1}{r\,(1+r\kappa\cos\theta)}\Bigg[2\left(\frac{(1+r\kappa\cos\theta)}{r}\frac{\partial u}{\partial\theta}+\frac{r\kappa\sin\theta}{(1+r\kappa\cos\theta)}\frac{\partial w}{\partial s}\right) \tag{$\downarrow$}$$

$$+u\left(-\kappa\sin\theta+\frac{r\kappa^2\sin\theta\cos\theta}{(1+r\kappa\cos\theta)}\right) \tag{$\downarrow$}$$

$$-\frac{v}{r}\left(\frac{r^2\kappa^2\sin^2\theta}{(1+r\kappa\cos\theta)}+(1+r\kappa\cos\theta\right)\Bigg]\Bigg\}\mathbf{e}_\theta \tag{$\downarrow$}$$

$$+\Bigg\{\nabla^2 w+\frac{1}{(r+r^2\kappa\cos\theta)}\Bigg[2\left(\frac{r\kappa\cos\theta}{(1+r\kappa\cos\theta)}\frac{\partial u}{\partial s}-\frac{r\kappa\sin\theta}{(1+r\kappa\cos\theta)}\frac{\partial v}{\partial s}\right) \tag{$\downarrow$}$$

$$-\frac{wr\kappa^2\cos^2\theta}{(1+r\kappa\cos\theta)}-\frac{wr^2\kappa^2\sin^2\theta}{r(1+r\kappa\cos\theta)}\Bigg]\Bigg\}\mathbf{e}_s \tag{$\downarrow$}$$

Applying steady-state ($\frac{\partial}{\partial s}=0$) and one-dimensional flow ($u=v=0$) approximations.

$$\nabla^2\mathbf{v}=\Bigg\{\nabla^2 w-\frac{w\kappa^2\cos^2\theta}{(1+r\kappa\cos\theta)^2}-\frac{w\kappa^2\sin^2\theta}{(1+r\kappa\cos\theta)^2}\Bigg\}\mathbf{e}_s \tag{$\downarrow$}$$

Substituting Eq. B.10 for the Laplacian of the axial direction fluid velocity, and considering an axis-symmetric flow, yields the form for the Laplacian of the velocity vector.

$$\nabla^2\mathbf{v}=\Bigg\{\frac{1}{h_1h_2h_3}\left[\frac{\partial}{\partial x_1}\left(\frac{h_2h_3}{h_1}\frac{\partial w}{\partial x_1}\right)+\frac{\partial}{\partial x_2}\left(\frac{h_3h_1}{h_2}\frac{\partial w}{\partial x_2}\right)+\frac{\partial}{\partial x_3}\left(\frac{h_1h_2}{h_3}\frac{\partial w}{\partial x_3}\right)\right] \tag{$\downarrow$}$$

$$-\frac{w\kappa^2\cos^2\theta}{(1+r\kappa\cos\theta)^2}-\frac{w\kappa^2\sin^2\theta}{(1+r\kappa\cos\theta)^2}\Bigg\}\mathbf{e}_s \tag{$\downarrow$}$$

$$=\Bigg\{\frac{1}{1rN}\left[\frac{\partial}{\partial r}\left(\frac{rN}{1}\frac{\partial w}{\partial r}\right)+\frac{\partial}{\partial\theta}\left(\frac{N1}{r}\frac{\partial w}{\partial\theta}\right)+\frac{\partial}{\partial s}\left(\frac{1r}{N}\frac{\partial w}{\partial s}\right)\right] \tag{$\downarrow$}$$

$$-\frac{w\kappa^2\left(\cos^2\theta+\sin^2\theta\right)}{(1+r\kappa\cos\theta)^2}\Bigg\}\mathbf{e}_s \tag{$\downarrow$}$$

$$= \left\{ \frac{(1 + 2r\kappa\cos\theta)}{r\,(1 + r\kappa\cos\theta)} \frac{\partial w}{\partial r} + \frac{\partial^2 w}{\partial r^2} - \frac{w\kappa^2}{(1 + r\kappa\cos\theta)^2} \right\} \mathbf{e}_s \qquad (.)$$

$$\mathbf{v}\cdot\nabla\mathbf{v} = \left[\mathbf{v}\cdot\nabla u + \frac{u}{1}\left(\frac{v}{r}\frac{\partial 1}{\partial\theta} + \frac{w}{N}\frac{\partial 1}{\partial s} \right) - \frac{v^2}{1r}\frac{\partial r}{\partial r} - \frac{w^2}{1N}\frac{\partial N}{\partial r} \right] \mathbf{e}_r \qquad \text{(B.15)}$$

$$+ \left[\mathbf{v}\cdot\nabla v + \frac{v}{r}\left(\frac{w}{N}\frac{\partial r}{\partial s} + \frac{u}{1}\frac{\partial r}{\partial r} \right) - \frac{w^2}{rN}\frac{\partial N}{\partial\theta} - \frac{u^2}{r1}\frac{\partial 1}{\partial\theta} \right] \mathbf{e}_\theta \qquad (^{\downarrow})$$

$$+ \left[\mathbf{v}\cdot\nabla w + \frac{w}{N}\left(\frac{u}{1}\frac{\partial N}{\partial r} + \frac{v}{r}\frac{\partial N}{\partial\theta} \right) - \frac{u^2}{N1}\frac{\partial 1}{\partial s} - \frac{v^2}{Nr}\frac{\partial r}{\partial s} \right] \mathbf{e}_s \qquad (^{\downarrow})$$

$$= \left[\mathbf{v}\cdot\nabla u - \frac{v^2}{r} - \frac{w^2}{(1 + r\kappa\cos\theta)}\kappa\cos\theta \right] \mathbf{e}_r \qquad (^{\downarrow})$$

$$+ \left[\mathbf{v}\cdot\nabla v + \frac{uv}{r} + \frac{w^2\kappa\sin\theta}{(1 + r\kappa\cos\theta)} \right] \mathbf{e}_\theta \qquad (^{\downarrow})$$

$$+ \left[\mathbf{v}\cdot\nabla w + \frac{w}{(1 + r\kappa\cos\theta)}\left(u\kappa\cos\theta - v\kappa\sin\theta \right) \right] \mathbf{e}_s \qquad (^{\downarrow})$$

Applying steady-state ($\frac{\partial}{\partial s} = 0$) and one-dimensional flow ($u = v = 0$) approximations.

$$\mathbf{v}\cdot\nabla\mathbf{v} = \left[-\frac{w^2}{(1 + r\kappa\cos\theta)}\kappa\cos\theta \right] \mathbf{e}_r + \left[\frac{w^2\kappa\sin\theta}{(1 + r\kappa\cos\theta)} \right] \mathbf{e}_\theta + \left[\mathbf{v}\cdot\nabla w \right] \mathbf{e}_s \qquad (.)$$

Substituting Eq. B.9 for the gradient of the axial direction fluid velocity, and considering an axis-symmetric flow, yields the form for the $\mathbf{v}\cdot\nabla\mathbf{v}$ term.

$$\mathbf{v}\cdot\nabla\mathbf{v} = \left[-\frac{w^2}{(1 + r\kappa\cos\theta)}\kappa\cos\theta \right] \mathbf{e}_r + \left[\frac{w^2\kappa\sin\theta}{(1 + r\kappa\cos\theta)} \right] \mathbf{e}_\theta \qquad (^{\downarrow})$$

$$+ \left[\mathbf{v}\cdot\left(\frac{1}{h_r}\frac{\partial w}{\partial r}\mathbf{e}_r + \frac{1}{h_\theta}\frac{\partial w}{\partial\theta}\mathbf{e}_\theta + \frac{1}{h_s}\frac{\partial w}{\partial s}\mathbf{e}_s \right) \right] \mathbf{e}_s \qquad (^{\downarrow})$$

$$= \left[-\frac{w^2}{(1 + r\kappa\cos\theta)}\kappa\cos\theta \right] \mathbf{e}_r + \left[\frac{w^2\kappa\sin\theta}{(1 + r\kappa\cos\theta)} \right] \mathbf{e}_\theta \qquad (^{\downarrow})$$

$$+ \left[(u\mathbf{e}_r + v\mathbf{e}_\theta + w\mathbf{e}_s)\cdot\left(\frac{1}{1}\frac{\partial w}{\partial r}\mathbf{e}_r \right) \right] \mathbf{e}_s \qquad (^{\downarrow})$$

$$= \left[-\frac{w^2}{(1 + r\kappa\cos\theta)}\kappa\cos\theta \right] \mathbf{e}_r + \left[\frac{w^2\kappa\sin\theta}{(1 + r\kappa\cos\theta)} \right] \mathbf{e}_\theta \qquad (^{\downarrow})$$

$$+\left[u\frac{\partial w}{\partial r}\mathbf{e}_r\cdot\mathbf{e}_r+v\frac{\partial w}{\partial r}\mathbf{e}_\theta\cdot\mathbf{e}_r+w\frac{\partial w}{\partial r}\mathbf{e}_s\cdot\mathbf{e}_r\right]\mathbf{e}_s \qquad (^{\downarrow})$$

$$=\left[-\frac{w^2\kappa\cos\theta}{(1+r\kappa\cos\theta)}\right]\mathbf{e}_r+\left[\frac{w^2\kappa\sin\theta}{(1+r\kappa\cos\theta)}\right]\mathbf{e}_\theta \qquad (.)$$

C – Cylindrical Equation Asymptotic Form Check

$$\frac{\partial p}{\partial r} = \frac{\rho\kappa\cos\theta}{N}w^2 + \rho f_r \tag{C.1a}$$

$$\frac{1}{r}\frac{\partial p}{\partial \theta} = -\frac{\rho\kappa\sin\theta}{N}w^2 + \rho f_\theta \tag{C.1b}$$

$$\frac{\partial p}{\partial s} = \rho N\nu\nabla^2 w - \frac{\rho\nu\kappa^2 w}{N} + \rho f_s \tag{C.1c}$$

The required vector operators are defined in the previous section, for one-dimension, as:

$$\mathbf{v}\cdot\nabla = \frac{w}{N}\frac{\partial}{\partial s} \tag{C.2a}$$

$$\nabla^2 = \frac{1}{rN}\left(\frac{\partial}{\partial r}\left(rN\frac{\partial}{\partial r}\right) + \frac{1}{r}\frac{\partial}{\partial\theta}\left(N\frac{\partial}{\partial\theta}\right)\right) \tag{C.2b}$$

In order to check the asymptotic form of the equation, Eqs. C.2 are substituted into Eq. 3.14c, resulting in the axial momentum equation,

$$0 = -\frac{1}{\rho N}\frac{\partial p}{\partial s} + \nu\frac{1}{rN}\left(\frac{\partial}{\partial r}\left(rN\frac{\partial w}{\partial r}\right) + \frac{1}{r}\frac{\partial}{\partial\theta}\left(N\frac{\partial w}{\partial\theta}\right)\right) - \frac{\nu\kappa^2 w}{N^2} + f_s \tag{C.3}$$

$$\frac{1}{\rho N}\frac{\partial p}{\partial s} = \nu\frac{1}{rN}\left(\frac{\partial}{\partial r}\left(rN\frac{\partial w}{\partial r}\right) + \frac{1}{r}\frac{\partial}{\partial\theta}\left(N\frac{\partial w}{\partial\theta}\right)\right) - \frac{\nu\kappa^2 w}{N^2} + f_s \tag{$^\downarrow$}$$

$$\frac{1}{\rho}\frac{\partial p}{\partial s} = \nu\frac{\partial w}{\partial r}\frac{\partial N}{\partial r} + \nu N\frac{\partial^2 w}{\partial r^2} + \frac{\nu N}{r}\frac{\partial w}{\partial r} + \frac{\nu N}{r^2}\frac{\partial^2 w}{\partial\theta^2} + \frac{\nu}{r^2}\frac{\partial w}{\partial\theta}\frac{\partial N}{\partial\theta} - \frac{\nu\kappa^2 w}{N} + f_s \tag{$^\downarrow$}$$

Noting $\frac{\partial N}{\partial r} = \kappa\cos\theta$ and $\frac{\partial N}{\partial\theta} = -r\kappa\sin\theta$, the axial momentum equation becomes,

$$\frac{\partial p}{\partial s} = \mu\kappa\cos\theta\frac{\partial w}{\partial r} + \mu N\frac{\partial^2 w}{\partial r^2} + \frac{\mu N}{r}\frac{\partial w}{\partial r} + \frac{\mu N}{r^2}\frac{\partial^2 w}{\partial\theta^2} - \frac{\mu\kappa\sin\theta}{r}\frac{\partial w}{\partial\theta} - \frac{\mu\kappa^2 w}{N} + \rho f_s \tag{.}$$

The cylindrical asymptotic form of the toroidal axial momentum equation is easily checked by letting the value of curvature, i.e. inverse of the coil radius, go to zero. Doing this produces Eq. C.4, which when compared to the cylindrical form of the

1-D, steady, incompressible, Newtonian momentum equation provided in Aris (1962) or any other fluids text, shows exact agreement.

$$\frac{\partial p}{\partial s} = \mu \frac{\partial^2 w}{\partial r^2} + \frac{\mu}{r}\frac{\partial w}{\partial r} + \frac{\mu}{r^2}\frac{\partial^2 w}{\partial \theta^2} \tag{C.4}$$